THE ADSORPTION OF NITROGEN ATOMS

ON METAL ~~SURFACES~~ FILMS

A thesis submitted for the Degree of Doctor of Philosophy of the University of London

by

JOHN CHARLES GREGORY

B.Sc., A.R.C.S., A.R.I.C.

Department of Chemistry,

Imperial College, London.

February, 1967.

ABSTRACT

The adsorption on nickel of nitrogen activated by a tungsten filament at temperatures between 2000 and 2600°K is described. The activation process on tungsten is identified with atomisation and an absolute reaction rate treatment is developed using a site adsorption model. When the surface coverage is small this rate equation for production of nitrogen atoms is identical to that presented by Nornes and Donaldson (1966), who did not postulate site adsorption.

An average experimental activation energy for production of nitrogen atoms on tungsten between 2300 and 2600°K and at 2×10^{-2} torr pressure was calculated to be 117 ± 3 K cals $mole^{-1}$, in good agreement with that derived theoretically ($\frac{1}{2}D(N.N) \pm 7 = 118$),

A study has been made of the adsorption of nitrogen, activated in a high frequency discharge, on glass and nickel surfaces, neither of which adsorb molecular nitrogen at ambient or higher temperatures. The adsorption is compared with that of the rare gases argon and xenon activated in the same fashion, and a clear distinction is apparent in the amounts of gas taken up.

Desorption from a nickel filament of nitrogen activated by both methods showed two desorption peaks. The first, which was evolved between 140 and 200°C was only about 1% of the second peak which was evolved at higher temperatures, (between 250 and 400°C).

Both peaks were identified with nitrogen by mass spectrometric analysis and other evidence.

Activation energies of desorption from a nickel filament of nitrogen activated by both methods were shown to be 28 ± 10 K cals $mole^{-1}$.

An analogy is drawn between the interstitial nickel nitride Ni_3N, and the nickel-nitrogen complex investigated in this work, which provides the basis for an explanation of the desorption characteristics.

ACKNOWLEDGEMENTS

I should like to express my gratitude to Professor R.M. Barrer for the provision of facilities for research in the Department of Physical Chemistry, Imperial College, and to J. Lyons and Company for the award of the J. Lyons Postgraduate Studentship for three years.

I am much indebted to Dr. David Hayward and Professor F. C. Tompkins for their guidance and encouragement, especially through the more difficult and frustrating times, and for their good-natured tolerance of my occasional absences during the regatta season.

College life has been made more profitable by the assistance of many friends in the workshops and stores, as well as in the laboratories of the group, and to all these, and to my wife for typing the manuscript, I extend my sincere thanks.

CONTENTS

SECTION 2 : EXPERIMENTAL

SECTION 1 : INTRODUCTION

Section 1:1 Chemisorption of diatomic gases on metal surfaces

The energy relations between a metal surface and a diatomic molecule approaching it are best discussed in terms of a potential energy diagram, (see figures 1, 2 and 3). Figures 1 and 2 represent the exothermic chemisorption of a diatomic molecule such as nitrogen as two atoms. The energy requirement is $2X - D > 0$ where X is the binding energy of a nitrogen atom to the surface, and D is the dissociation energy of the nitrogen molecule. The shallow depression in the energy curve of the molecule represents physical adsorption due to Van der Waal's forces. If the free atom—metal surface P.E. curve crosses this free molecule —metal surface P.E. curve while the Van der Waal's forces are still operative there is no energy of activation for dissociative chemisorption of molecules, as shown in figure 1. This is shown experimentally for very many transition metal—diatomic gas systems (H_2, N_2, O_2 on Mo, W, Ti, Zr, Nb; Hayward and Trapnell, 1964). If the activation energy E_A is small it is not likely to be noticed except at low temperatures. Figure 2 shows the relative positions of the P.E. curves when

NON ACTIVATED CHEMISORPTION

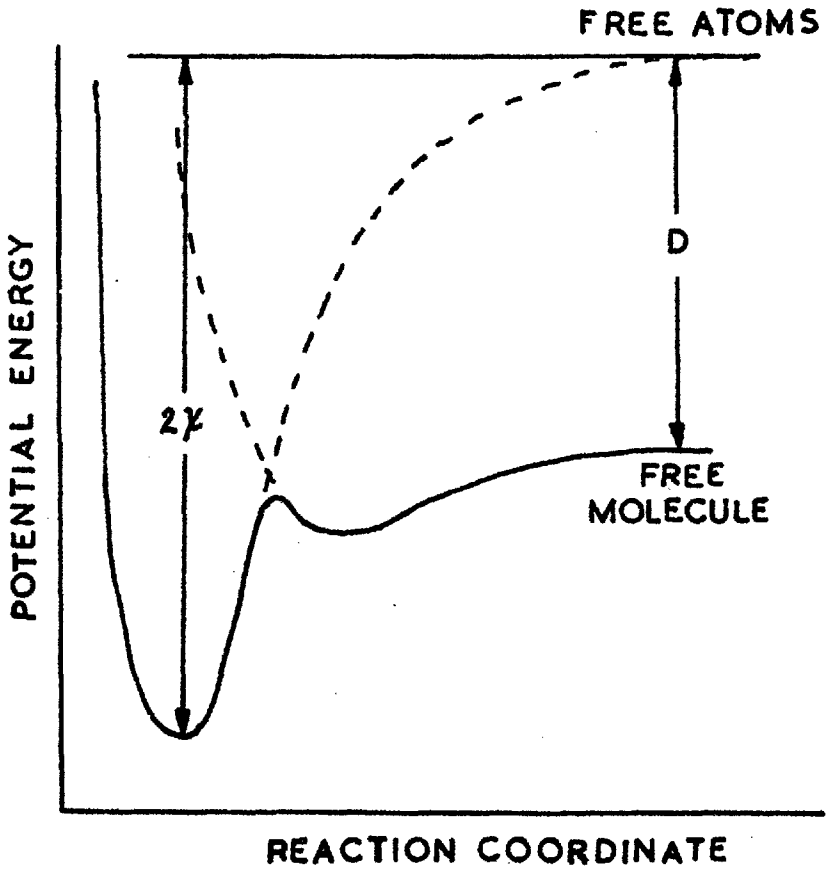

FIG. 1.

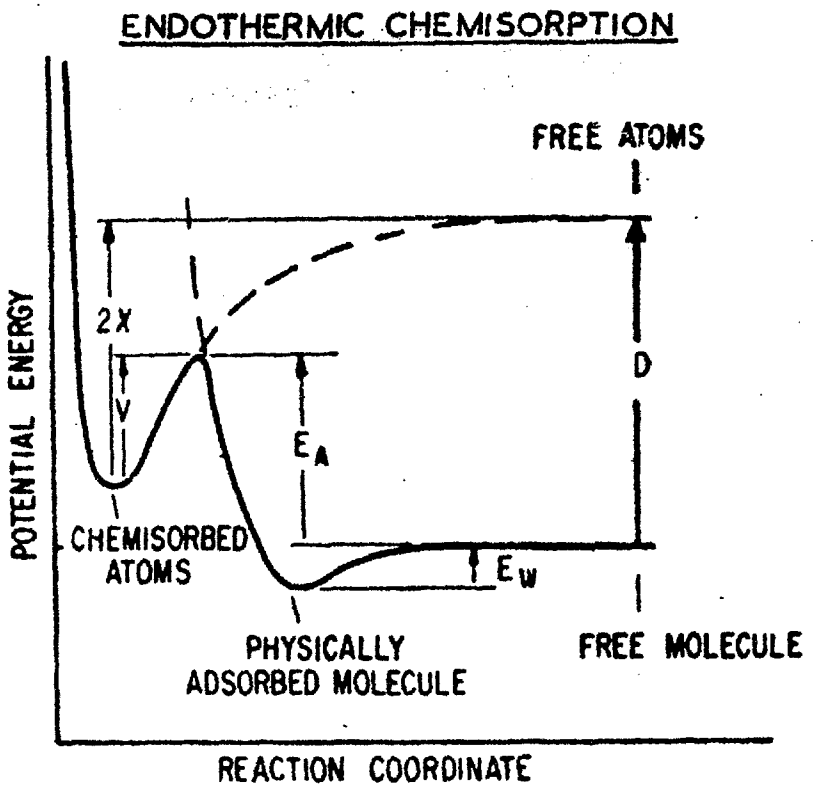
ENDOTHERMIC CHEMISORPTION
FREE ATOMS
2X
V
E_A
D
POTENTIAL ENERGY
CHEMISORBED ATOMS
E_W
PHYSICALLY ADSORBED MOLECULE
FREE MOLECULE
REACTION COORDINATE

FIG. 3.

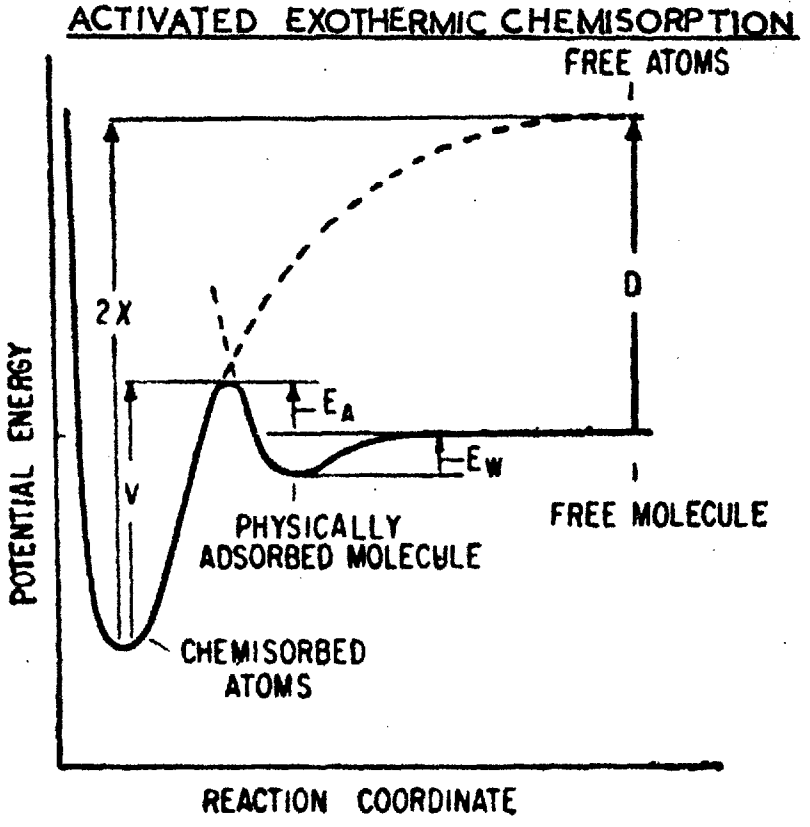
ACTIVATED EXOTHERMIC CHEMISORPTION
FREE ATOMS
2X
D
E_A
V
E_W
POTENTIAL ENERGY
PHYSICALLY ADSORBED MOLECULE
FREE MOLECULE
CHEMISORBED ATOMS
REACTION COORDINATE

FIG. 2.

there is a finite value of E_A.

Figure 3 shows the case for endothermic chemisorption, $2X - D < 0$.

If a diatomic molecule is not chemisorbed on a metal surface at low temperature, either the activation energy E_A is too high or the system is non-bonding, which means the process is endothermic and thermodynamically unstable. If the diatomic molecule is not adsorbed at intermediate temperatures, (several hundred degrees Kelvin), either E_A is improbably high, or again the system is thermodynamically unstable. Even though molecules are not dissociatively adsorbed, figure 3 shows that atoms might be adsorbed if the potential well was deep enough. Thus, one would expect atoms, or activated molecules, to be chemisorbed on many surfaces which do not chemisorb molecules.

1.2. Selection of a system of study

Nitrogen molecules do not chemisorb on several Group VIII metals (Ni, Pt, Pd, Rh), and the system Ni-N_2 was selected for special study. Experiments described in this thesis were devised to elucidate the potential energy structure of this apparently non-bonding system by investigating the adsorption of nitrogen atoms on nickel surfaces and their subsequent desorption.

1.3. Nickel-Nitrogen interaction

1.3.1. Adsorption of molecular nitrogen

From adsorption measurements on evaporated films several authors have concluded that nitrogen does not chemisorb appreciably on nickel at room temperature and pressures < ca. 10^{-3} torr, (Wagener, 1957; Hickmott and Ehrlich, 1958; Trapnell, 1953; Beeck, Smith and Wheeler, 1941). This has been confirmed by field-emission observation of nickel tips by Ehrlich and Hudda (1961) and by low energy electron diffraction (LEED) measurements of nickel single crystal surfaces under pressures of nitrogen up to 10^{-3} torr and between 0 and 300°C, (Madden and Farnsworth, 1961). The LEED observations of Germer, Scheibner and Hartman (1960) who reported observing a Ni-N_2 interaction under similar conditions were regarded doubtfully even by the authors, and it now seems almost certain that their results were due to contamination.

However, many authors have claimed that molecular nitrogen is reversibly chemisorbed on nickel at low temperatures, 78°K and 195°K, (Beeck, Smith and Wheeler, 1941; Kokes and Emmett, 1960; Gundry, Haber and Tompkins, 1962; Schuit and DeBoer, 1954). As the heat of adsorption of molecular nitrogen may be as high as 10 K cals $mole^{-1}$ (Gundry, 1961), the interaction appears

to be chemical, although the influence of the adsorption of nitrogen on both electrical conductivity (Suhrmann and Schultz, 1955) and the surface potential, (Gundry et al., 1962; Mignolet, 1950) of nickel does not exceed the effect produced by the physical adsorption of Xenon.

Recent infrared spectroscopic work by Eischens and Jacknow, (1965), has shown beyond doubt that molecular nitrogen is chemisorbed on finely divided nickel powders at room temperature. The lowest pressure at which they detected the adsorption was 1×10^{-2} torr, and a pressure of 10-100 torr was needed to bring the band to maximum intensity. The molecular nature of the adsorbed nitrogen (structure Ni - N ≡ N) was proved by observation of three infrared absorption bands upon adsorption of a mixture of isotopes, $^{28}N_2$, $^{29}N_2$, and $^{30}N_2$, instead of the two bands to be expected in the case of atomic adsorption of ^{14}N and ^{15}N.

Van Hardeveld and Van Montfoort (1966) repeated the work of Eischens and Jacknow, and found the occurrence of the Ni - N ≡ N species to be dependent on the manner of preparation of the finely divided nickel substrate, and, in particular, on the nickel crystallite size. In a well-argued paper they present evidence that nitrogen is only adsorbed on sites where

coordination is possible with 5 nickel atoms, (called B_5 sites). Such sites do not occur on the normal crystal faces of nickel. Examination of marble and computer models showed that a maximum number of B_5 sites occurs on particles of the size range (20-40Å) which is precisely the size range found to be experimentally necessary for the occurrence of the infrared-active nitrogen adsorption at room temperature. They point out that similar behaviour is shown for N_2 - Pt, N_2 - Pd, and conclude the adsorption is physical and of the form:-

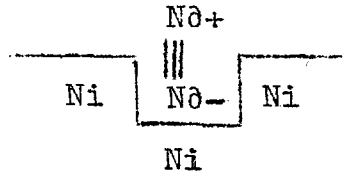

1.3.2. Nickel-nitride formation.

No evidence is known of nitrogen molecules reacting with nickel to form a bulk nitride.

A study of the transformation of the nickel lattice under the influence of inserted nitrogen has been made by Trillat, Tertian, Terao, and Lecomte, (1957), and Terao and Berghezan, (1959). Thin polycrystalline and monocrystalline layers of evaporated nickel were heated in an atmosphere of ammonia. The

ammonia was decomposed, and the nitriding process was followed kinetically by electron diffraction. A considerable expansion of the f.c.c. lattice of nickel, from α = 3.52A to α = 3.72A, was observed in the temperature range 150-175°C with the formation of Ni_4N. Continued nitriding changes this f.c.c. structure into the hexagonal lattice of Ni_3N. This interstitial nitride was formed at about 175°C, and was destroyed by heating in vacuo. In the decomposition experiments performed, the nickel f.c.c. pattern was only observed to reappear at 450°C, but the authors (Trillat et al.) point out that their rate of temperature rise was quite fast (20° per minute), so that their method of detection would not be sensitive to the decomposition until it was proceeding at a fast rate. They did, however, observe an increase in magnetic susceptibility at 250°C.

Trillat et al. also found that the action of a 10KV discharge in air produced the hexagonal Ni_3N phase in the nickel cathode identical to that previously obtained from ammonia cracking, except for increased formation of NiO, as might be expected.

Mathis (1951) measured the rates of decomposition of Ni_3N at various temperatures over 300°C. He estimated the temperature of onset of decomposition to be 290°C.

Using the micro-bombcalorimeter method of Juza and Hahn (1939) for Cu_3N, Hahn and Konrad (1951) have measured the heat of formation of Ni_3N at 20°C and one atmosphere pressure to be 0.20 $\pm$ 0.1 K cal. mole^{-1}. Ni_3N is thus endothermic and approximate entropy considerations would seem to make the free energy of formation more positive and therefore the compound less likely to be spontaneously formed.

The work on Ni_3N in the preceeding papers is discussed in relation to the present results in Section 3.

While this work was in progress, two papers appeared describing the adsorption of electron activated nitrogen on nickel surfaces, (Winters, Horne, and Donaldson, 1964; Winters, 1966). These authors recognise separate contributions of atoms and ions to the adsorption.

1.4. Production of nitrogen atoms

Nitrogen atoms were produced in two ways; by dissociation of molecules on the surface of a hot tungsten filament, and by a high frequency electrodeless discharge.

1.4.1. Production of nitrogen atoms on a tungsten filament.

Farber and Darnell (1953) investigated the influence of a hot tungsten filament on molecular

nitrogen. They did not detect any dissociation even at temperatures up to 3000°K for reasons which will be discussed in Section 3.

The attempt to produce nitrogen atoms in this way was inspired by a paper by Ricca and Saini (1964) on the influence of the ionisation gauge on the chemisorption of nitrogen on tungsten. Ricca and Saini noticed increased uptakes of gas when the gauge was operated at higher filament currents (and higher emission currents), and considered that activated nitrogen molecules were being formed by the hot cathode, or by the electron current of the ionisation gauge.

Very recently two papers have appeared on the atomisation of nitrogen on tungsten, (Nornes and Donaldson, 1966; Mimeault and Hansen, 1966). However the results of these two groups differ fundamentally as to the value of the activation energy and its theoretical justification, and it is believed that the present work can resolve the disparity.

1.4.2. Production of nitrogen atoms in the discharge

The nitrogen discharge is well-known for the phenomenon of the yellow afterglow. This is sometimes called the Lewis-Rayleigh afterglow after two early investigators; Lewis (1900) having first observed that when a nitrogen discharge was switched off a golden-

yellow afterglow remained. Three reviews of the extensive literature on active nitrogen are available; the first by Mitra (1945) in his book, which is a complete survey up to 1945, and more recently by Jennings and Linnett (1958) and Mannella (1962) which brings the coverage up to 1961.

The light emission is believed to be due to the recombination of nitrogen atoms, and may last a few seconds, or a few hours, depending on the efficiency of removal of nitrogen atoms from the system. In the present work no afterglow was observed, but it was noted early (Lewis 1929) that absolutely pure nitrogen in a baked out system did not give the afterglow. This is almost certainly due to the rapid removal of nitrogen atoms by recombination at the walls. This recombination can be slowed down enormously by the application of certain surface coatings to the glass, but these are incompatible with the requirements of U.H.V. techniques.

Thus, nitrogen atoms do not remain uncombined for long in a system clean enough for surface reactions to be meaningfully investigated, and the adsorption had to be studied with the nickel surface in contact with the gas discharge, and not just with the afterglowing gas.

The processes taking place in a nitrogen discharge are exceedingly complex and in spite of the vast

literature, as yet not completely elucidated. The species of interest with regard to adsorption on a nickel surface are

(1) nitrogen atoms

(2) various ions of nitrogen, N^+, N_2^+ etc., and

(3) excited nitrogen molecules.

Electrons, produced by ionisation of nitrogen moleclues

$N_2 + e \rightarrow N_2^+ + 2e$ are accelerated in the high frequency (20 Mc/s) field and produce collision dissociation, ionisation and activation of other nitrogen molecules

$$N_2 + e \rightarrow N_2^+ + 2e$$
$$N_2 + e \rightarrow N_2^* + e$$
$$N_2 + e \rightarrow N + N + e$$

It is interesting to note that the direct collision dissociation of nitrogen has not been observed (Massey and Burhop, 1952).

In the case of a hydrogen discharge about 90% hydrogen atoms may be produced in this way, but the proportion of nitrogen atoms in a nitrogen discharge is much lower, and has been estimated by many workers at about 0.1-1%.

An investigation of the populations of various species was not attempted after a trial operation of an

Omegatron mass spectrometer during the discharge showed that the instrument did not work properly with the discharge field switched on.

A summary of species population measurements in the literature is therefore the only guide to the concentration obtained in the present work. Determinations of nitrogen atom concentrations in active nitrogen reported in the literature are of interest if the system permitted a long lifetime of the nitrogen atoms compared to the time of flow of the atoms from the discharge region to the sampling point. The nitrogen atom concentration is then approximately equal to that in the discharge itself. The following methods of atom concentration are commonly used:-

(1) Both the mass spectrometer and the Wrede gauge are sensitive to mass difference. The mass spectrometer is more specific and may be used to measure concentrations in the actual discharge.

(2) Calorimetric methods based on the heat liberated by recombination of atoms. They are unreliable in the presence of other excited species.

(3) Electron spin resonance (e.s.r.) is a very sensitive technique for observing nitrogen

atoms, and also excited nitrogen atoms.

(4) Chemical reactions. Owing to the abnormal chemical activity of N atoms, several reactions have been used. The most useful appears to be the nitric oxide titration. N atoms are removed as follows:-

$$N + NO \rightarrow N_2 + O$$

(5) Spectral methods.

Investigations using general methods.

As the mass spectrometric studies give much more interesting information as far as the present work is concerned, they will be reviewed in a separate section.

Atoms. Using a Wrede-Harteck gauge, Groth and Warneck (1957) determined the N atom concentration in a condensed discharge to be about 1% at 1 torr. Hemstreet and Hamilton (1961) trapped from a discharge both ground state and excited state nitrogen atoms at 4.2°K in a matrix of solid N_2. The operating conditions were similar to those in the present work, and a 10Mc/s, 100W oscillator was used to maintain the discharge. They deposited ca 10^{22} molecules, and determined the

atom concentration to be about 0.1%. ^2D atoms were present in comparatively small numbers. Hildebrandt, Barth and Booth (1961) estimated the $N(^4S)$ concentration in a microwave discharge by an e.s.r. technique. They found 2% of $N(^4S)$ at 1 torr pressure and their results indicate that the proportion of atoms falls off rapidly at lower pressures. Campbell and Thrush (1966), using a power source similar to that in the present work, though operating at a lower power and higher pressures (2 - 10 torr), determined their nitrogen atom concentration to be 0.5% by NO titration.

Metastable species

Excited atoms or molecules with lifetimes > 1μ sec. are generally described as metastable, the transition to the ground state by the emission of electric dipole radiation being forbidden by one or more selection rules. The following metastable species have been produced in radiofrequency discharges and studied in molecular beams:

Species	P.E. above g.s.(eV)	Author
$N(^2D)$	2.38	Foner and Hudson (1962)
$N(^2P)$	5.38	
$N_2(A^3\Sigma^+u)$	6.16	Lichten (1960)
$N_2(a'^1\Pi g)$	8.54	

Mass spectrometric investigations

Jackson and Schiff, (1953, 1955), found ca.1% nitrogen atoms in the gas leaked into their mass spectrometer from a 1 torr condensed discharge. Ionisation efficiency curves (plots of normalised ion intensities against applied electron voltage) show an appearance potential of 14.7 ± 0.2 eV for N^+, which can only be explained by the ionisation of ground state ^4S atoms. There was no evidence of metastable atoms which would have had a lower appearance potential. Evidence for ^2D atoms has however been provided by Tanaka (1956, see Schiff, 1956), and Broida and Lutes (1956), but both estimate the concentration to be ca.1% of the ground state (^4S) concentration.

The second electron impact process giving rise to N^+ observed by Jackson and Schiff (1955) could have been due to N_2^* or N_3. N_2^* was discounted as there was no low appearance potential for N_2^+. No peak was observable at mass 42, but this does not dispose of the possibility of N_3 being present.

Berkowitz, Chupka, and Kistiakowsky (1956) also report a 1% concentration of N atoms in the discharge. Their results indicate a small proportion, ca. 2 p.p.m., of an excited molecular species, N_2 ($A^3\Sigma_u^+$).

Although Thompson (1961) was only able to detect

the nitrogen molecule-ion, N_2^+, among the charged species in a d.c. glow discharge at 1-5 x 10^{-2} torr, Knewstub and Tickner (1962) report several other charged species. A summary of their results is given. They do not give an absolute concentration for N_2^+, and other ions concentrations are normalised with respect to N_2^+.

Pressure range: 2 x 10^{-2} - 4 x 10^{-1} torr.

Ion	relative concentration
N_2^+	1
N_4^+	0.1
N^+	0.05
N_3^+	0.02

The ions are produced by the following processes:-

(N^+) $\quad N_2 + e \longrightarrow N^+ + N + 2e$

(N_2^+) $\quad N_2 + e \longrightarrow N_2^+ + 2e$

(N_3^+) $\quad N_2^{+*} + N_2 \longrightarrow N_3^+ + N$

$\quad N^+ + 2N_2 \longrightarrow N_3^+ + N_2$

(N_4^+) $\quad N_2^+ + 2N_2 \longrightarrow N_4^+ + N_2$

1.4.3. The mechanism of the nitrogen afterglow

The afterglow emission is definite evidence of the presence of nitrogen atoms in the ground state (^4S). Berkowitz, Chupka and Kistiakowsky (1956) show that under all conditions they studied,

$\frac{I}{[N]^2}$ = a constant (where I = afterglow intensity).

POTENTIAL CURVES OF NITROGEN

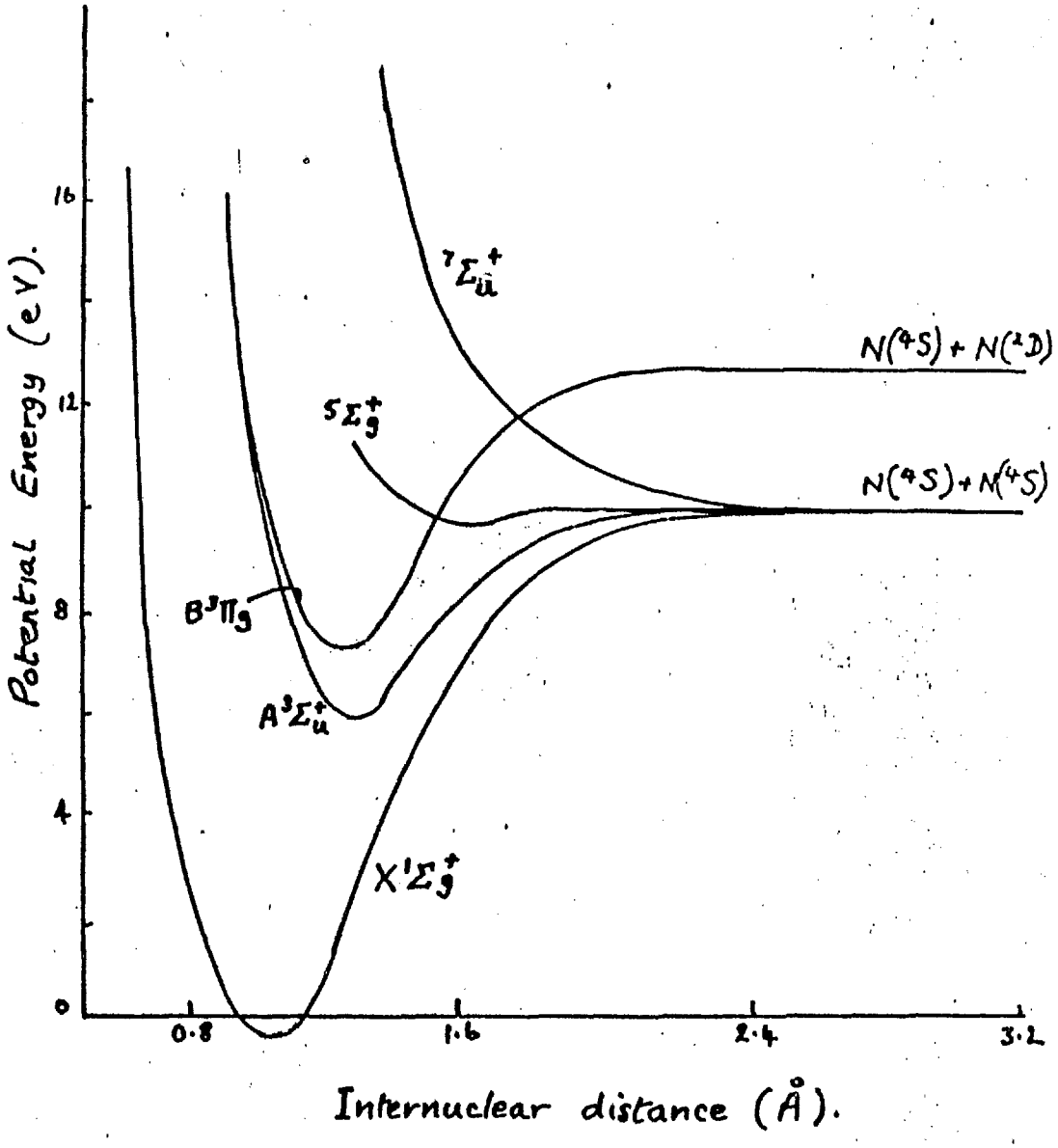

FIG. 4.

Thus the kinetic law governing afterglow intensity is second order in $N(^4S)$atoms. Rayleigh (1940) found that $I \alpha [N]^2 [M]$ (where M is a third body) at pressures of the order of 10^{-1} torr. The mechanism of afterglow undoubtedly involves three-body collisions as the rate determining step.

Figure 4 shows some of the relevant potential curves of nitrogen, (Gilmore, 1965). The following discussion shows the great ease with which predissociation and preassociation can occur in the nitrogen system, and is relevant both to the formation of nitrogen atoms by electron impact, and the processes occurring after Auger neutralisation of a N_2^+ ion at a metal surface.

The possible products arising from the collision of two ^4S nitrogen atoms (electronic configuration $1s^2\ 2s^2\ 2p_x\ 2p_y\ 2p_z$) are shown in figure 4. Two such atoms may approach each other along four different paths, corresponding to the pairing of 6, 4, 2, and 0 electrons, according to the Wigner-Witmer rules, (Herzberg, 1950). The spectroscopic designation of the states of the N_2 molecules thus formed are, in the same order $^1\Sigma g^+$, $^3\Sigma_u^+$, $^5\Sigma_g^+$, $^7\Sigma_u^+$. Whichever path the two atoms follow they will fly apart again at the end of the first molecular vibration unless collision with a third body

prevents this. Even such a collision will not prevent the non-bonding molecular system $^7\Sigma_u^+$ from dissociating.

The visible emission comes mainly from the $B^3\Pi g$ state of N_2, with a small contribution from the $Y^3\Sigma_u^-$ state, although neither of these states correlate with two ground state atoms. The emission is, however, confined to levels with energies less than that of $N(^4S) + N(^4S)$. It has been generally accepted (Berkowitz et al 1956, Jennings and Linnett 1958) that these levels of the B state just below this threshold are populated by collision-induced transitions from the very shallow $^5\Sigma_g^+$ state of N_2.

$$N(^4S) + N(^4S) + M \longrightarrow N_2(^5\Sigma_g^+) \longrightarrow B^3\Pi g \longrightarrow A^3\Sigma_u^+ + h\nu$$

This mechanism is disputed in a recent paper by Campbell and Thrush (1966). They argue that instead of preassociation to the B state occurring from the shallow $^5\Sigma_g^+$ state, which they maintain could not have a high enough steady state population to account for the high rate of formation of nitrogen molecules, the precursor of the radiating B state is the $A^3\Sigma_u^+$ state. The $A^3\Sigma_u^+$ and $B^3\Pi g$ states lie close enough together, and although the selection rules prohibit the radiationless transition $^3\Sigma_u^+ \longrightarrow {}^3\Pi g$ this would probably occur readily in collisions.

$$N(^4S) + N(^4S) + M \longrightarrow A^3\Sigma_u^+ \xrightarrow{+M} B^3\Pi g$$

$$\longrightarrow A^3\Sigma_u^+ + h\nu \text{ (afterglow).}$$

1.4.4. Summary of nitrogen species probably occurring in the discharge.

Atoms:	$N(^4S)$	0.1-1% of total nitrogen species.
	$N(^2D)$	ca. 1% of $N(^4S)$ concentration.
	$N(^2P)$	concentration unknown, but very small
Ions:	N_2^+	concentration not given, but presumably quite high.
	N^+	5% of $[N_2^+]$
	N_3^+	2% of $[N_2^+]$
	N_4^+	10% of $[N_2^+]$
	N^{++}, N^{+++}	have been reported, but only present in very small proportion.

Metastable molecules

$N_2(A^3\Sigma_u^+)$	ca. 0.0002% of total $[N_2]$.
$N_2(a'\Pi g)$	concentration unknown but very small.

Of this considerable array of activated species fortunately not many are considered to have a significant effect on the main adsorption processes. Among atomic species, the ^4S atoms are present in sufficient quantities to swamp any effect of the ^2D and ^2P atoms.

The ion-surface interaction process is discussed briefly in the next section, but the theory is not well enough developed to be able to differentiate between the various ions. As N_2^+ ions are present in a large

preponderance, the other varieties are, for the purpose of this work, ignored.

Metastable molecules are only present in minute quantities, and, apart from their important role as intermediates in the adsorption of N_2^+ ions, are not mentioned further.

1.5. Adsorption of gases activated by electron impact

The gradual disappearance or clean-up of gas subjected to bombardment by energetic electrons was first observed by Plücker in 1858. Since then many investigations of these phenomena have been undertaken, and many explanations have been offered. The older literature has been reviewed by Pietsch (1926), while the more recent work has been reviewed by Stout and Vanderslice (1961) and Carter (1959).

Several different mechanisms have been proposed to account for clean up, e.g. ion-burial, creation of metastable molecules, molecular dissociation, burial by sputtering etc.

The adsorption of noble gas ions has been studied by a number of investigators:

Blodgett and Vanderslice (1961), Carmichael and Knoll (1958), Smeaton, Carter, and Leck (1962), Kornelsen (1961), and Carter and Leck (1961).

Investigations of the reemission of noble gases from metal surfaces have shown in many cases the rate of gas release has an inverse time dependence. Blodgett and Vanderslice (1961) found the reemission rate varied as $t^{\frac{1}{2}}$ for glass surfaces and interpreted their results as ion-burial and subsequent diffusion to the surface. However, Carter et al. (1961, 1962) found neither of these time dependences and interpreted their results as indicating that the gas is bound close to the surface and that it can be desorbed in a single activated jump.

James and Carter (1962) maintain that noble gases must be adsorbed on or near the surface because a small amount of sputtering liberates most of the adsorbed gas. This argument is not conclusive as Bowden and Brandon (1963) have shown that low energy ion bombardment produces damage to a depth of at least 100Å. It is likely the defects created by ion bombardment are surrounded by strain fields which might cause a large diffusion rate for trapped gas.

The mechanism which leads to sorption of nitrogen is probably different from that of the noble gases. By plotting a graph of pumping speed of electron-activated nitrogen over a nickel surface against electron energy, Winters, Horne and Donaldson (1964)

showed that changes in the slope of this curve could be correlated with known ionisation potentials and electronic states of the molecule. They identified four discontinuities in their pumping speed curve with limits of predissociation from the $B^3\Pi g$, $a'\Pi g$, $C^3\Pi u$, $y'\Pi g$ states, with energies corresponding to values from 9.8 to 14.2 eV. A further discontinuity at 15.7 eV corresponds to the ionisation energy of N_2. The authors suggest that the non-ionic part of the pumping results from predissociation and subsequent adsorption of the atomic nitrogen.

A gas ion approaching a metal surface with a kinetic energy of less than 1 KeV is neutralised by an Auger transition (Hagstrum 1956) before it strikes the surface. In this process an electron from the conduction band in the metal neutralises the ion near the surface. The energy released by the electron is absorbed by a second electron from the metal because the wave functions of the two electrons overlap. If the energy transferred to this second electron is large enough and its momentum properly oriented, this electron can escape from the metal. The neutral gas atom or molecule then makes elastic collisions with metal lattice atoms during which momentum is transferred. Surface atoms are sputtered (Wehner 1962), lattice disorders produced

and electrons ejected from the surface of the metal (Hagstrum, 1956). The gas atom or molecule comes to rest in the metal lattice and is trapped or sorbed. Sticking probabilities of ions, induced reemission of adsorbed gas, and the phenomenon of target saturation have been reported using ion pumping techniques, but there is still a lack of experimental data concerning the interaction of an ion of known energy with a clean metal surface. A review of this work is given by Yarwood and Close (1963).

Brown and Davies (1963) and Kornelsen (1962) have established that for an integrated ion flux of $<10^{13}$ ions cm^{-2} (for rare gas ions on tungsten) the total number of ions adsorbed (found by flashing the target) is proportional to the total number incident for all ion energies. Above this value of total flux, significant interaction occurs between incident ions and atoms already trapped in the surface layers of metal atoms. This affects the saturation condition which is therefore not entirely governed by target sputtering as suggested by Nielsen (1956) and Carter, Colligon and Leck (1962).

Winters (1966) has measured the sticking probabilities of Ar^+ and N_2^+ ions on nickel surfaces as a function of ion energy. The larger differences

make it clear that different mechanisms of adsorption are operating. It is known that the adsorption of noble gas ions results from their being physically trapped at or near the surface. This mechanism is probably operative with N_2^+ ions, but is overshadowed by a much larger effect.

The sticking probability, s, for N_2^+ ions on nickel is about 0.1 for ions of a few eV, 0.5 for ions of 15 eV and nearly 1 for ions of energy > 50 eV, whereas for argon $s < 10^{-2}$ for ion energies < 60 eV, and 0.5 at energies > 300 eV. In addition Winters records the much greater reemission, due to impact on the surface, in the case of Ar^+ than with N_2^+.

These results indicate that a N_2^+ ion has a large probability of dissociating upon impact with a nickel surface, thus leading to its sorption as atomic nitrogen. It has been suggested (Propst and Lüscher, 1963) that a N_2^+ ion, upon approaching the surface, is Auger neutralised into a variety of molecular states. An Auger electron, ejected from the surface of the metal may scatter from an electron in the ground state around an 'adsorbed' molecule, exciting it to a higher state. Predissociation may occur from one of these states, yielding two atoms which then interact with the metal surface.

2. EXPERIMENTAL

2.1 Introduction

Achievement of Ultra High Vacua

Many modern methods of investigating gas-surface interactions, such as flash desorption, and ion and electron microscopy, are dependant on the researcher's being able to establish and maintain pressures below 1×10^{-9} torr. At 10^{-6} torr and a sticking probability of unity a large fraction of the surface is covered with adsorbed gas in a matter of seconds. Therefore a clean surface is contaminated too quickly for its characteristics to be established. At 10^{-10} torr this degree of contamination is achieved only in a matter of hours. Figure (5) shows the approximate time in which a monolayer is formed (t_m) versus P for two values of s (sticking probability). Using ultra high vacuum techniques therefore the properties of clean surfaces, or of surfaces contaminated in a known manner may be investigated.

The techniques for achieving these vacua were known thirty years ago (Anderson, 1935, Nottingham, 1937) but these workers had not the means of measuring them. Although much work done at pressures of 10^{-6} torr (background) is perfectly valid, there

FIG. 5

Variation of Surface Monolayer Time with pressure for 2 values of S.

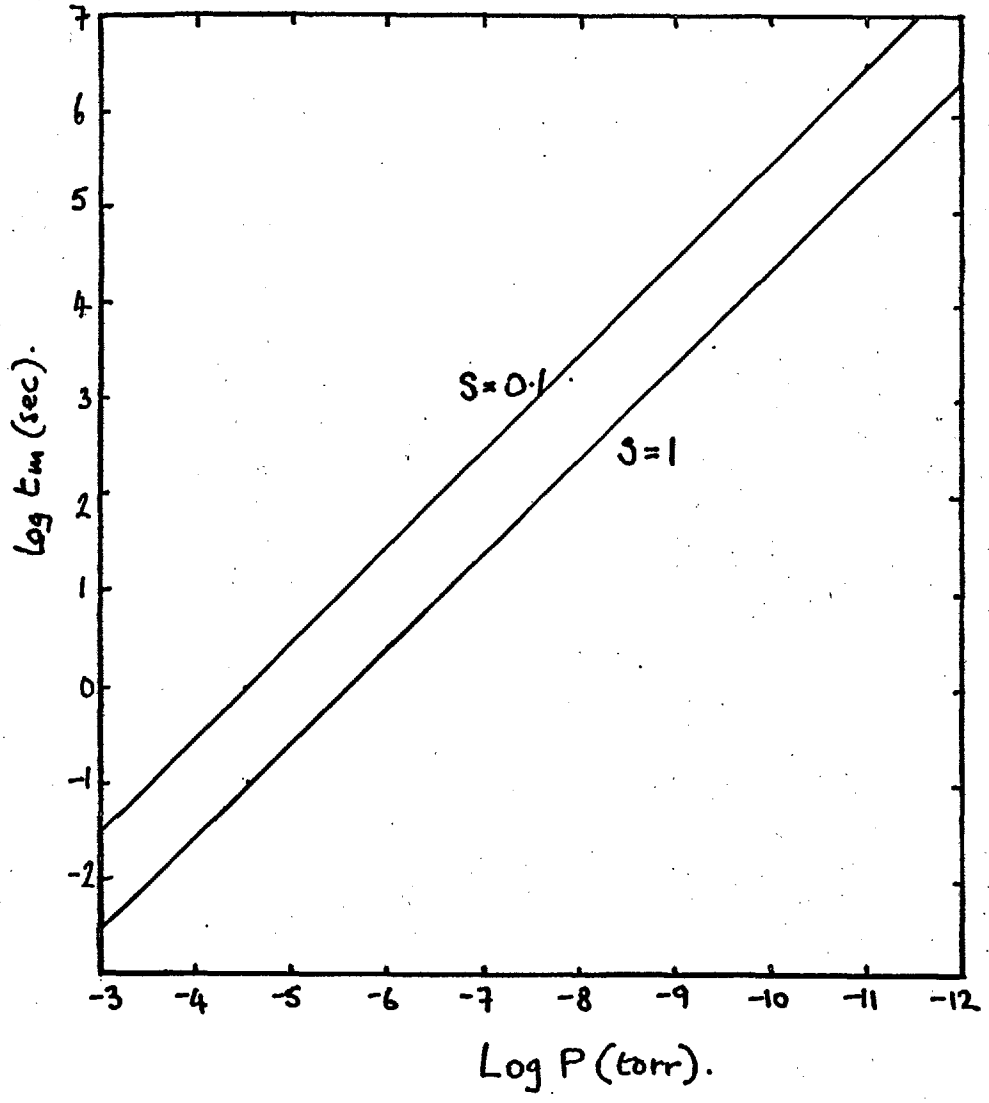

is no insurance that contamination by foreign gases will not give misleading or at least irreproducible results.

To achieve these ultra high vacua the rate of outgassing of surfaces in the ultra high vacuum part of the system at the operating (experimental) temperature must be reduced by heating that entire part whilst maximising the pumping to reduce the pressure over the surface involved.

The techniques required to pump down to pressures of 2×10^{-10} torr are well known (Ehrlich, 1963) but the procedure followed during this work will be briefly given.

The vacuum envelope was constructed of borosilicate glass (Pyrex). This is permeable to helium and Redhead (1961) has shown the residual gas at 1.3×10^{-10} torr to be 40% He. The advantages of glass over metal are its chemical inertness, simplicity in leak checking, ease of manipulation, dielectric strength, and low cost. Metal envelopes are less fragile, more easily demountable, and generally more suitable for large volume systems (> 5 litres).

2.2 The Vacuum Apparatus

A diagram of the apparatus is shown in Figure (6)

LEGEND TO FIGURE

A	Nitrogen generator (Sodium Azide)
C	Cell
D_{1-3}	Magnetically operated Dekker valves
D_4	Capillary Dekker
F	Breakseal flasks of pure gases
G	High frequency generator
IG	Ionisation gauges
K	Klemperer high speed diffusion pump
LV	Low vacuum system
M	McLeod Gauge
MC	Mercury cut off
NRV	Oil no-return valve
P	High speed diffusion pump
P3	3 stage diffusion pump
R	Rotary pump
RB	Rose bowl trap
S	Safety shut off float valve
$T_{1,2}$	Liquid nitrogen traps
SL	Ballast volume

Area enclosed by dashed line - part of apparatus bakeable in furnace.

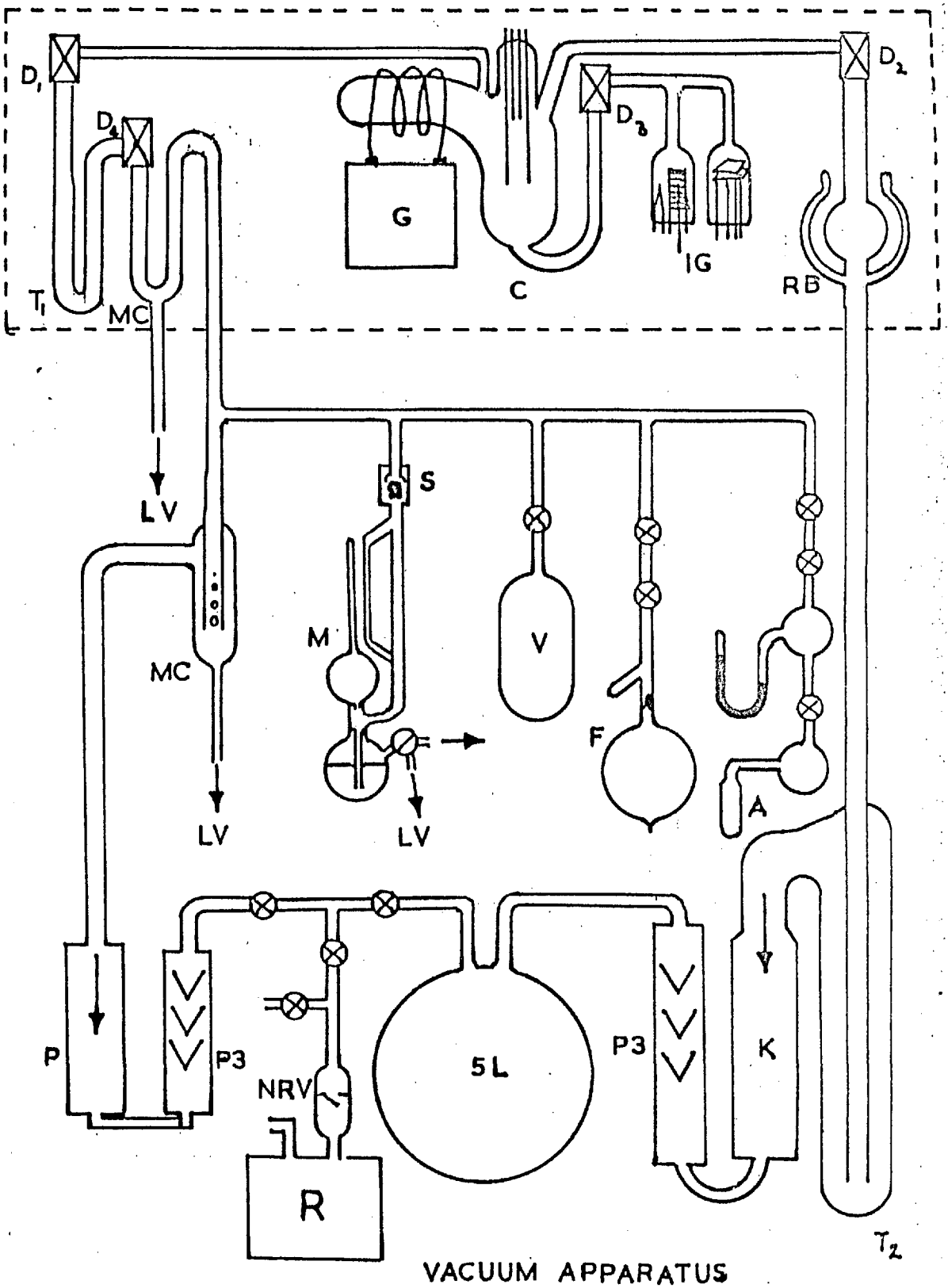

VACUUM APPARATUS

FIG. 6

It was constructed in an aluminium slotted angle box frame (Dexion Ltd.), 4 feet high, and mounted on wheels. The top surface of the frame was covered in ½" thick asbestos sheet (Syndenyo) in which holes were cut to allow pumping leads, thermocouple and gauge control wires to pass through. The part of the apparatus above this sheet was baked to 420°C inside the furnace. A heat shield of aluminium sheet just underneath the Syndenyo sheet prevented failure of greased stopcocks in the dosing system during bakeout.

The vacuum system employed had mercury rather than oil diffusion pumps because penetration of mercury into the system on trap failure does no permanent harm, while oil vapour can cause extremely serious contamination due to cracking and deposition of carbon. Carbon monoxide is an especially undesirable contaminant in this work. The only permanent effect of the mercury penetration during bakeout was the discolouration of the gold plated box of the Omegatron. However, its performance was not affected. The reaction cell, which was the same for both film and filament studies, contained a metal filament. Nitrogen atoms could be produced in one section of this cell either by gas discharge or by

dissociation on a hot tungsten filament. A side arm contained gauges. One pumping lead from the cell was of large bore (2-3 cm. dia.) and could be isolated by a dekker valve (Dekker 1954) D_2 from the cold trap and pumps, (an 8 cm. bore high speed Klemperer mercury diffusion pump, backed by a 3-stage umbrella type mercury diffusion pump). The tubulation between cell and dekker was sometimes sealed off when experiments were being conducted of sufficiently long duration that pumping across the seat of the dekker would have made an appreciable error.

The other pumping lead passed through a dekker D_1, a cold trap, and a mercury cut-off to the dosing system. A second mercury cutoff was interposed between the cell and the second pumping system which consisted of a high speed single stage diffusion pump backed by a 3-stage pump. This cutoff had some small conductances in between the fully open and the fully closed positions.

The dosing system comprised a McLeod gauge, a calibrated volume, and the gas bulbs themselves. It was necessary to have several greased stopcocks in this part of the apparatus.

2.3 Valves used in the apparatus

Greased stopcocks. The main disadvantage of these

is the permanent gas which is evolved from the grease when the taps are turned. Vapours are retained in the liquid nitrogen trap, but even after long outgassing of the grease, each revolution of a tap produced a burst of gas of about 1×10^{13} molecules. An analysis was made of this gas ~~made of this gas~~ with the Omegatron mass spectrometer.

Diaphagm valves. These taps had a diaphagm of Viton C which was chemically inert, and safe up to 200°C. They were fitted on parts of the apparatus where taps became heated during bake-out. Two out of four had to be removed because of leaking, either across the seat or to atmosphere. Leaks in the taps are not easy to locate.

Bakeable metal valve. A one inch bore bakeable stainless-steel tap (Vacuum Generators Ltd.) for which a closed conductance of 10^{-14} litres sec^{-1} was claimed, (3.5×10^{5} molecules $torr^{-1}$ sec^{-1}), was fitted in place of D_1 in Figure (6) during early experiments. Later the metal valve had to be replaced by the dekker valve and mercury cutoff after a series of mechanical failures.

Mercury cut-off. The chief disadvantage of the mercury cut-off is the necessity for a cold trap in the

enclosed volume, with the resulting possibility of physical adsorption in the trap, and the necessity of making thermal transpiration corrections.

Dekker valves. These are magnetically operated bakeable ground-glass ball and socket valves. They are very useful for isolating gas at pressures in the molecular flow region for reasonably short periods of time, but their conductance becomes noticable after long periods and at higher pressures. The conductance may not be reproducible if the dekker is lifted out and reseated.

2.4 Safety device for failure of water supply to the diffusion pumps.

The diffusion pump heater supply was controlled by a Sunvic relay so that when the temperature of the water jackets of the pumps rose above 40°C or failure of the water supply, the heaters on the pumps were shut off. The sensitive element was a small thermistor strapped to the side of one of the water jackets, and connected into one arm of a wheatstone bridge, so that an out of balance signal, amplified, operated the relay.

2.5 The cell

The cell was cylindrical, 6 cms. in dia. and 18 cms. long, including the rounded off portions.

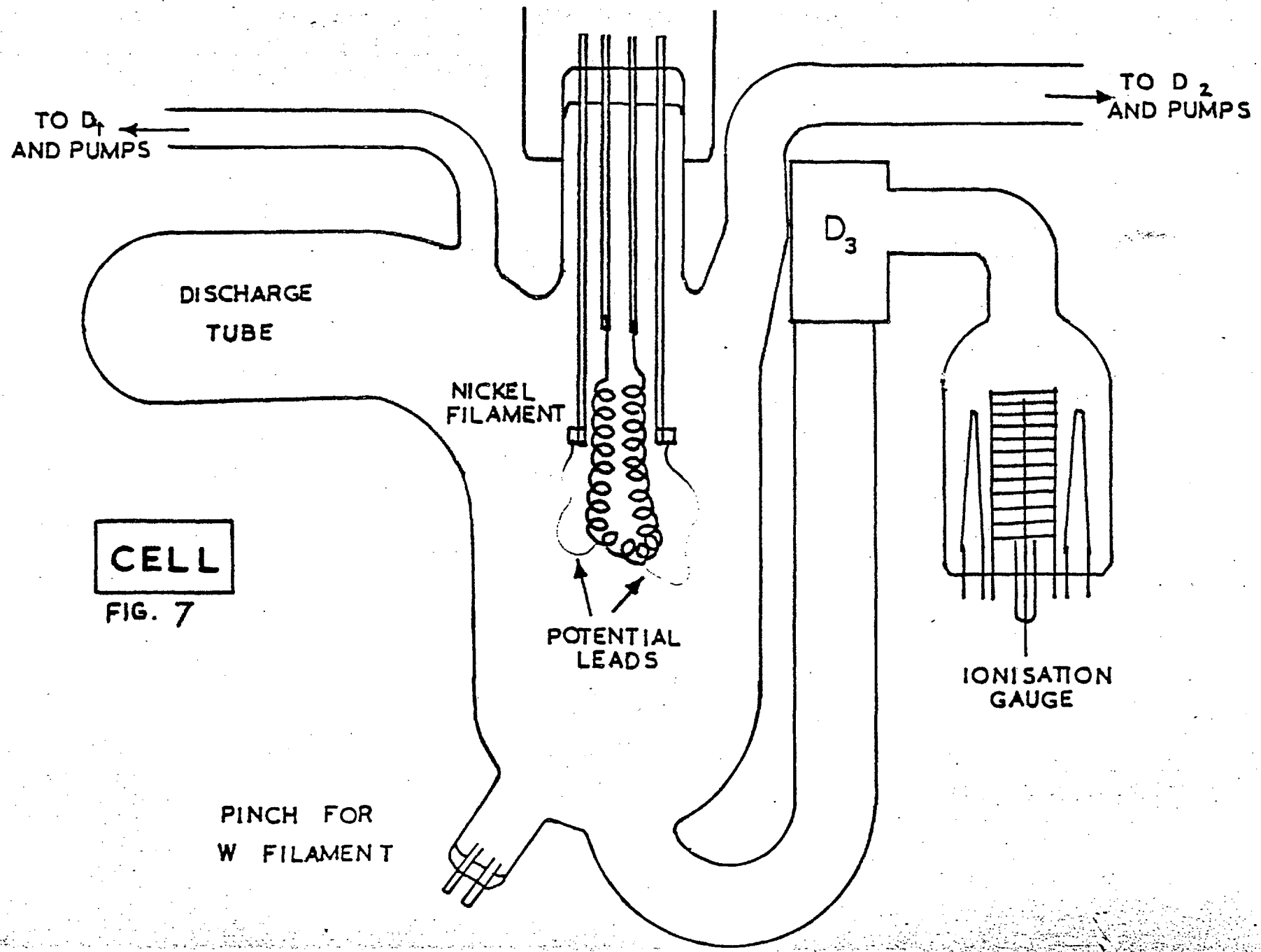
TO D1
AND PUMPS
TO D2
AND PUMPS
D3
DISCHARGE
TUBE
NICKEL
FILAMENT
POTENTIAL
LEADS
IONISATION
GAUGE
PINCH FOR
W FILAMENT

CELL

FIG. 7

The discharge tube was a horizontal projection out of the cell. Two leads passed via dekker valves to the pumps, and one via another dekker to the gauges. The volume of the cell and gauges including the tubing up to the two pumping lead dekkers was about 1 litre. This was measured by expansion from a standard 1 litre volume incorporated in the dosing system. Pressures were measured on the McLeod gauge, and were in the 10^{-2} - 10^{-3} torr range. The gas used was nitrogen, no cold-traps were used for the purposes of the calibration and Boyle's Law was assumed. As small alterations were often made to the volume of the topwork, the exact volume between the pumping lead dekkers is given with the respective result.

The dekker, D_3, leading to the gauges was closed during all atomisation, whether by the discharge or by the hot tungsten filament. This was to prevent take up of active species in the gauges. When uptakes were not being measured, the initial gas dose was let in only after the dekker D_3 was closed. During the time of a typical experiment the pressure might rise to 1×10^{-3} torr in the gauges due to leakage across the seat, while the pressure in the cell was 3×10^{-2} torr. This measure enabled quicker return of the gauges to

stable pressure readings after the gas was pumped out.

The nickel filament was supported from two tungsten pins, (2 mm. dia.) glass covered for most of their length. The potential leads were of very fine tungsten wire (0.025 mm. dia.). These were attached to a second pair of tungsten rods by means of platinum foil sheaths around the ends of the rods. The exposed parts of the tungsten rods were etched with A.C. and polished with D.C. in the same bath of aqueous caustic soda before spotwelding was attempted. The potential leads were very carefully spotwelded to the Ni filament about 2 cms. apart in the centre of the Ni filament.

The ends of the tungsten rods outside the cell were similarly cleaned and attached to 8 cm. lengths of 1 mm. diameter silver wire by means of platinum foil wrapped round the join and heavily spotwelded. By these means connections to the filament controller leads could be made with reproducible low contact resistance.

The glass construction round the main cell pinch-seal was to contain liquid nitrogen. During the latter stages of this work the filament was cooled by this means, and though the filament temperature was

never measured under these conditions, it certainly never reached 78°K. The coolant had the effect of preventing the nickel filament from being heated during the atomisation process. The filament and pinch were allowed to return to room temperature before any desorption run was carried out, in order to avoid including any low temperature nitrogen on nickel species in the desorption spectrum.

2.6 Operation of vacuum system

No experiments were done at very low pressures, but pressures of $2 - 5 \times 10^{-10}$ torr were obtained before dosing in order to test for sources of gas impurity, and to standardise as much as possible the impurity levels.

After attaining a vacuum of 10^{-5} torr or better the apparatus was baked out under the furnace at 400°C overnight with the cold traps on. The temperature of the furnace was monitored using a chromel-alumel thermocouple and a Cambridge potentiometer, and controlled with a 30A Variac. The traps were removed in the morning and outgassed at about 250°C with heating tapes for 2 hours, after which the latter were removed. When the traps were cool, they were immersed in liquid nitrogen. The furnace was switched

off, and when it had cooled to less than 200°C it was removed.

2.7 Outgassing of metal parts

Outgassing of the gauges and filament was then done as quickly as possible while the glass was still hot. A new nickel filament was outgassed normally for 12 hours at a temperature just below that required to produce a film (about 1200°C). After thorough outgassing another bakeout would be performed.

Outgassing by electron bombardment was usually sufficient for both Bayard-Alpert and high-pressure Schulz-Phelps gauges, but when these became heavily oxidised more rigourous methods were required. Electron bombardment was discontinued if the pressure rose much above 1×10^{-5} torr as a discharge in the gas which struck at pressures of about 1×10^{-4} torr caused sputtering of the filament. Film throwing in the gauge leads to the possibility of leak paths and spurious emission or ion currents. The structure of the Edwards 1G3H gauge usually prevents the latter.

The ionisation gauge control circuit made in these laboratories was capable of supplying about 60 watts for electron bombardment, (grid voltage 700 V.A.C.),

but this was not sufficient to heat a well blackened gauge grid to a high enough temperature, (1300°C), owing to the enhanced thermal emissivity of the blackened surface and increased loss of heat because of the higher gas pressure. Badly contaminated grids were therefore outgassed by eddy-current heating, the power for which was supplied by a 500W 500Kc/S oscillator built in these laboratories. It was also used to outgas the omegatron mass spectrometer at 800°C.

For the worst contamination of grids, it was necessary to 'hydrogen-fire' the gauges by heating them with the eddy-current heater in an atmosphere of hydrogen at several torr pressure. If a heavy film had been thrown in the gauge, it was demounted and steeped in a hot mixture of caustic soda and potassium ferricyanide solutions. The quantities of ingredients here are not critical, and a minute or two of this treatment was sufficient to remove the thickest films, and also any oxide on the grid.

2.8 Leak detection

If the vacuum was not of the order of $2 - 5 \times 10^{-10}$ torr and contamination was not suspected, the standard methods of leak detection were employed. These were:

FIG. 8

GENERAL VIEW OF THE APPARATUS

From left to right: Filament control circuit, ionisation gauge control circuit; vacuum line and gas discharge oscillator; Omegatron magent and support, and eddy current heater; Omegatron control equipment.

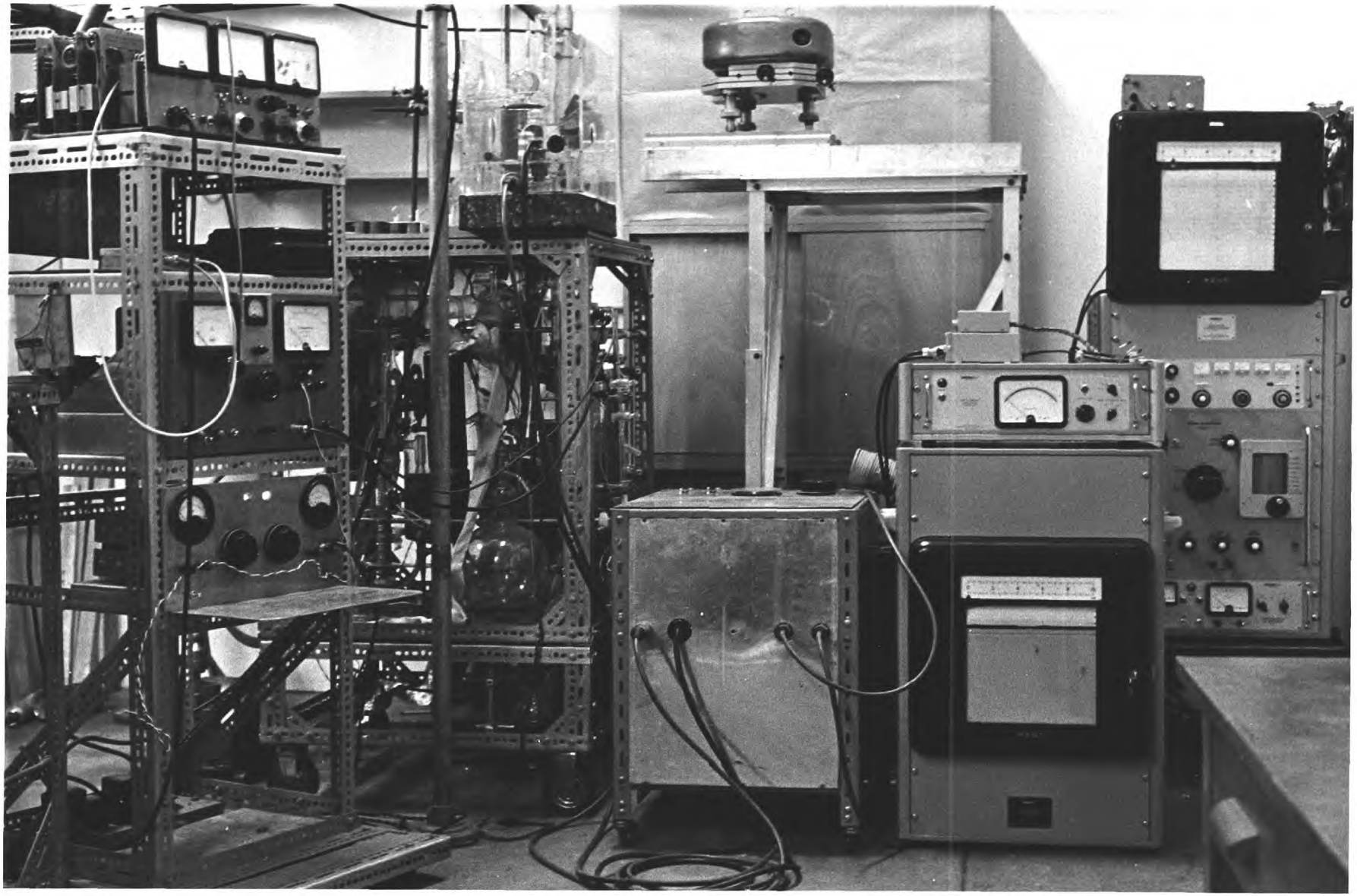

FIG. 9

VIEW OF TOP OF APPARATUS

Showing reaction cell and discharge oscillator in position round finger.

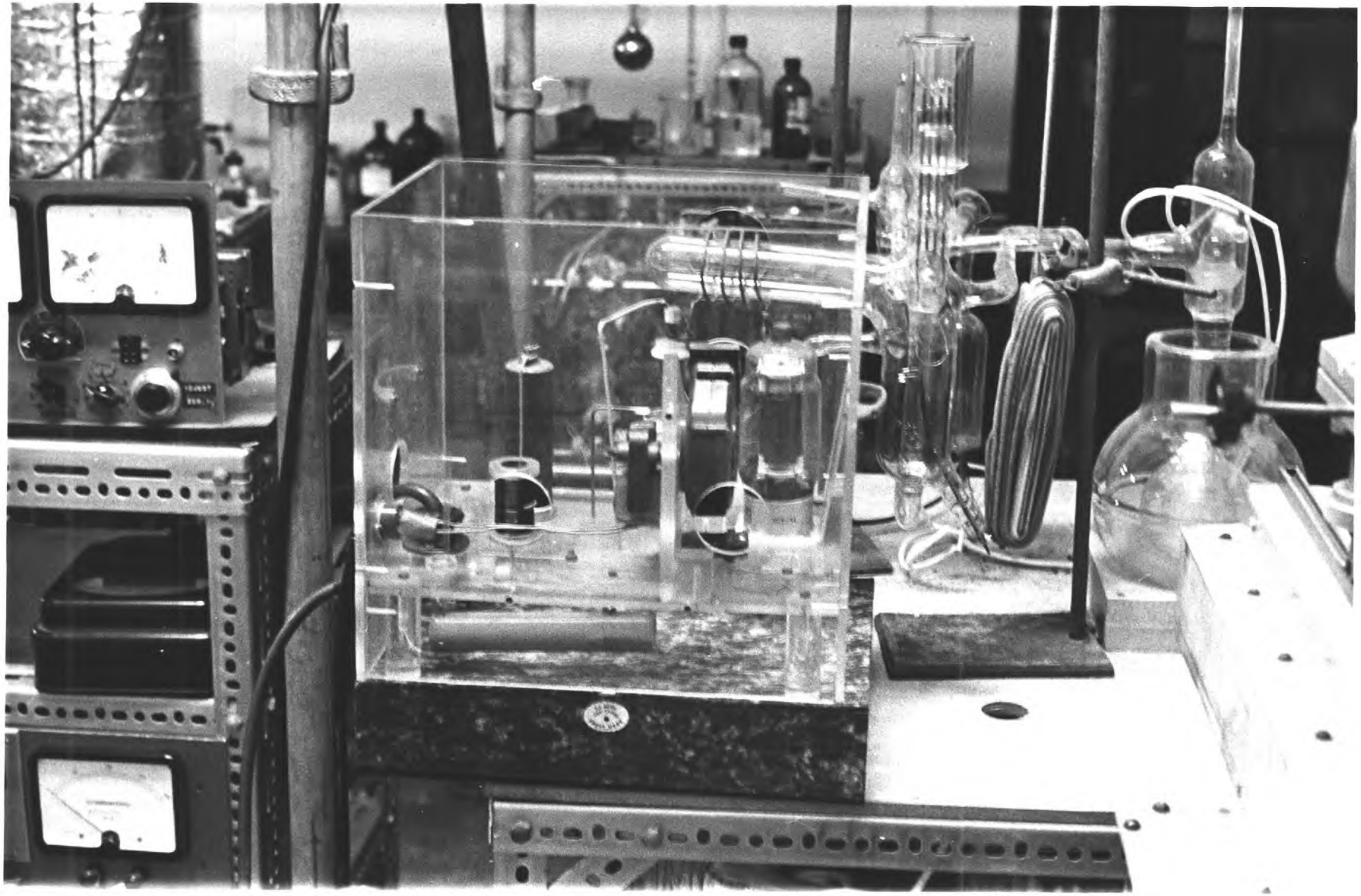

inspection (for streaky greased taps, cracked pinch seals etc.), isolation of various sections of the apparatus to pinpoint the source of gas, use of Tesla coil, particularly on newly blown sections of glass, and painting on the vacuum envelope of liquids such as carbon tetrachloride or water, and watching for any variation in the ion current from the ionisation gauge. When liquid passes into a small hole or crack in the apparatus, the ion gauge characteristically shows a sharp increase, often followed by a fall to below the previous steady pressure as liquid blocks the hole and cannot pass through the hole as freely as air. A more sensitive variation of this method, suitable for very small holes, is to spray a small hydrogen or helium jet over the apparatus using a mass spectrometer set on the appropriate mass number as the detector.

2.9 Materials

Nickel. 0.5 mm. and 0.1 mm. wire was supplied by Johnson Matthey and Co. Ltd. and designated Grade I. The spectrographic report is summarised below:

Iron	4 ppm	Aluminium	<1
Silicon	2	Calcium	<1
Magnesium	1	Copper	<1

Unfortunately the carbon figure cannot be given

as the spectra were obtained by means of a D.C. arc between two graphite electrodes.

Palladium and Iridium. Wires of these elements of diameter 0.5 mm. were obtained from Johnson Matthey. They were described as 'spectrographically pure'. Metallic impurities 10 p.p.m. (mainly Pt and Rh.).

Nitrogen. Nitrogen was produced in a small bulb in the dosing system by heating previously outgassed Analar sodium azide.

$$2NaN_3 \longrightarrow 2Na + 3N_2$$

The first dose of Ca. 10^{21} molecules was pumped out and a second quantity prepared.

Some samples of sodium azide exploded violently on heating. This was found not to depend on whether or not a Tesla coil was used to initiate decomposition, but appeared to be a function of the batch number on the sodium azide bottle.

A mass spectrometric analysis of the nitrogen did not reveal any impurities.

Argon and Xenon. These gases were supplied in 1 litre bulbs (B.O.C. Ltd., Grade X).

Impurities:	Grade X Ar	Grade X Xe
N_2	< 5 p.p.m. (vol)	< 25 p.p.m.(vol.)
O_2	< 1	< 5
H_2	< 1	
CO_2	< 0.5	< 5
Kr		< 50

2.10 Construction of auxiliary pieces of equipment

2.10.1 Furnace. This was in the form of a 3' cube and was constructed of aluminium sheet. Two open bottomed boxes of this material were placed one inside the other with a gap of $1\frac{1}{2}$'' between all faces, so that the open sides of each were coplanar. They were fastened together in this plane so that they could expand independently. The space was filled with expanded mica (Micafil).

The heating was effected by four 1 KW elements, (Tetra Ltd.), fixed on the inner walls of the furnace and controlled from a 30A Variac variable transformer.

The furnace weighed about 60lbs and was raised and lowered by a Haltrac midget hoist. It could be rested in the raised position on moveable bars placed across members of rigid framework of $1\frac{1}{2}$'' steel tubes (Geo. Gascoigne, Ltd.) which also held the hoist.

Now that Caposil magnesium silicote slabs are

available, furnace construction in this material is recommended as involving much less work, and being about half the weight.

2.10.2. 500Kc/s Eddy-Current heater. A 500W 500 Kc/s eddy current heater was constructed to enable metal parts to be outgassed in vacuo and to use in hydrogen-firing ionisation gauges.

The circuit which was supplied by the General Electric Research Laboratories, Schenectady, New York, is shown in figure (10).

The oscillators are two 813 beam tetrodes supplied with 0-2000 VDC. The two capacitors in the tank circuit and the other 2 capacitors in the oscillating circuit were found to be under-rated when operated in the laboratories. As this heater had to be used mainly at its maximum output capacitors of high current rating should be used. It is recommended that the 50A leads in the tank circuit be water cooled.

The work coil was made of copper tube supported on an insulating handle (see figure 11). The heater was capable of heating the body of the Omegatron mass-spectrometer to 1000°C in vacuo and of heating the grid of an Edwards 1G3H ionisation gauge to 1200-1300°C in hydrogen at several torr pressure.

FIG. 10

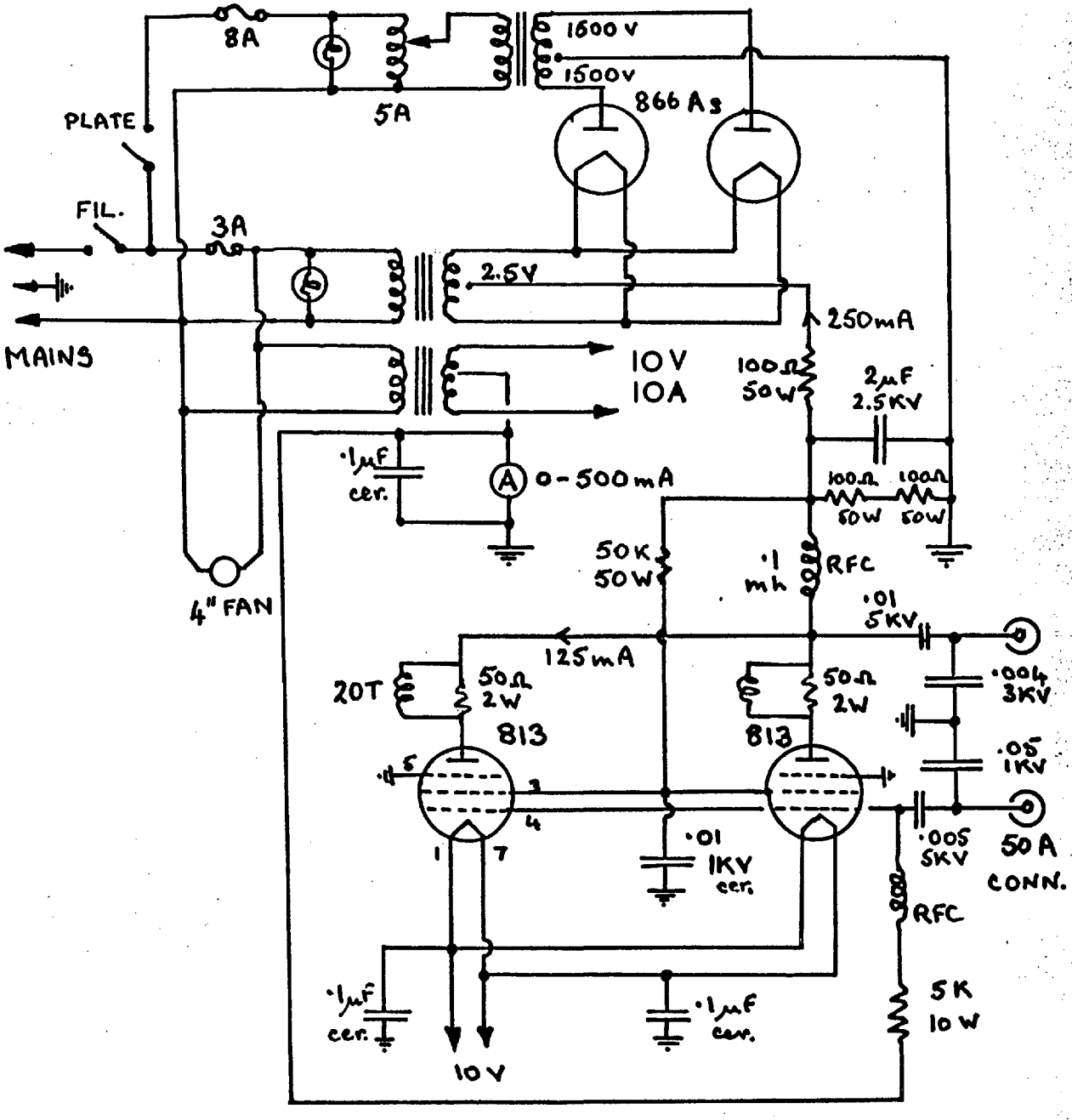

500 W OSCILLATOR

DESIGN: GENERAL ELECTRIC RES. LABS.

WORK COIL FOR 500W HEATER

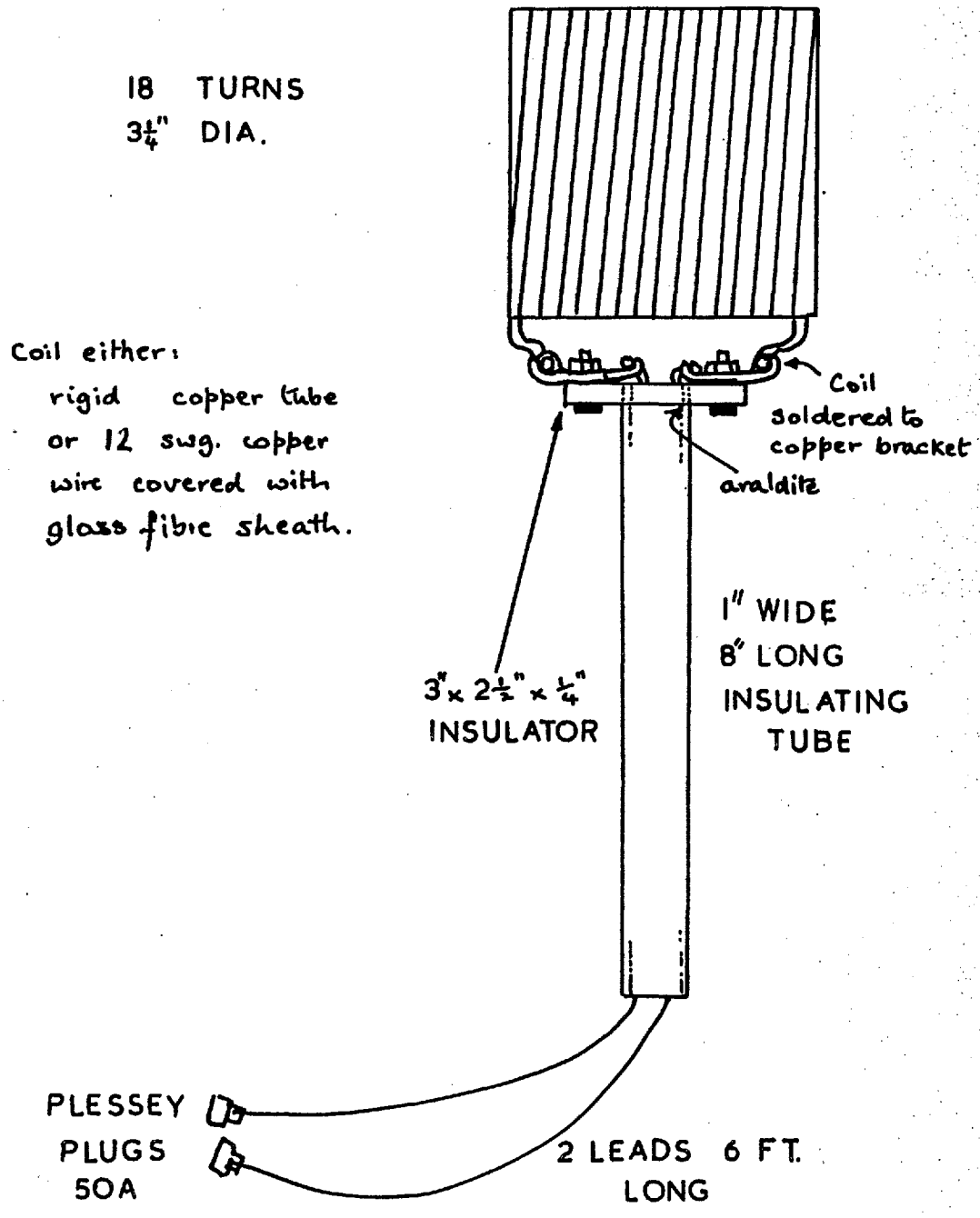

FIG. 11

2.10.3. 300W. 20Mc/s oscillator to excite gas discharges. A simple high frequency oscillator capable of supplying 2-300W to a nitrogen discharge was constructed. The circuit was provided by the AERE Harwell and was similar to that used there to atomise hydrogen molecules for subsequent ionisation and use in aproton linear accelerator.

The power supplies in the 500W eddy current heater were used to supply the single 813 oscillator. The output was 200-300 watts at 22.5 Mcs. The oscillating circuit was mounted in a perspex box which could be placed on the vacuum apparatus in such a way that a 5 cm. dia. glass tube projecting from the reaction cell passed through a hole in the side of the perspex box and into the work coil of the oscillator. A small electric fan was incorporated to improve air circulation round the discharge finger and the oscillator valve, which otherwise became very hot.

2.11. Preparation of nickel films

Nickel films were thrown from previously outgassed 0.5 mm. dia. wire onto the glass walls of about 50°C in vacua of the order of 1×10^{-9} torr to 2×10^{-10} torr. This required a filament current of 5.6 to 6.0 amps. depending on the rate of throwing. These throwing

FIG. 12

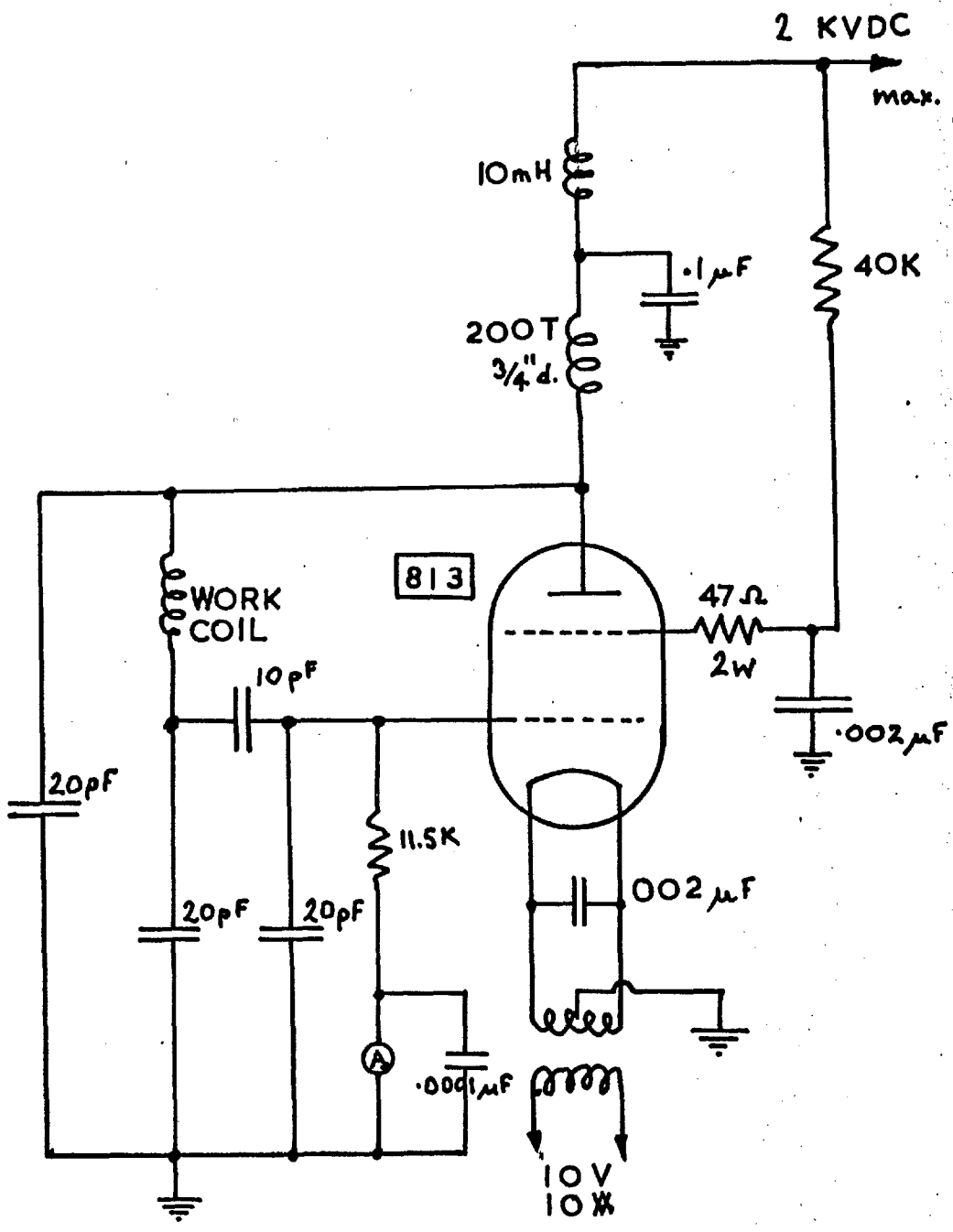

300W 20 Mc. OSCILLATOR.

pressures are in contrast to the findings of King (1966) who observed pressures as high as 1 x 10^{-8} torr during the first part of the throwing period. Evaporation was stopped when the film appeared opaque. It was found that several films could be thrown from the same filament.

After each run the cell was cleaned with either nitric or hydrofluoric acid, followed by distilled water.

2.12 Procedure for studying adsorption and desorption of nitrogen atoms on nickel films

After the film had been thrown, nitrogen was dosed in to a pressure of about 1 x 10^{-2} torr. With all dekkers down to prevent the discharge reaching the gauges or the cold traps, the power to the oscillator was turned on. Initial experiments were done with the work coil of the 500Kc/s oscillator round the main part of the cell, but it was found that the film acted as a screen and the discharge was not very effective. The 500 Kc/s oscillator did not create a very brilliant discharge and a 20 Mc/s oscillator was constructed which was much more effective.

Take-up of nitrogen was measured in between intermittent bursts of power of 30 secs or 1 minute's duration.

Total desorption was measured by heating the cell under the furnace with the system closed to the pumps. Desorption at different temperatures was achieved using an oil bath heated with a gas ring.

Pressure measurements during desorption and adsorption were made with the McLeod gauge, the Schulz-Phelps gauge, and also, initially, with a Pirani gauge.

2.13 Adsorption on and desorption from filaments

When the limitations of the film technique became apparent, i.e. too little known about the adsorption process and not enough range and control of temperature variation for the desorption, flash filament techniques were tried.

In this case, however, adsorption quantities were not meaningful because of parallel adsorption on glass surfaces and on any film that was thrown during outgassing. Usually a small amount of film was thrown deliberately in an attempt to produce a cleaner surface on the filament. A difficulty with nickel filaments is that they may not be heated much beyond 1200°C without throwing heavily, by which temperature it would not be expected that all impurities would be desorbed.

It is not claimed that the technique does in fact produce a clean surface, as there was no way of

determining this. Gomer (1953) and Farnsworth and Tuul (1958) have made direct observations of carbon and oxygen on nickel surfaces using field emission microscrope and low energy electron diffraction techniques respectively. A more detailed discussion of this subject is given in Results and Discussion, Section 3.

There was no pumping on the cell during desorption as is commonly practised in flash filament work, (Becker and Hartmann (1953), Hickmott and Ehrlich (1958), and Ehrlich (1963)), and the desorptions were therefore integral. As gauge pumping and conductance through dekker valves was minimised or corrected for, a value of the total amount desorbed at any time from the filament was obtained directly from the pressure reading. The total amount of adsorption is also thus given if it is assumed that very little gas remains on or in the filament after flashing to 1200°C, a reasonable assumption for the systems investigated.

Because of the high background pressure in the apparatus after atomisation, large surface area filaments were used. For most runs, unless otherwise indicated, 40 cm. filaments of 0.5 mm. dia. wire were used. These had a surface area of 6.25 cm^2. This

area does not include that of the length, approximately 1 cm. at each end, which was thinned down, as explained in Section 2.15:7 (Variations of temperature along an electrically heated wire). A nickel filament of 0.1 mm. dia. was used in order to reduce end effects (see Section 2.15.7.). This had a length of 2 metres, and therefore the same surface area as the 40 cm. 0.5 mm. dia. filaments, and was helically wound into about 130 turns of 5 mm. dia. During outgassing at about 850°C, it collapsed to the bottom of the cell. A second filament similarly wound was outgassed at a temperature below the collapsing point, and an adsorption-desorption run was performed using it. It was found that the desorption spectrum had little resolution due to the uneven temperature distribution which arose because of the self heating effect of the turns of the helix, which could not in practice be evenly spaced.

2.14. Dosing and basic run procedure

The N_2 reservoir was normally at about 3 cms. pressure. The whole system was dosed to about 2 x 10^{-2} torr, and dekkers D_2 and D_3 closed. Atomisation was then carried out followed by pumping down to background. As there was adsorption on the glass

during atomisation, and subsequent slow desorption the background after atomisation was much higher than if a similar dose had been let in and pumped out without atomisation. Immediately after atomisation with the system open to the pumps the steady background would be about 1 x 10^{-6} torr. This would slowly decrease. An improvement was made by heating the walls of the cell which had been in contact with N atoms to about 80°C, either with the hot air blower or by lowering the furnace. On subsequent cooling of the cell, the background would have improved to < 10^{-7} torr, with the system open to the pumps. Normally D_1 and D_2 would be closed when this pressure was reached and a desorption carried out.

2.15 Filament temperature control

2.15.1. D.C. heating, manual control.

The first method of filament temperature control employed a 10V. 10 A.D.C. power supply, controlled by a variable transformer. Although different temperatures could be attained, there was no proper control of the rate of rise of temperature, thus limiting the amount of information obtainable. Some interesting results were obtained, however, with this arrangement, while a filament temperature controller

was being built.

2.15.2. Filament temperature controller.

The controller built is similar to that designed by Gomer and Zimmerman (1965) (see figs.13,14,15) for the temperature control of the filament supporting the tip in a field emission microscrope. Potential leads tap off a section of the filament and compare the potential across it with that across a variable standard resistor in a Kelvin bridge. The out of balance current is amplified and after passage through a phase sensitive detector, is passed on to a power amplifier which can supply 6 or 7 amps through the filament. The device is capable of altering the temperature of the field emission tip by many hundreds of degree in less than 1 second, but due to the different characteristics of the nickel filament, (e.g. low specific resitivity), the heating time in this case is much longer, depending on the size of the temperature jump. The temperature jumps were kept to a minimum for this reason, compatible with their producing changes in rate of gas evolution suitable for measurement. The controller behaved rather erratically at first, sometimes not controlling at all and sometimes oscillating with a period of 1 to 2 secs. This was

FIG. 13

KELVIN BRIDGE

R = Ω

+ = 1%

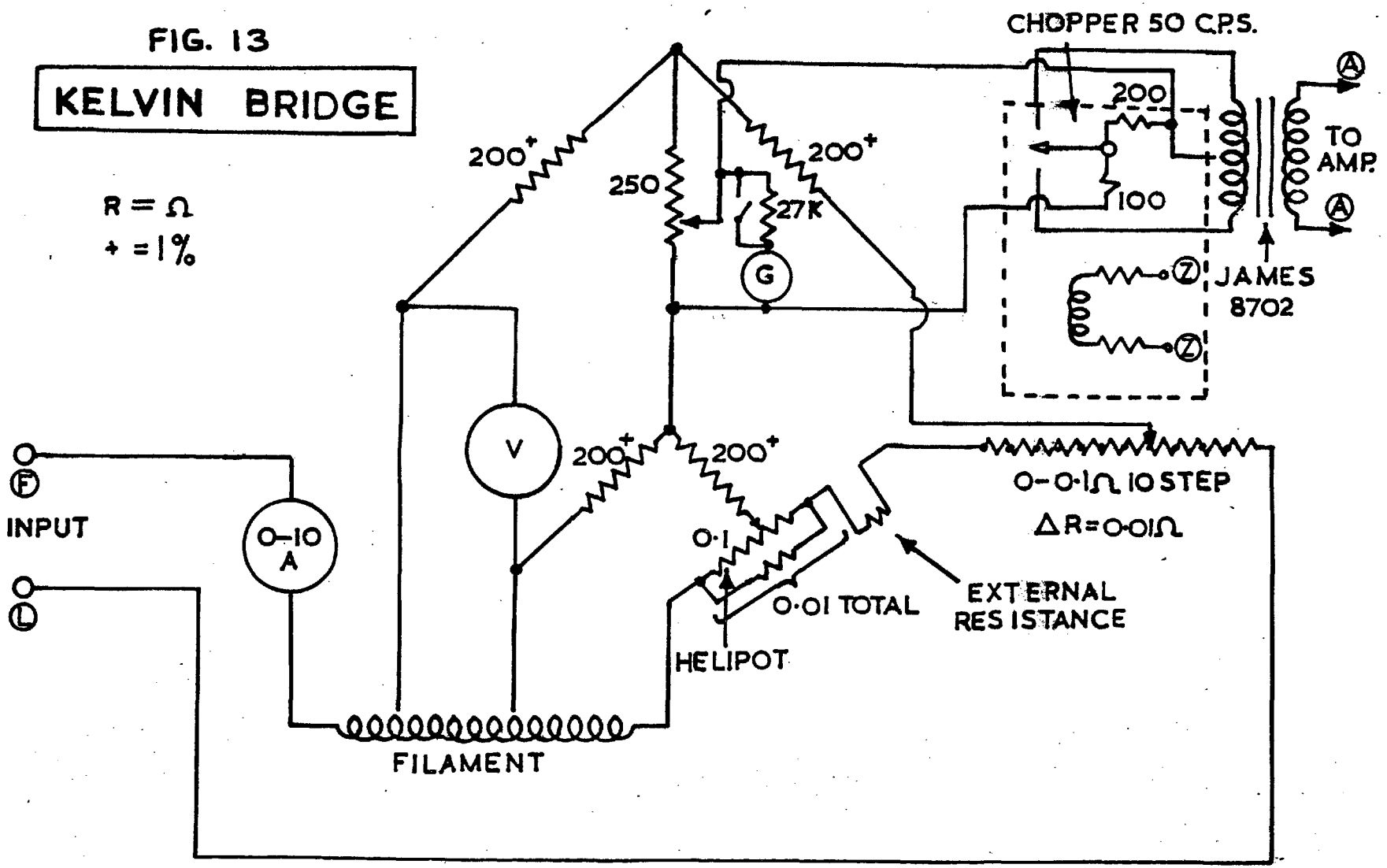

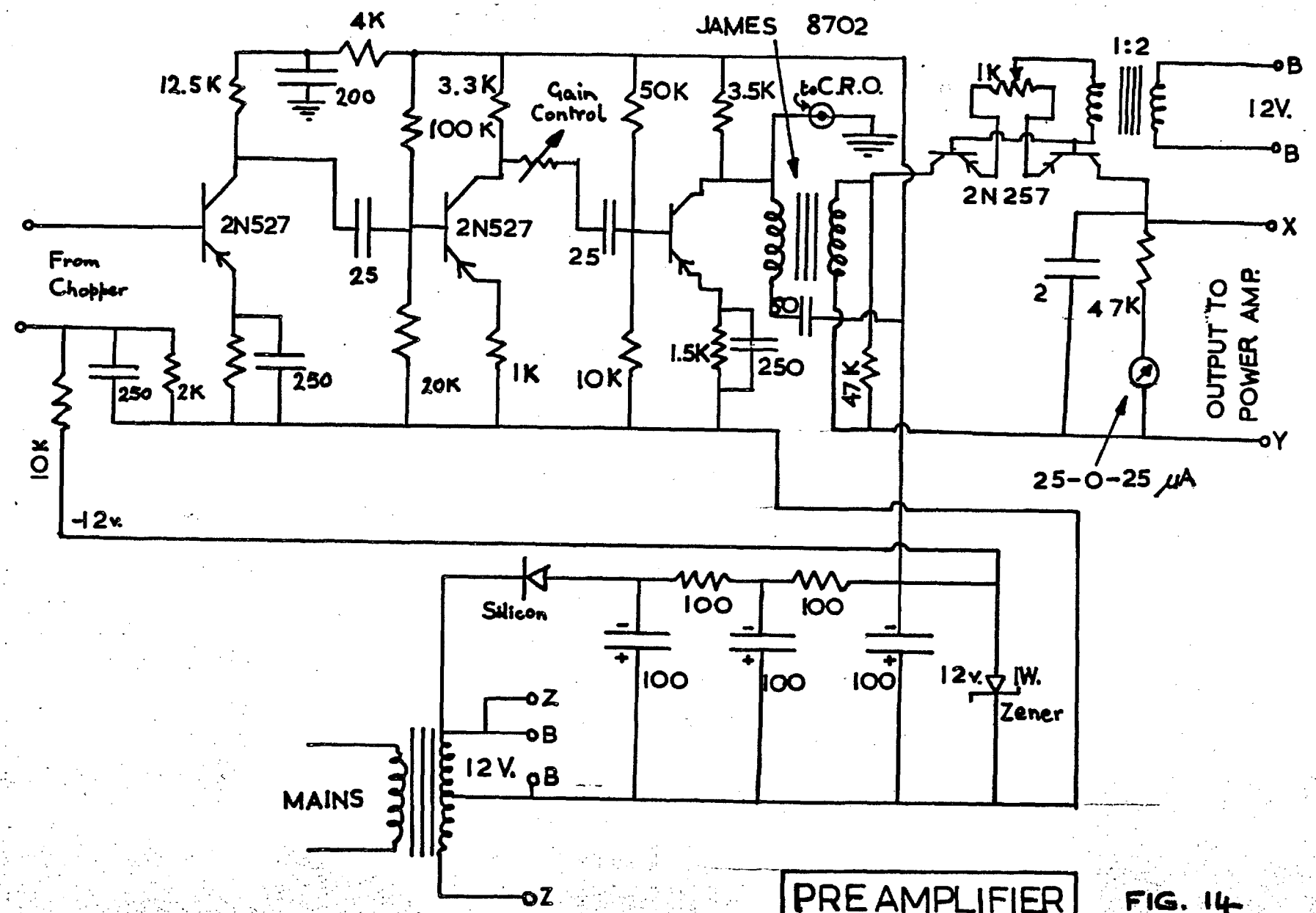

PREAMPLIFIER

FIG. 14

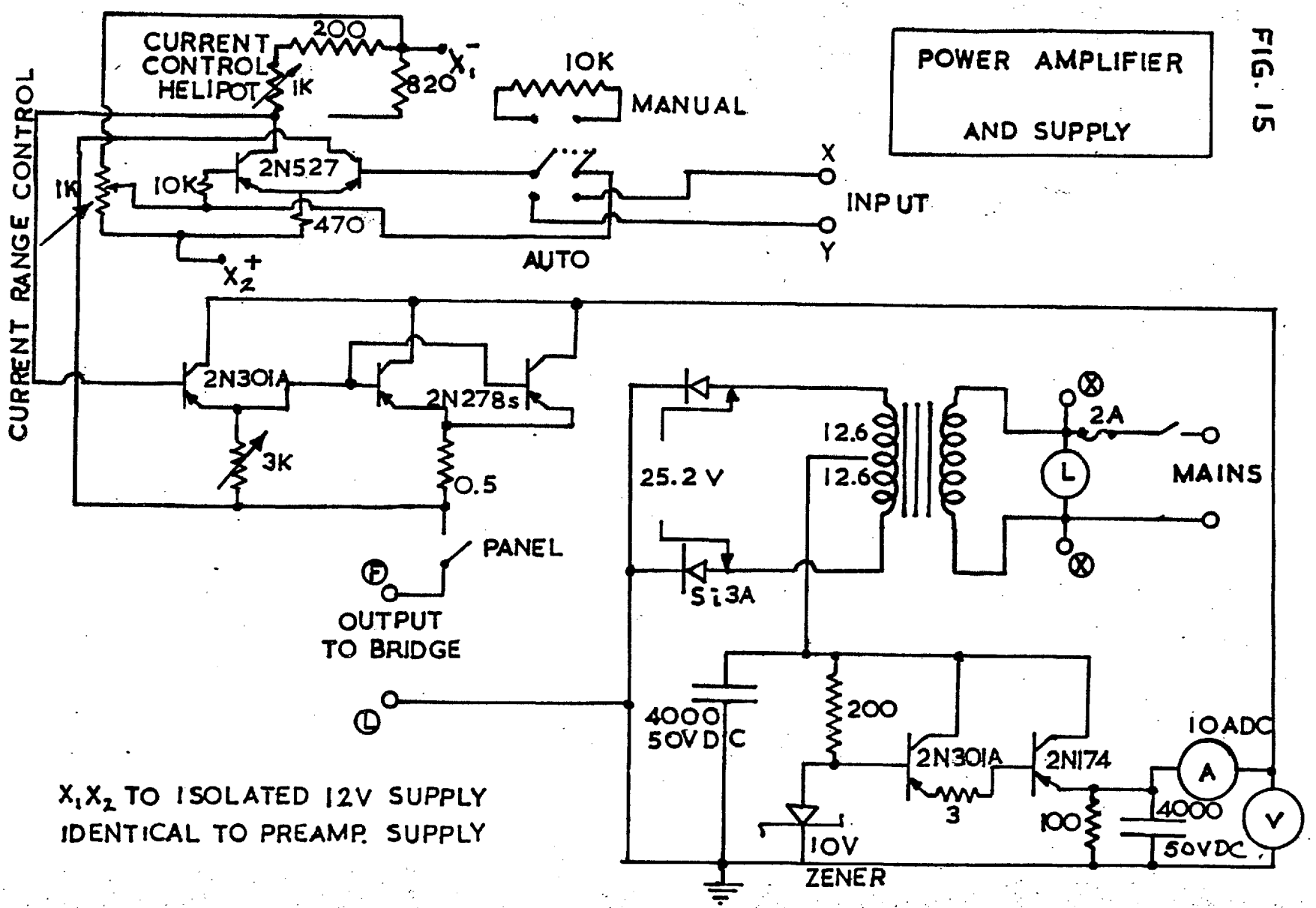
POWER AMPLIFIER
AND SUPPLY
CURRENT CONTROL HELIPOT
200
1K
820
X_1 -
10K
MANUAL
CURRENT RANGE CONTROL
1K
10K
2N527
470
X_2 +
AUTO
X
Y
INPUT
2N301A
2N278s
3K
0.5
PANEL
OUTPUT TO BRIDGE
25.2 V
12.6
12.6
2A
MAINS
Si3A
4000 50VDC
200
2N301A
2N174
3
100
4000 50VDC
10ADC
A
V
10V ZENER
$X_1 X_2$ TO ISOLATED 12V SUPPLY IDENTICAL TO PREAMP. SUPPLY

FIG. 15

cured by altering the capacitor in the phase sensitive detector, which also had the effect of reducing the maximum heating current to 4.5-5 amps.

The temperature of the nickel filament was determined by resistance measurements obtained from direct simultaneous recording of voltage across the potential taps and current through the filament. The voltage from the potential leads was suitably divided as shown in figure (16) and passed to a 10 mV potentiometric recorder. Potential taps were also taken from across a standard 0.01 ohm resistor in the heavy current part of the Kelvin bridge, and after dividing, was passed to another 10 mV recorder synchronised with the first. Both recorders required careful calibration, and the potential dividers were mounted in a separate box which was not touched during a series of runs. The calibrations were checked after such a series of runs. On some occasions when the circuit failed to control properly it was found that by reversing the polarity of the filament, control could be restored.

2.15.3. Operation of the controller.

Two controls, the sensitivity control which is a variable resistance through which the out of balance current flows, and the amplifier gain control, affect the magnitude of the output to the power amplifier.

FIG. 16

MONITORING OF FILAMENT RESISTANCE

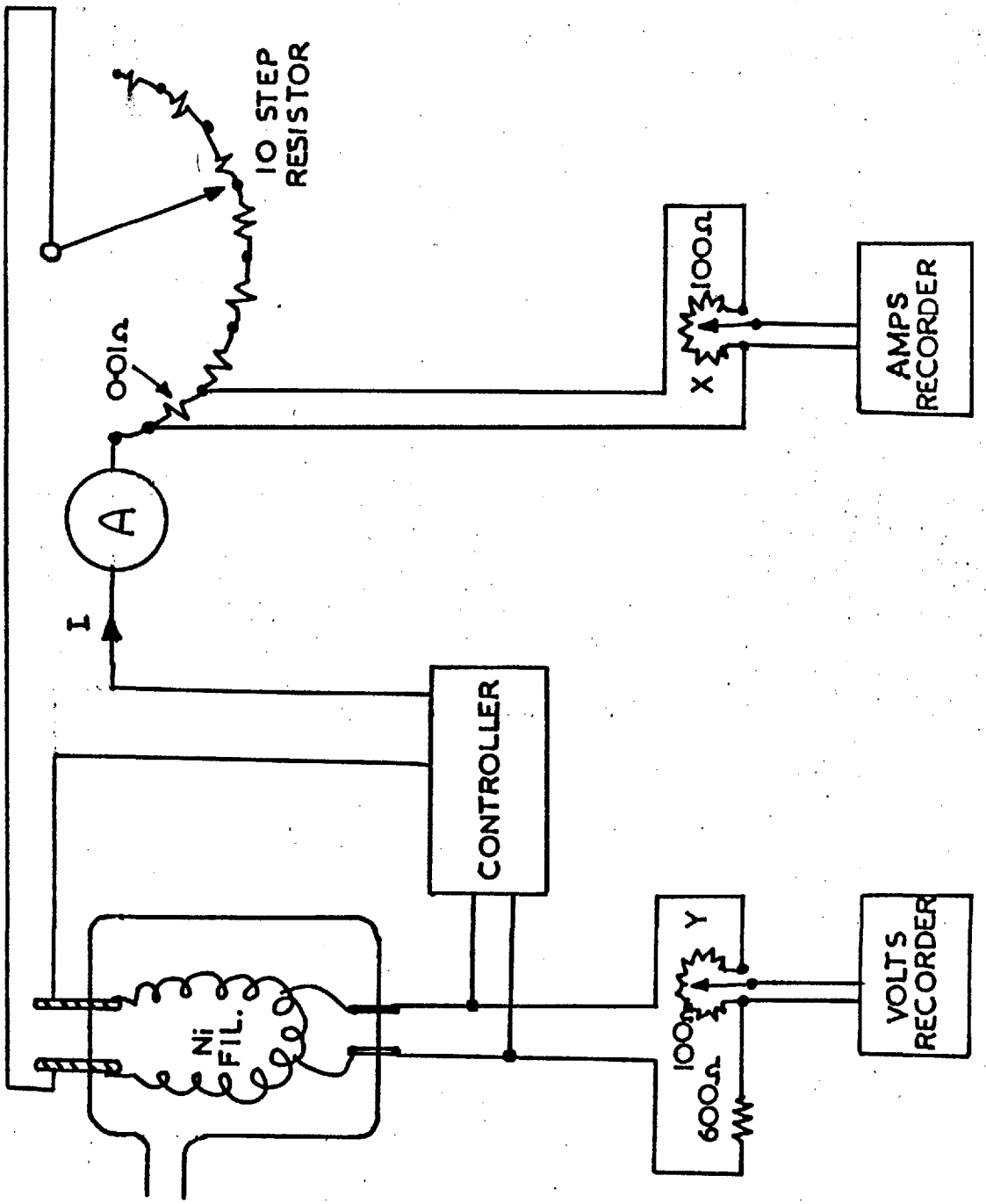

Both controls were operated near their limits for maximum sensitivity. Values of the two current range controls were found by experiment to permit stable operation over the temperature range desired. These controls were then not touched. When the controller was connected to the filament and switched on, operation of 0.1 ohm 10 step resistor enabled temperatures between room temperature and about 500°C to be selected, the increments of temperature being about 70°C per 0.01 ohm change in the 10 step resistor. The shunted helipot in series with the latter resistor enabled each 0.01 ohm step to be subdivided further.

2.15.4 Calibration of current and voltage recorders

(a) Current recorders. The potential divider X (a 100 ohm potentiometer) in figure (16) was set so that the steady current required to maintain the nickel filament at about 500°C produced nearly full scale deflection on the current recorder. The filament was allowed to cool, an accurate D.C. ammeter was connected in series with the filament, and a dummy run was carried out. For each step on the 10 step resistor, the steady current through the filament written on the recorder chart.

CALIBRATION OF VOLTAGE RECORDER

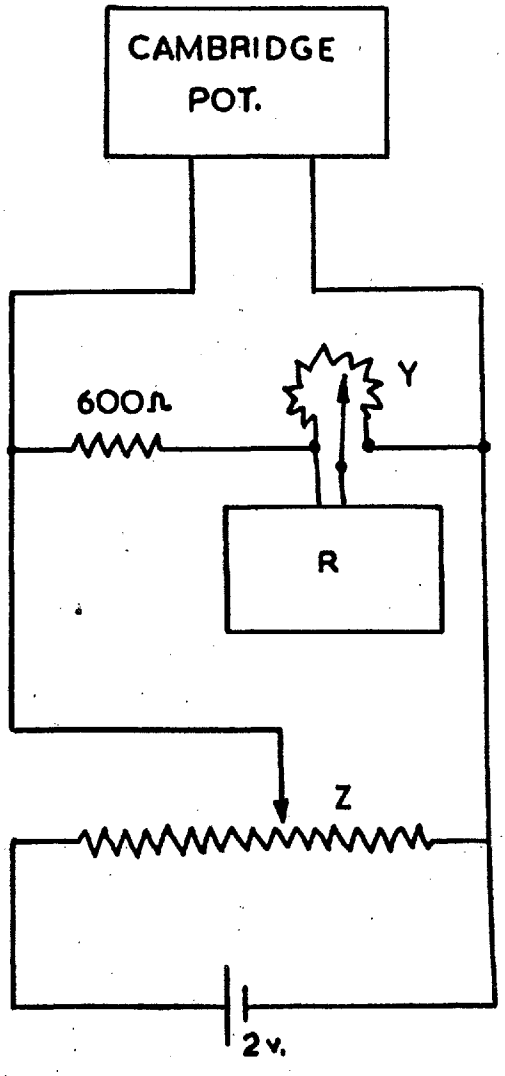

FIG. 17

(b) Voltage recorder calibration. This could not be done by measuring the voltage across the potential taps directly with a sensitive potentiometer as the fluctuations made the balance point too difficult to find. After a suitable value of Y had been selected in a similar manner to the procedure for X, the filament was taken out of the circuit, and the arrangement shown in figure (17) was constructed. The potentiometer Z is set to select a fraction of 2v placed across it. This was applied across AB and measured on a sensitive Cambridge potentiometer bridge. The affect produced on the recorder was thus calibrated across the range of the recorder by altering the potentiometer Z.

2.15.5. Measurement of temperature

The resistance of the section of filament between the potential taps is thus known at each temperature. The resistance is then found at one known temperature, in this case at 298°K, and by extrapolation from resistance data, calculated for 273°K. Gmelin (1959) gives tables of values of $\frac{R_T}{R_{273}}$ against T°K for nickel and a calibration curve was constructed from these to enable the temperature of the filament to be determined (figure 18). The discontinuity in this

FIG. 18

TEMPERATURE DEPENDENCE OF RESISTANCE OF PURE NICKEL, (GMELIN 1959).

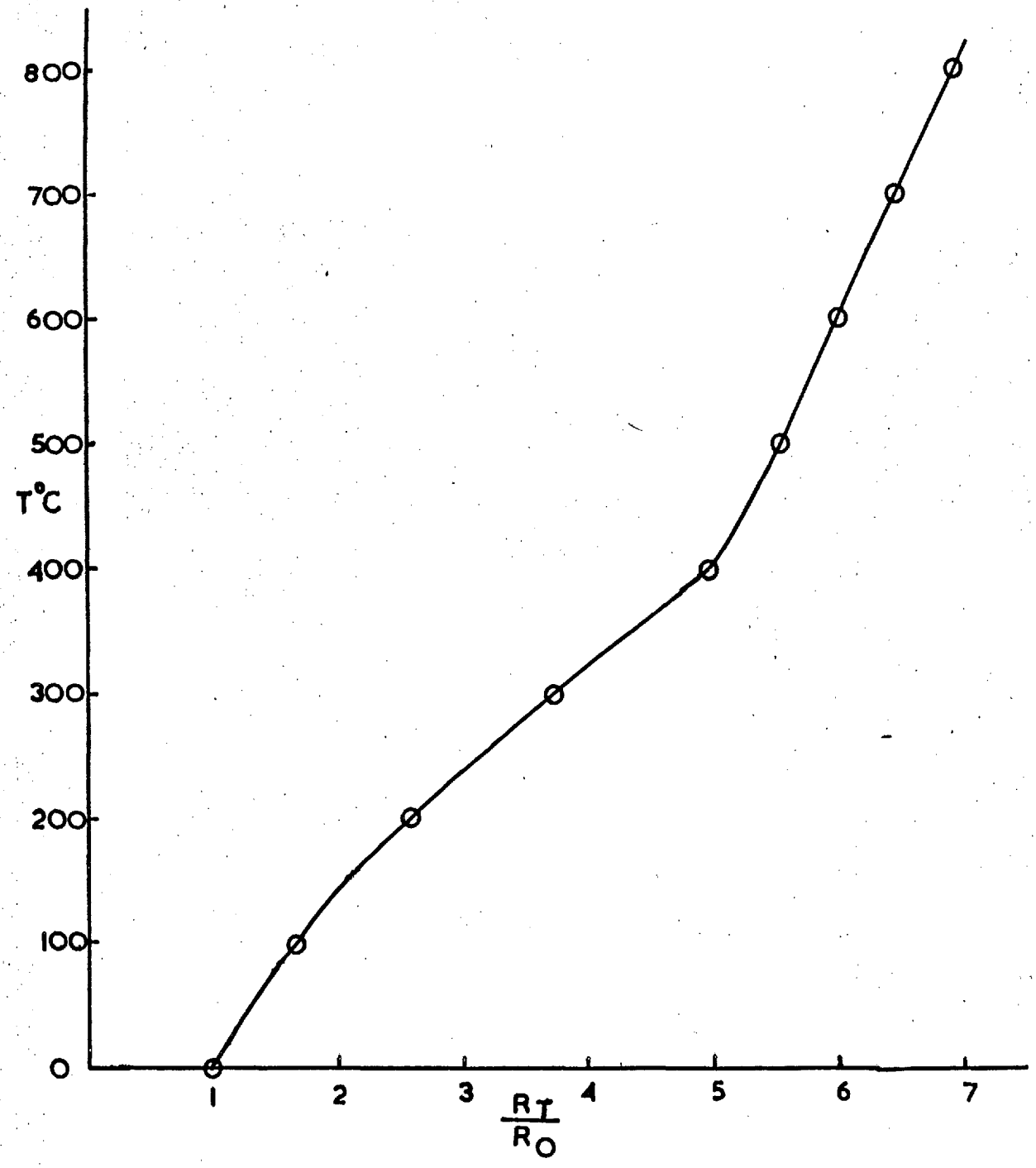

curve at 400°C makes the accuracy of the measurement of R_{298} very important.

2.15.6 Determination of R_{298}

A very small direct current was passed through the filament and measured on an accurate milliameter. The voltage across the potential taps was measured with the Cambridge potentiometer (capable of reading down to 1×10^{-5} volt). The current and voltage readings were taken over a period of minutes and the corresponding resistances calculated. Though the heating effect was very small, from a current of about 80 mA, a correction could be made for the temperature rise.

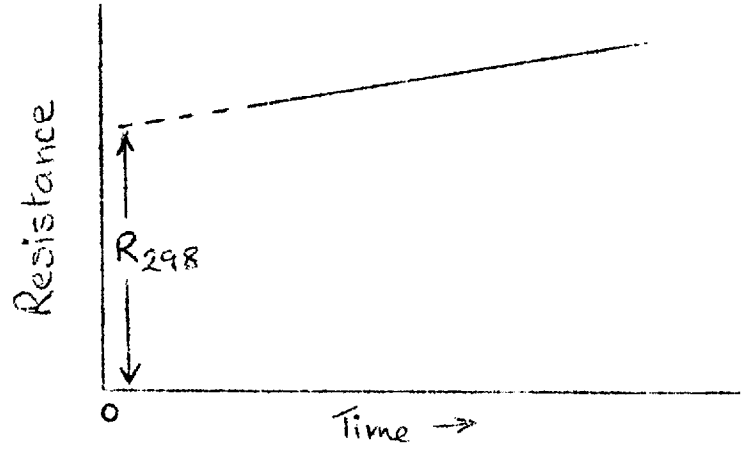

2.15.7. Variations of temperature along an electrically heated wire.

Ehrlich (1963) has shown that the temperature along

an electrically heated wire welded to low temperature supports is not constant. In the present work no attempt was made to investigate the temperature profile, but an interpolation was made from Ehrlich 's results. He noted that for a tungsten wire of 15.6 cms. length and 0.25 mms. dia., the temperature difference between a point 4 cms. from one end and the centre of the wire was $\sim$ 50°C for a temperature difference of 200°C above the surroundings, and $\sim$100°C for a temperature difference of 450°C above the surroundings (the maximum encountered in the present work). It is important to note that these temperature variations are for the steady state. The nickel filament used was 0.5 mm. in dia. and the length was 40 cms. A measure to reduce heat loss down the filament supports was made by thinning down the ends of the wire and attaching it to the supports with a single small spot weld.

The effect of variations of temperature along the filament is to reduce resolution of the desorption peaks; the strongly held gas starting to come off the hotter central part of the filament before the more weakly held gas has desorbed completely from the cooler parts. Nevertheless, good resolution was obtained of the two peaks observed in this work.

The temperature variation was shown by Ehrlich in the same paper to be greatly reduced during flash heating. The parts of the filament near the supports, when rapidly heated, take up much more nearly the temperature of the centre of the wire, and only cool slowly when the flash current is reduced to the steady state current. Thus in the present experiments where the temperature of the filament was rapidly changed during the field emission tip controller, the variation in temperature along the filament will not be as large as indicated for the steady state.

2.16 Measurement of Pressure

2.16.1. The McLeod Gauge

An ordinary McLeod gauge (McLeod(1874)) was used as a means of measuring steady pressures in the range 1×10^{-4} to 1×10^{-1} torr, and as a check on the calibrations of other types of gauges. The performance is compared with that of a Bayard-Alpert gauge in figure19and with that of a high-pressure ionisation gauge in figure 20.

The volume of the bulb was measured by filling it with water from a burette. A 25 cm. length of 0.1 mm. bore tubing was used as the closed capillary. The uniformity of cross-section of this tube was

checked by measuring with a cathetometer the length of a mercury thread introduced into the tube. This also gave an average value for the radius.

McLeod parameters. Length of mercury thread: (mean of 15 readings) = 3.293 cms. (standard deviation = 0.005 cms.)

Weight of mercury thread = 0.3530g.
radius of tube = 0.0502 cms.
volume of bulb = 198.8 ml.
volume of capillary = 0.196 ml.
total enclosed volume = 199.0 ml.

Assuming Boyle's Law is obeyed, if the mercury in the comparison capillary is level with the closed end of the McLeod capillary, and the meniscus is 1 cm. from the end in the latter tube, the required pressure is:

$$P_{1cm.} = \frac{1 \times \pi(0.0502)^2}{199}$$

$$= 3.977 \times 10^{-4} \text{torr}$$

The factor used throughout was 4.0×10^{-4} torr. Similarly for a depression of h cms. in the closed capillary the pressure is given by

$$P_h = h^2 \times 4 \times 10^{-4} \text{ torr}$$

Calculations by Jansen and Venema (1959) show that errors arising from non-ideal gas behaviour are

much less than other errors arising in the McLeod, gauge, even for vapours, so long as the maximum vapour pressure is not exceeded in the closed limb.

According to Porter (1933), the angle of contact of clean mercury on clean glass is altered appreciably in tubes of bore less than 4 mm., and may vary between 30° and 60° depending on whether the mercury rises or falls to its equilibrium position. For a capillary of 1 mm. bore, the measured values of h are for this reason only accurate to $\pm$ 0.5 mm. This gives a possible error of $\pm$ 10% at 5×10^{-4} torr and more than 100% at 5×10^{-6} torr. In the calibrations in figures 19 & 20 the scatter in the 10^{-5} torr region is attributed to this effect.

That roughening of the inner surfaces of the capillary tubes greatly reduces the uncertainty in the capillary depression has been shown by both Rosenberg (1938 and 1939) and Klemperer (1944). The work of Rosenberg (1939) enables a calculation to be made of the improvement of accuracy possible if the capillary is roughened and the McLeod operated most carefully. For an instrument of dimensions used in this laboratory the accuracy at 6.5×10^{-4} torr could be not better than $\pm$ 2%, and at 6.5×10^{-5} torr not better than $\pm$ 6%.

2.16.2 Ionisation gauges

Those used were of two types, the normal Bayard-Alpert or inverted gauge, (Bayard and Alpert, 1950), obtained from Edwards High Vacuum Ltd., and designated 1G3H, and the Schulz-Phelps, or high pressure gauge, which was made in this laboratory, (Schulz and Phelps, 1957).

The operational range of the Bayard-Alpert gauge is from almost 1×10^{-2} torr to 1×10^{-10} torr, and of the Schulz-Phelps, 5×10^{-1} torr to 5×10^{-6} torr.

2.16.2(a) Comparison of ionisation gauges with the McLeod Gauge.

The comparison of the McLeod gauge with the Edwards 1G3H gauge is shown in figure (19), and with the Schulz-Phelps in figure(20). The comparison of the McLeod with the 1G3H is only possible over 2 orders of magnitude of pressure as the McLeod errors are too large below 1×10^{-4} torr, but within the two ranges linearity is found, giving a sensitivity of 11 per torr with the 1G3H operating at the rather low voltages of; collector, earthed; filament 75V; grid (electron collector) 150V.

Good linearity over three orders of magnitude of pressure was obtained with the McLeod-Schulz-Phelps

FIG. 19

IONISATION GAUGE CALIBRATION

AGAINST McLEOD GAUGE.

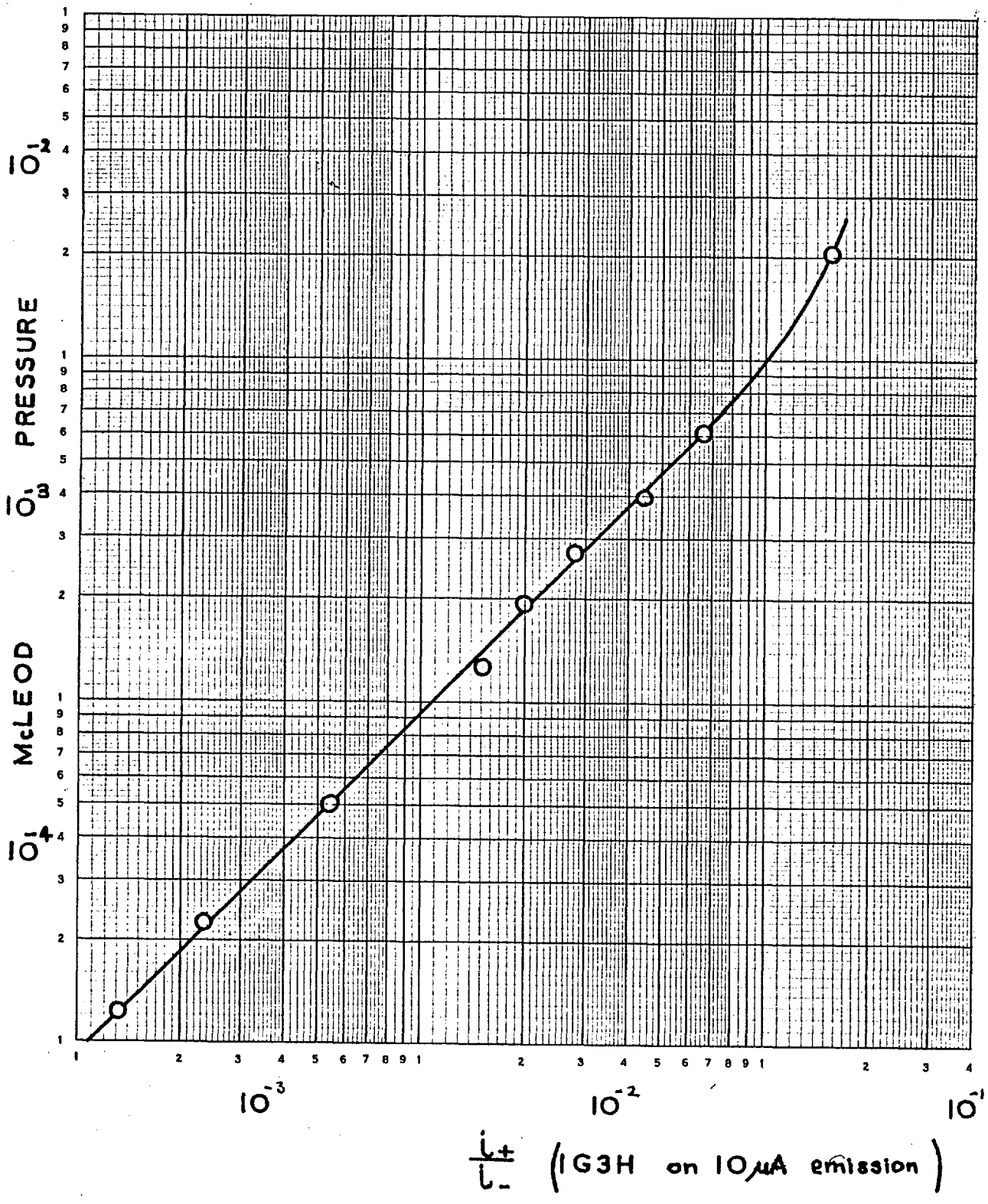

FIG. 20

CALIBRATION OF SHULZ-PHELPS GAUGE WITH McLEOD GAUGE

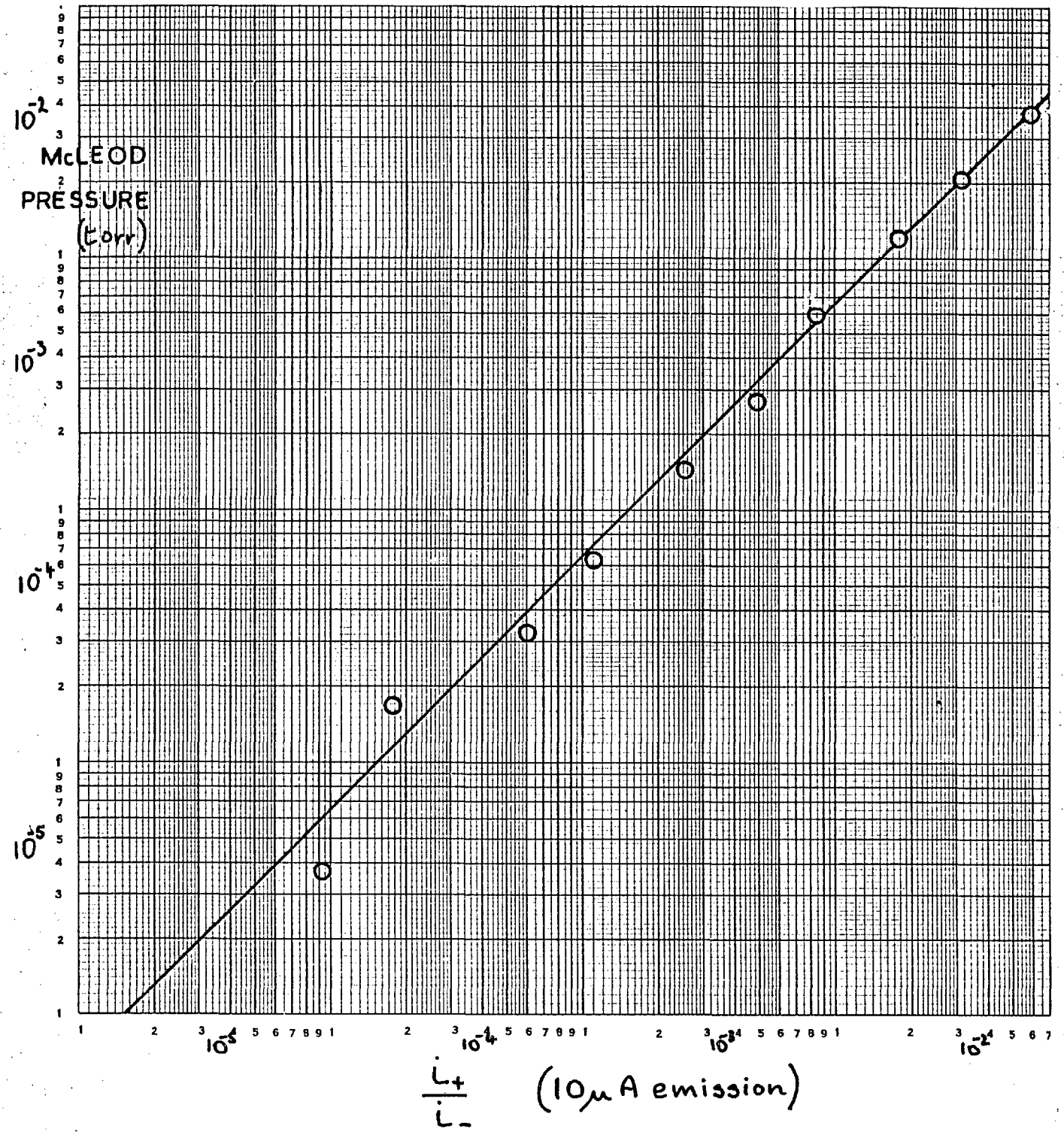

FIG. 21

COMPARISON OF SCHULZ-PHELPS WITH IG3H

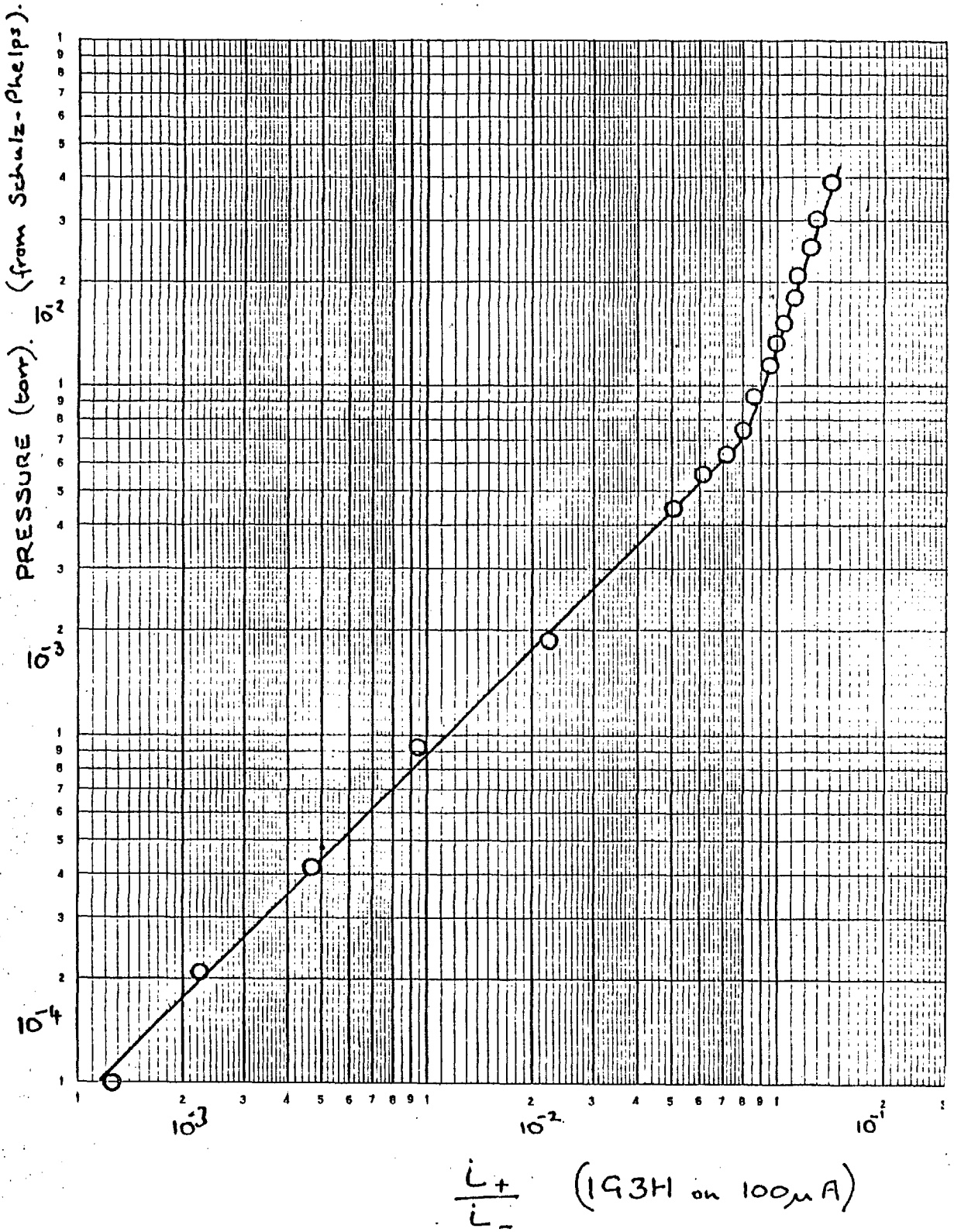

calibration, giving a sensitivity of 1.53 $torr^{-1}$ for this gauge.

The sensitivities of both gauges were checked by a flow method.

2.16.2(b) Molecular pumping effect due to mercury vapour from the McLeod gauge

A possible error introduced by the use of a McLeod gauge and cold trap was first noted by Gaede (1915). The continuous stream of mercury vapour from the McLeod gauge to the cold trap causes a pressure gradient of gas in the tube. Leck (1964) shows that the pressure gradient of permanent gas $\frac{\Delta P}{P}$ in the simple case where the gauge and trap are connected by a long tube of radius R cm.can be calculated in terms of the diffusion coefficient of mercury.

$$\frac{\Delta P}{P} = 0.905\ R.p_m.\ \sqrt{\frac{T}{D}}$$

where pm is the saturated vapour pressure of mercury at T^oK and D is the diffusion coefficient of mercury at atmospheric pressure.

For	$T = 15^oC$	$\Delta P/P = 0.13\ R$
	$T = 20^oC$	$\Delta P/P = 0.196\ R$
	$T = 25^oC$	$\Delta P/P = 0.30\ R$

Thus the error introduced increases with the temperature and the radius of the connecting tube, but for a tube

of varying diameter, most of the pressure drop occurs across the narrowest portion. Leck (1964) suggests the insertion of a short piece of capillary, 1 cm. long, 1 mm. dia. between trap and gauge to reduce the error to 2% at 20°C. Such a piece of capillary was incorporated into a dekker valve, (D_4 in figure 6), so that the normal high conductance of the system to the pumps would not be reduced. It was found during calibration of the ion gauges with the McLeod that no significant difference could be detected with the capillary in position from when the capillary dekker was raised.

This is probably because the tube connecting McLeod and trap is of 1 cm. dia., and contains several 90° and 180° bends. Ishii and Nakayama (1961) however observed changes in apparent sensitivity of 25% for their ionisation gauges when the laboratory temperature varied from 10°C to 30°C, which they attribute to this effect. The pumping is only significant at pressures lower than the mercury vapour pressure (10^{-3} torr).

2.16.2.(c) Flow method for measuring gauge sensitivity

In figure 22 c' and c are capillary conductances, and M is a manometer. The volume V is known by expansion from standard volume S, therefore from the

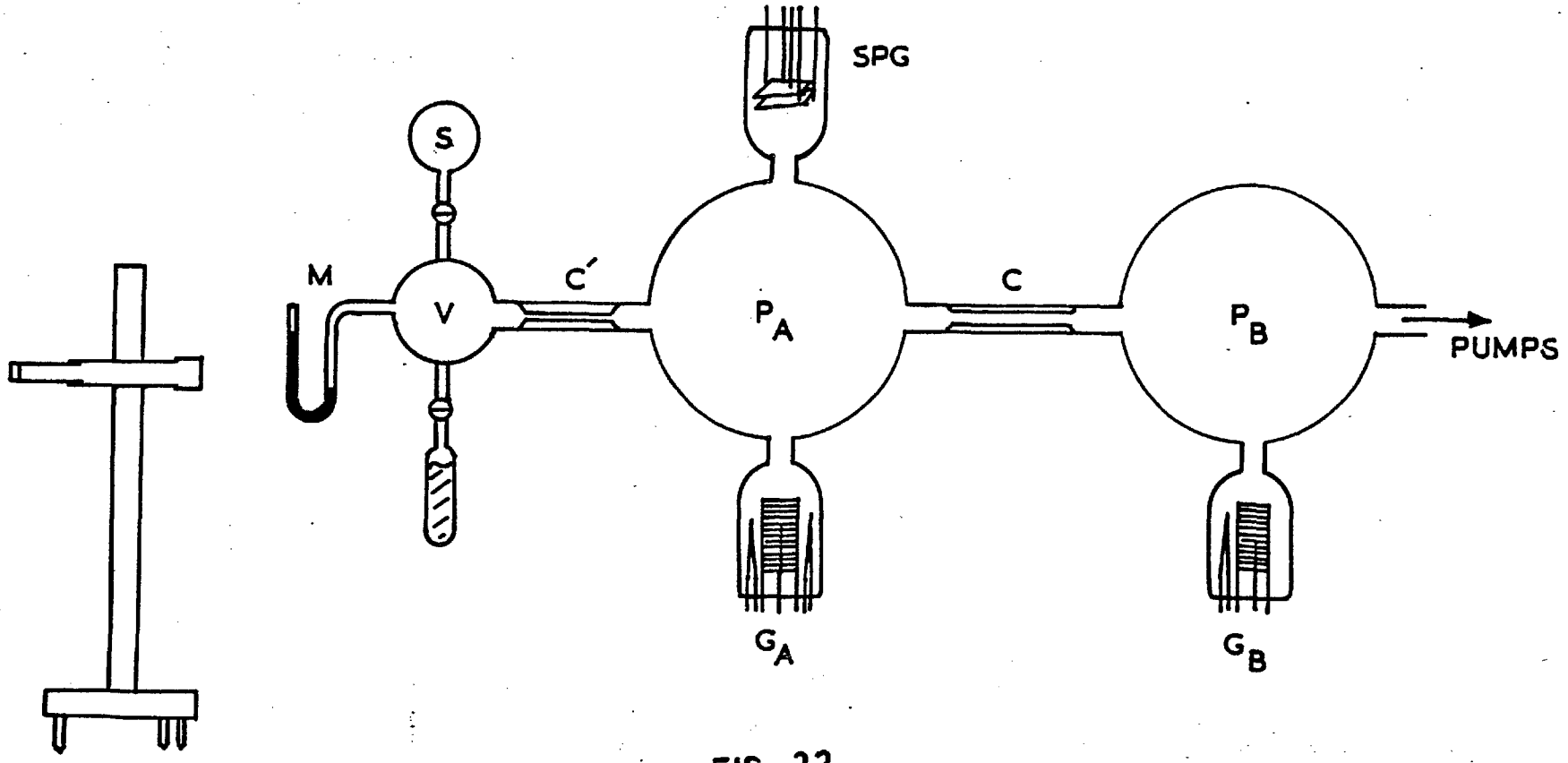

FIG. 22

FLOW METHOD FOR GAUGE SENSITIVITY

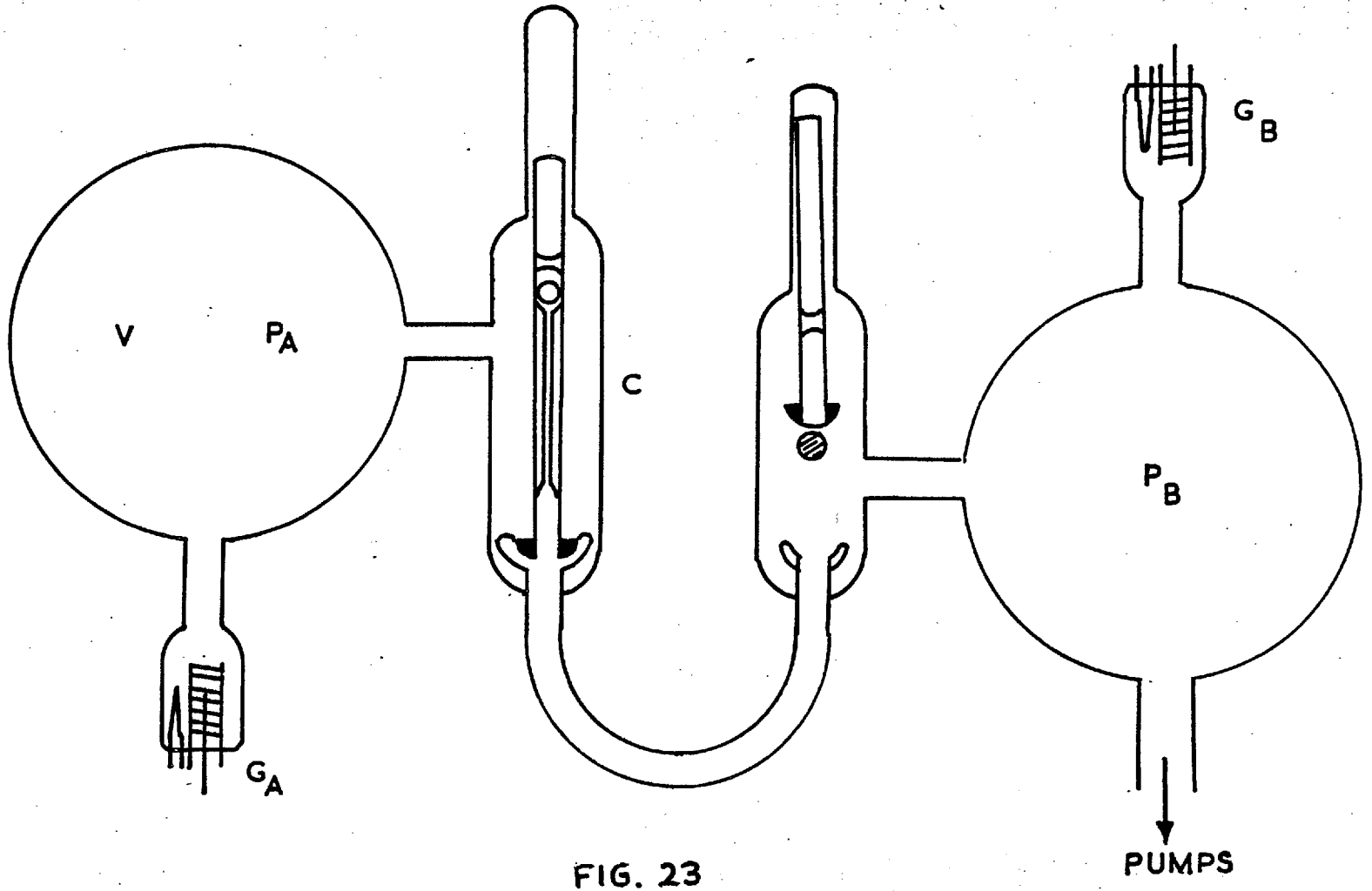

FIG. 23

DETERMINATION OF CONDUCTANCE OF CAPILLARY C

rate of fall in pressure as indicated by the manometer, the rate of outflow of molecules $\frac{dn}{dt}$ through c' and c to the pumps, is known.

In practice, the conductance required is of the capillary and the tubulation leading to bulb B. This conductance is F molecules $torr^{-1}$ $sec.^{-1}$.

$$\text{Then } \frac{dn}{dt} = F\,(P_A - P_B)$$

$$= FP_A \quad [\text{as } P_A \gg P_B]$$

$$= F.\frac{1}{g}.\frac{i+}{i-}$$

where g is the sensitivity of the gauge and $\frac{i+}{i-}$ the normalised ion current.

As gauge pumping is also removing molecules in addition to the pumps at the rate of G per torr per sec., we should write:

$$\frac{dn}{dt} = (F + G).\frac{i+}{gi-} \qquad \text{.....(1)}$$

The quantity (F + G) is found by the following experiment (see figure 23).

The volume V is filled with nitrogen to a pressure of 1×10^{-3} torr, and both dekkers C and D are lowered. The ionisation gauge G_A, which may be of any type as the method is independent of the sensitivity of G_A, is switched on and allowed to stabilise. Then dekker D is opened. The process is similar to the discharge

of a charged capacitor through a resistor.

$$-\frac{dn}{dt} = \frac{VdP_A}{dt} = (G + F)(P_A - P_B)$$

$$= (G + F)P_A \qquad [P_A >> P_B]$$

$$V\int \frac{dP_A}{P_A} = (G + F)\int dt$$

$$V \ell n\, P_A = (G + F)t + k$$

$$\ell V \ n \frac{i+}{gi-} = (G + F)t + k \qquad .....(2)$$

A graph of ℓn i+ against t has a slope of $\frac{(G + F)}{V}$. See figure 24.

Slope of curve in figure 24 $= 1.942 \times 10^{-3}$

$$\therefore \frac{\ell n\ i+}{t} = 2.303 \times 1.942 \times 10^{-3}$$

Volume of cell plus gauge and tube volumes (calculated) = 1.84 litres

$$\therefore G + F = 8.23 \times 10^{-3} \text{ litres sec}^{-1}.$$

$$= 2.71 \times 10^{-17} \text{ molecules torr}^{-1} \text{ sec}^{-1}.$$

The results of the gauge sensitivity calibration are given below for two rates of flow

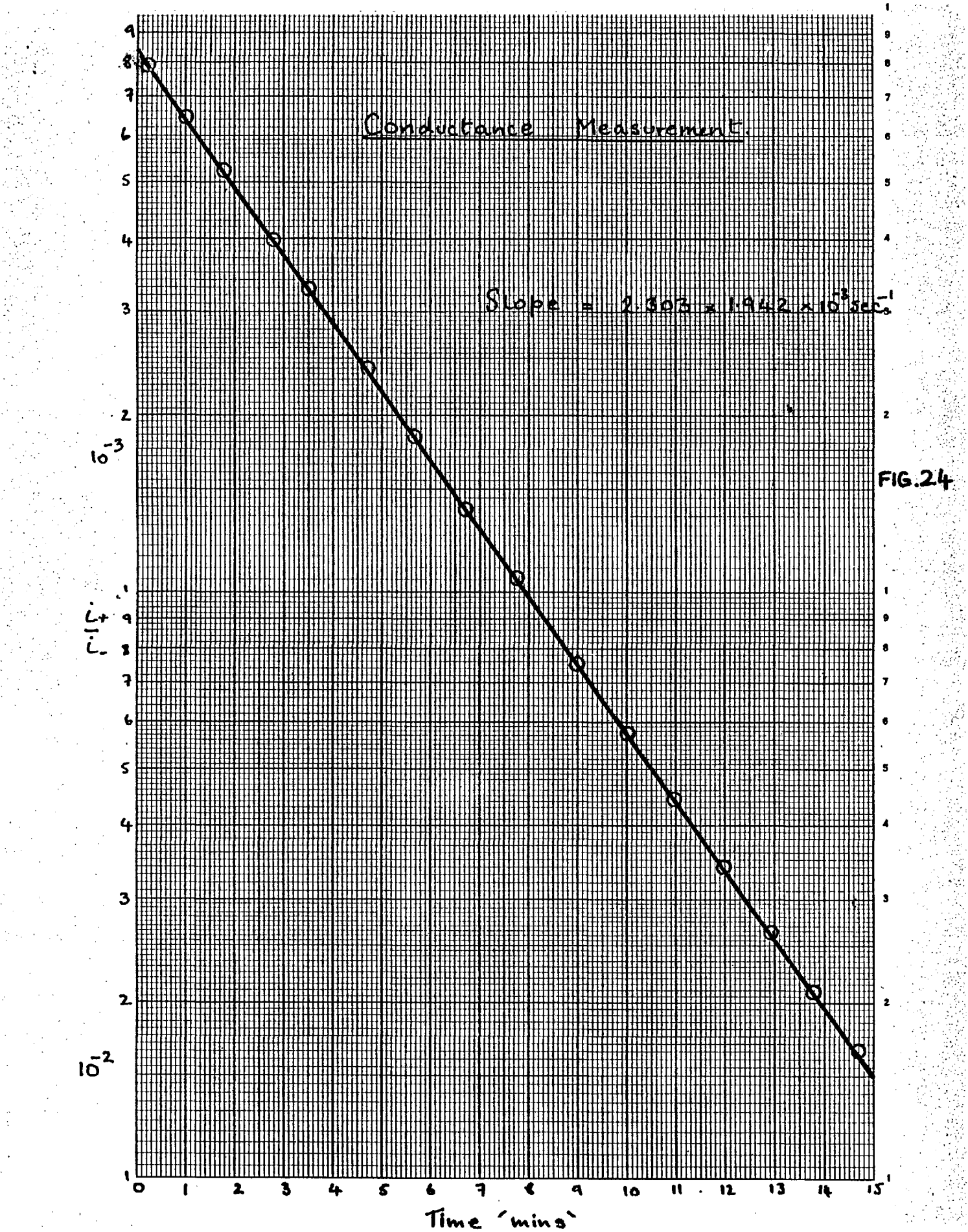
Conductance Measurement.
Slope = 2.303 × 1.942 × 10⁻³ sec⁻¹
10⁻³
10⁻²
C+ / C-
Time 'mins'
0 1 2 3 4 5 6 7 8 9 10 11 12 13 14 15

FIG. 24

$\frac{dn}{dt}$ (mols sec^{-1})	T^oK	(G + F) mols $torr^{-1} sec^{-1}$	g_{s-p} low voltage ($torr^{-1}$)	g_{1G3H} normal voltage ($torr^{-1}$)	g_{1G3H} low voltage ($torr^{-1}$)
8.17×10^{15}	293	2.71×10^{17}	1.32	16.7	12.8
2.80×10^{15}	293	2.71×10^{17}	1.46	18.4	

The values for the 1G3H at normal operating voltages are in good agreement with those of Hayward, King and Tompkins (1966) of 17-23 $torr^{-1}$ for identical Edwards 1G3H gauges and are in marked disagreement with the manufacturers' values of sensitivity for nitrogen of 12.5 $torr^{-1}$.

The values are in reasonable agreement with those obtained from comparison with the McLeod Gauge.

2.16.2(d) Summary of gauge sensitivities

Gauge	Method	Voltage	Sensitivity
1G3H	McLeod	low	11 $torr^{-1}$
1G3H	Flow	low	12.7 $torr^{-1}$ (mean)
1G3H	Flow	high	17.5 $torr^{-1}$ (mean)
S-P	McLeod	low	1.39 $torr^{-1}$
S-P	Flow	low	1.53 $torr^{-1}$

2.16.2(e) Theoretical calculation of capillary conductance.

As the combined pumping effects of the capillary, tubulation, and gauge appear in both equations (1) and (2) there is no need to separate the terms. It is

interesting however to compare the value of the conductance of the capillary derived from the experiment with that calculated from Knudsen molecular flow theory, (Dushman and Lafferty,1961). Using the formula of Dushman (1922) for the approximate total conductance of a cylindrical tube*;

$$C = \frac{3.64}{1+\frac{3}{8}\frac{\ell}{a}} \cdot A \cdot \frac{T}{M}^{\frac{1}{2}} \text{ litres sec}^{-1}.$$

where a = radius in cm.

ℓ = length in cm.

$A = \pi a^2$

for N_2 at 20°C

and $= 4.9$ cm, and $a = 0.075$ cm.

$C = 2.75 \times 10^{17}$ mols $\text{torr}^{-1}\text{sec}^{-1}$.

The removal of molecules from the gas volume may be represented by three conductances;

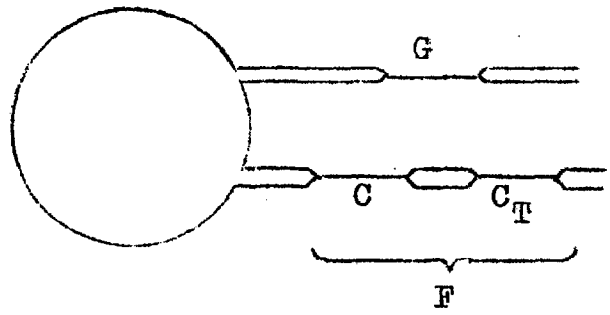

*Footnote: A useful approximation to this for air or N_2 at 20°C is $C = 100\frac{a^3}{\ell}$ litres sec^{-1}.

two in series and one in parallel; where G is the effect of gauge pumping, C is the capillary and C_T is the conductance of the tubulation, all in molecules $torr^{-1}sec^{-1}$.

$$\text{Total conductance} = G + F$$
$$= G + \frac{C.C_T}{C + C_T}$$

The effects of G and C_T oppose one another. As the gauges were normally operated on 10μA emission G is not large and is at the most 3×10^{15} mols $torr^{-1}$ sec^{-1}. This is about 2% of C. Allowing for the high conductance of C_T in series with C, and opposing the effect of G, the calculated value of C is in good agreement with experiment.

2.16.2 (f) Molecular flow and viscous flow under the conditions of the experiment

The mean free path of N_2 at 20°C

$= 5 \times 10^{-3}$cm. approx. at 1 torr

$= 2 \times 10^{-1}$cm. at P_A (2.5×10^{-2}torr)

As molecular flow takes place when

$$\frac{\lambda}{a} > 1.0$$

we may apply molecular flow theory to the flow in capillary C.

The capillary C' may not be so treated as its

diameter is 0.006 cm. and

$$\lambda_{N_2} \text{ at 1 cm. pressure} = 5 \times 10^{-4} \text{ cm.}$$

Thus the flow under these conditions is in an intermediate region between viscous or Poiseuille flow ($\frac{\lambda}{a}$ <0.01) and molecular flow.

2.16.2(g) Operation of the ionisation gauges at low grid currents.

Redhead (1961) has pointed out that operation of the ionisation gauge at low electron emission has the following advantages:

(1) ionic pumping is reduced to a minimum,

(2) pumping due to formation of atoms or activated molecules on the hot filament is reduced,

(3) there is less heating, and consequent outgassing of the glass envelope, and

(4) the filament has a longer life.

This reduction in grid current can however have undesirable side-effects. Ackley, Lothrop, and Wheeler (1962), have shown that the apparent sensitivity of a gauge can rise by a factor of up to 100 when the gauge is operating at low emission currents, and at pressures lower than 1×10^{-7} torr. They suggest this effect is due to the raising of the X-ray limit by adsorption on the grid of residual impurity gases, or from ionisation

by electron impact of these adsorbed gases.

As measurements in the ultra-high vacuum region were only made in the present work in the period immediately after bakeout to test for cleanliness and absence of leaks, any such errors are not very important. Nevertheless measurements were taken with higher emission currents (1mA).

Similarly, Redhead (1962) has shown that the residual current can vary very greatly with the nature of adsorbed gas on the grid, due to enhanced emission of photons or of excited species or ions.

Redhead (1961) also stated that for a system at 3×10^{-10} torr with the gauge envelope at 50°C, the pressure dropped to 1.4×10^{-10} torr when the envelope was cooled with an air blast. This was not observed in the present work.

Thus although the background after bakeout and subsequent outgassing of the gauge might vary from 3×10^{-10} to 1×10^{-10} torr for various reasons, this does not necessarily mean such a variation in true pressure. Redhead (1960) has devised a modulated gauge which is capable of resolving true ion current from residual current.

2.16.2(h) Construction of Schulz-Phelps (1957) high pressure gauge.

The dependence of the ion current on the pressure in the Bayard-Alpert gauge becomes non-linear at pressures approaching 10^{-2} torr for three reasons:

(1) The path of the ionising electrons and therefore the sensitivity becomes pressure dependent.

(2) At high pressures the efficiency with which positive ions are collected by the probe is altered, and

(3) secondary electrons formed during ionising collisions with gas molecules contribute significantly to the electron current. These contribute little to the ionisation, but still count as far as the emission stabiliser is concerned.

The simpler of the two Schulz and Phelps designs which reduces the above three effects is shown in figure 25.

(1) is reduced by making the electron path short and straight.

(2) is satisfied by making the ion collector large enough to collect essentially all the ions at all pressures. This is done by making the

SCHULZ-PHELPS HIGH-PRESSURE IONISATION GAUGE

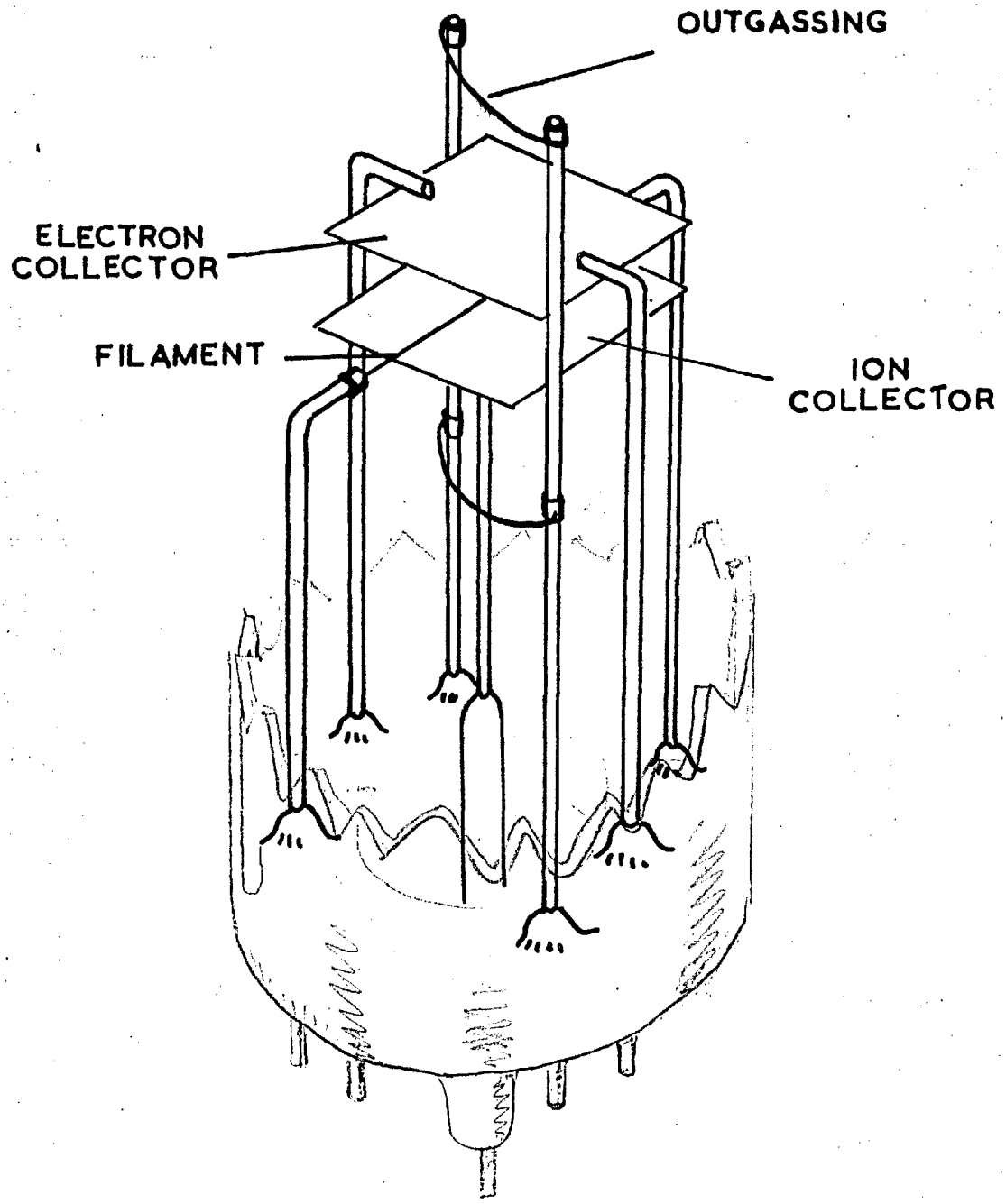

FIG. 25

collector very large with respect to the filament.

(3) is satisfied by making the sensitivity low. If $\frac{i+}{i-} = gP$, (where g is the sensitivity), (see Dushman, 1949),

Schulz (1957) has shown that in any ionisation gauge saturation at $\frac{i+}{i-} = 1$ is due to the collection of secondary electrons produced by ionisation. Thus reducing the sensitivity by reducing the volume traversed by electrons and altering voltages, enables a higher pressure to be reached before the normalised ion current $\frac{i+}{i-}$ approaches unity.

Constructional details were as follows:

Electron and ion collectors; $\frac{3}{4}$" squares of polished molybdenum or platinum sheet 0.006" thick spaced $\frac{1}{8}$" apart. Pt has the advantage of not chemisorbing N_2. The filament was 0.004" tungsten wire made by etching down some 0.008" wire with A.C. in aqueous NaOH solution. The twin outgassing filaments were 0.008" tungsten wire, and all supports were 1mm. tungsten rods. As tungsten-tungsten or tungsten-molybdenum spotwelds are difficult to make, tantalum sheet inserts were used.

The outgassing circuit in the laboratory built

ion-gauge control circuit proved, with proper control of filament current to prevent film being thrown, capable of heating the plates to 1250°C. Care must be taken not to outgas the gauge using the centre filament, which is not capable of carrying enough current because of the design condition in (2) above.

The Schulz-Phelps gauge was linear between about 3×10^{-1} torr, and 5×10^{-6} torr. Deviation at the low pressure end of the scale was due to x-ray emission.

2.16.2(i) Construction of ion-gauge control circuit

An ionisation gauge control circuit was built according to the circuit diagram shown in figure 26.

The circuit provided stabilised emission currents of 10mA, 1mA, and 100μA, and 150mA unstabilised emission for outgassing, is provided by a 700V transformer connected from filament to grid. The stabilised and outgas emission currents were controllable and displayed separately on the control panel. The ion current was amplified by a Knick picoammeter, the most sensitive range of which was 8×10^{-12} A f.s.d. (accuracy: $>1 \times 10^{-8}$A; ± 3%; $>1 \times 10^{-9}$A, ± 5%; $<1 \times 10^{-9}$A, ± 10%.). The output from the amplifier was both displayed on the control panel and also automatically recorded.

FIG. 26

IONISATION GAUGE CONTROL CIRCUIT

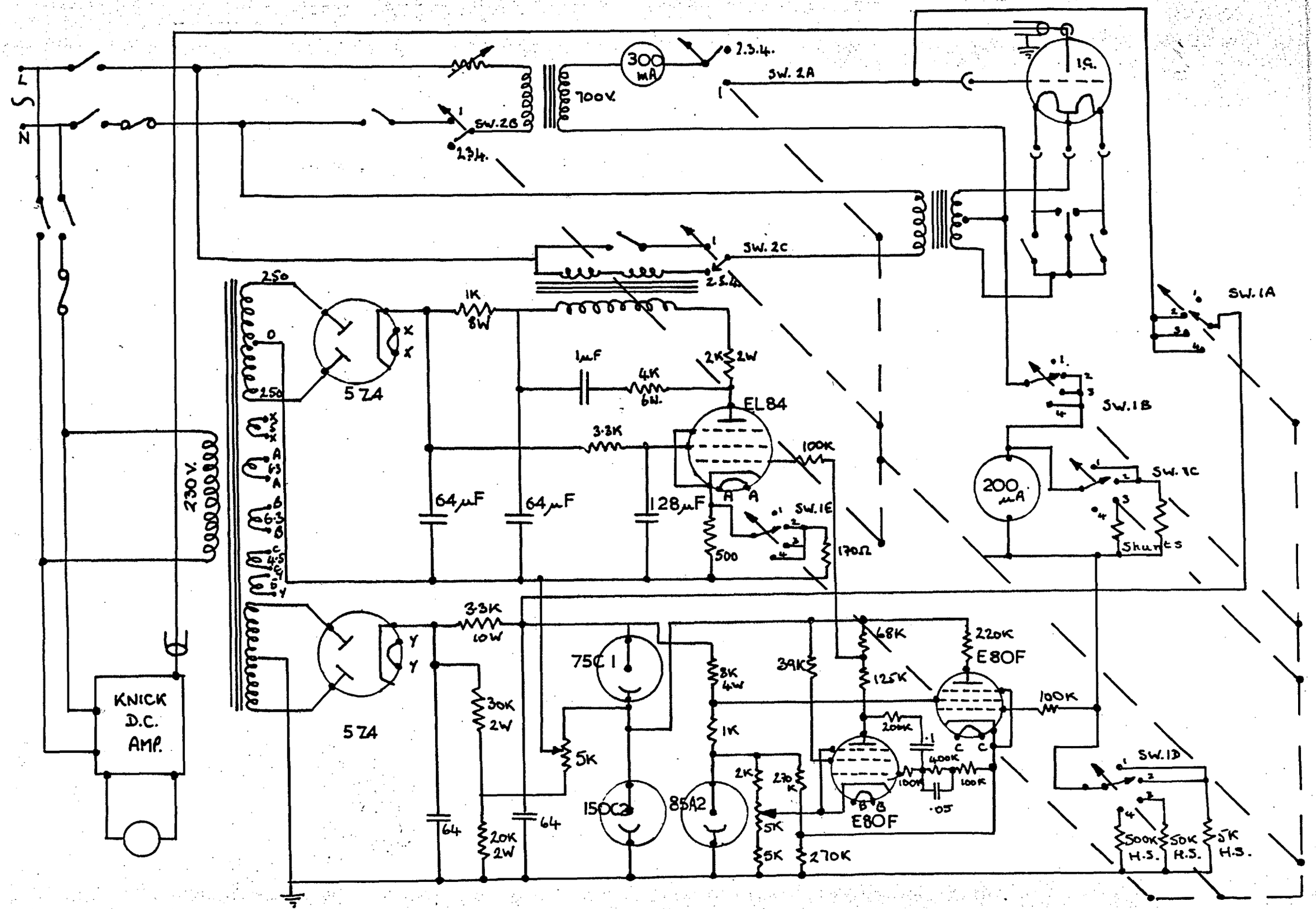

The following modifications were made to the circuit:

(1) The electrode potentials were lowered to conform to those recommended by Schulz and Phelps for use with their gauge. These are: Collector, 0 filament 75V, electron collector 150V.

(2) An extra stabilised emission of 10μA was included. This involved the use of an external sensitive DC ammeter to measure it. The circuit behaved very well at this low emission.

(3) The outgas control was altered from the H.T. to the L.T. supply to the filament. This gave more control of the filament temperature to prevent evaporation of tungsten.

The normal recommended electrode voltages for the Bayard-Alpert gauge are: 0, +25, +170, Ehrlich (1963) and this circuit normally provided 0, +50, +225, but it was found that the 1G3H operated well on the lower voltages used for the Schulz-Phelps, and both gauges were used on the lower voltages. Since many desorptions were done from the 10^{-6} torr range to the 10^{-3} torr range it was advantageous to operate the 1G3H at these voltages as the sensitivity was reduced from 18 to 12.5 thus raising the high pressure limit of linear operation almost to 1×10^{-2} torr (see figure 21).

2.16.3. Pirani gauge (see figure 27)

The sensing filament in this gauge was a helical 200V. 40W. tungsten lamp filament, unflashed and uncoated, and slightly stretched. At atmospheric pressure and ambient temperature its resistance was about 80 ohms. The centre-zero galvanometer across the Wheatstone net in figure (27) could be replaced by a microammeter, enabling the gauge to be used as a direct reading instrument. The Pirani gauge was found however to be violently affected by the operation of the 300W oscillator required to maintain the gas discharge, even though plasma did not come into contact with the filament, and even when the gauge tube was shielded with an iron cylinder. The effect appears to be due to eddy currents being formed by aerial pick-up by various wires forming the Pirani circuit. That it was not due to active species, such as atoms recombining on the filament, was shown by Pirani gauges on other apparatus, ten feet away, being similarly affected. When the Schulz-Phelps gauge was made, the use of the Pirani was discontinued.

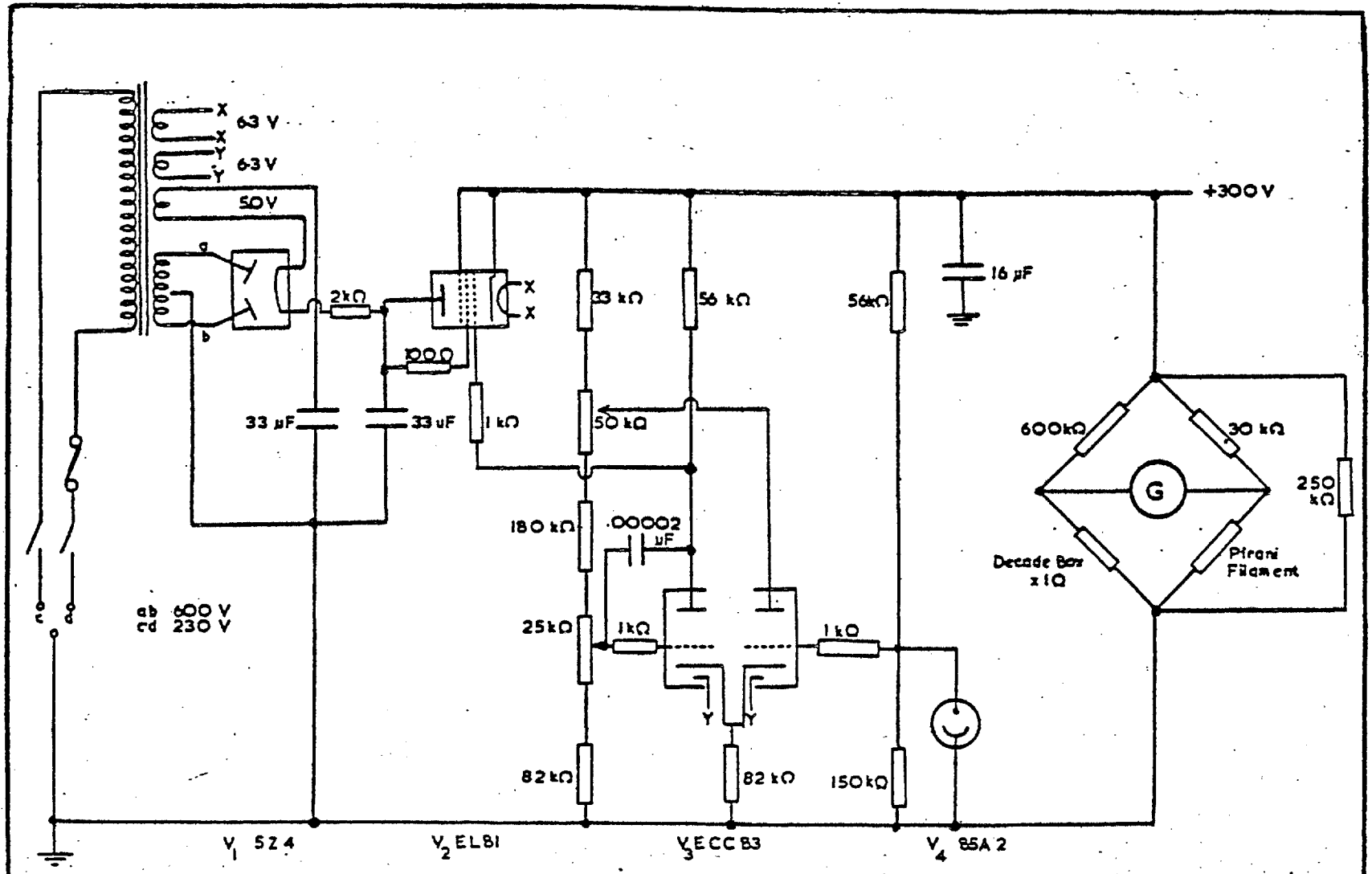

FIG.27 PIRANI CONTROL CIRCUIT

2.17. The Omegatron Mass-Spectrometer (Edwards High Vacuum Ltd.)

The Omegatron was used to analyse gas at pressures up to 2×10^{-5} torr. A diagram of the Omegatron head is shown in figure 28. The head consists of a rigid box-shaped formation of twelve electrodes, with ceramic spacers, mounted within a cylindrical glass envelope. Electrode connections are brought out to thirteen pins in the base, the centre ion collector lead being internally shielded.

The head is fused directly to the vacuum system and is mounted centrally between the poles of a large magnet.

The four RF grids, referred to as the trap, are held at a common potential and together with the potential on the side plates, help to obtain correct operating conditions. The filament with accelerators form an electron gun. RF is applied to the top plate.

The filament shield, at the same potential as the filament, repels electrons emitted in a direction reverse to that required.

Soft X-rays, which travel in straight lines and are generated when the electron beam strikes the electron collector, are prevented from falling on the

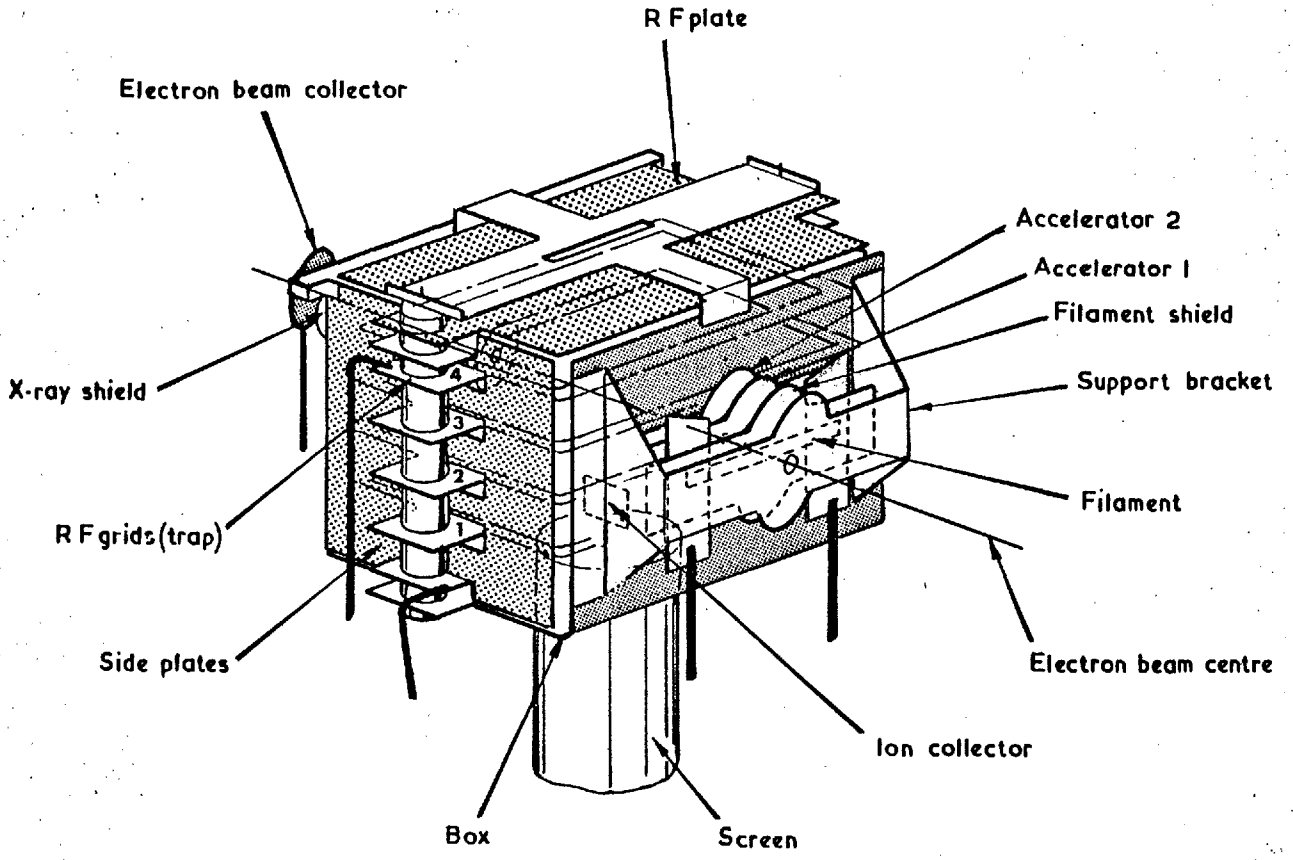

THE OMEGATRON HEAD - ELECTRODES

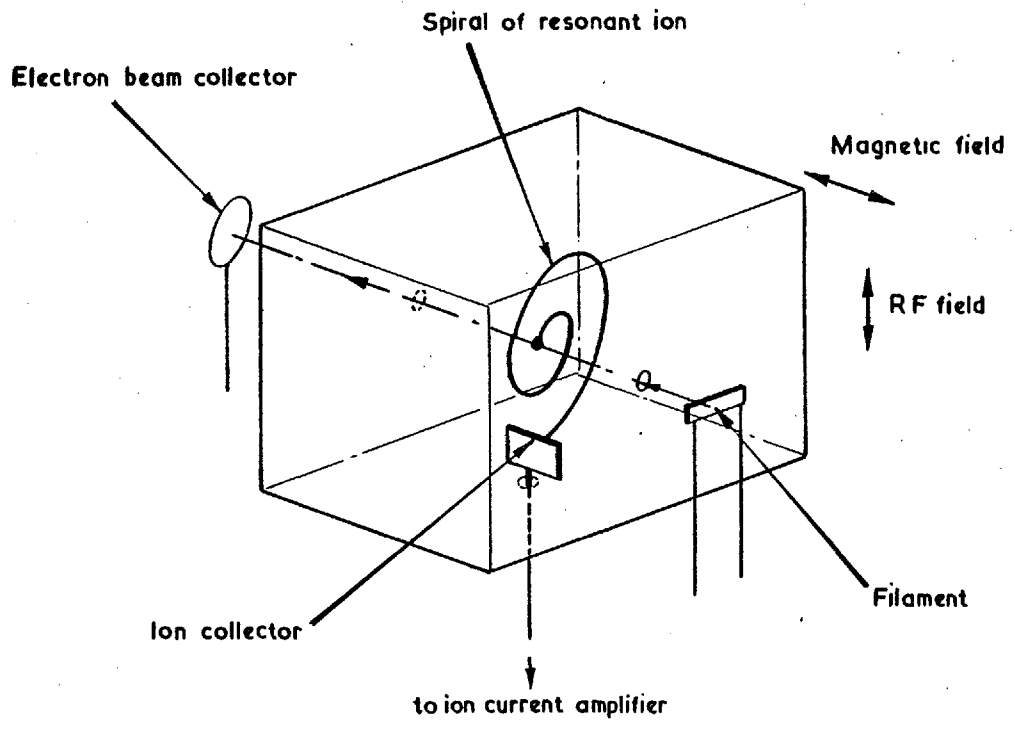

FIG.28 THE OMEGATRON HEAD - WORKING PRINCIPLE

ion collector by an X-ray shield. The head is mounted so that the electron beam is parallel to and in the centre of the magnetic field. Emitted electrons are accelerated and collimated by the electron gun and the magnetic field. The electrons traverse the box and are withdrawn by the electron collector. When an electron strikes a gas molecule another electron is emitted and an ion formed.

A radio frequency field, distributed uniformly by the RF grids is applied between the top and bottom of the box, which is at earth potential. When the RF is equal to the cyclotron resonance frequency for ions of a particular charge to mass ratio, these ions are accelerated and move in an expanding spiral to the ion collector. The ion current so obtained is amplified and passed to a recorder. By varying the RF, ions of different charge to mass ratios are collected, producing a mass spectrogram.

Operation

After system bakeout, the Omegatron head was outgassed for several hours at 800°C using the eddy current heater. The filament, which was coated with lanthanum boride, was heated gradually at first, as too rapid evolution of gases can detach the coating.

The setting-up instructions given by Edwards were followed. The electron current to the electron collector and to the box are both monitored, and the magnet is moved in three dimensions and rotated to give maximum beam current and minimum box current. Rotation was found to be the most critical adjustment.

A peak was located by operating the RF tuner; the frequency is given by:-

$$f(\text{Kc/s}) = \frac{1.52\ B}{m}$$

where B is the field strength in Gauss

and

$$m = \frac{\text{mass in AMU}}{\text{no. of charges on ion}}$$

Further adjustments are made for optimum sensitivity and resolution.

The field in the pole gap of the magnet was 4700-5000 Gauss and was stated to be homogenous to better than $\pm$ 2% in the central one inch cube. The magnet was supported on a three wheeled trolley of non magnetic material which could be adjusted in three directions and rotated by means of screw drives. A large frame of $1\frac{1}{2}$'' dural angle was built to support the rails of the trolley at the correct height.

The RF signal was provided by a signal generator which spanned the range 30 Kc/s to 30 Mc/s in seven ranges. The ranges could be swept automatically or

manually.

Scale calibration error was given as $< \pm 1\%$, but as the field strength B was only given to 6%, it was not important. The method of calibration was as follows:

A rough calculation was made of the cyclotron frequency of N_2^+. A peak was then obtained by operating the Omegatron with nitrogen in the apparatus at 10^{-7}torr. The peak frequency was then substituted back into the equation to obtain an accurate value for B. The assumption that the frequency scale calibration was accurate was born out by correct prediction of the characteristic frequencies of other ions such as N^+, O^+, H_2O^+, O_2^+, and CO_2^+. The identification of CO in N_2 is discussed later.

Ion currents were measured with the Edwards Speedivac Model 2A Ion Current Amplifier.

The most sensitive scale is 10^{-13}A p.d. A variable time-constant, and backing-off potential are other very useful facilities.

SECTION 3: RESULTS AND DISCUSSION

3.1. Calculation of approximate ion energy in a high-frequency field

Consider a singly charged ion of mass m in an electric field of gradient X volts cm^{-1}.

$$\frac{Xe}{300} = mf$$

Distance travelled by ion during one half-cycle

$$s = \tfrac{1}{2}ft^2$$

$$= \frac{0.5.Xe.1}{300\ m\ (2n)^2} \text{ (n = frequency of oscillator)}$$

$$= 0.5 \times 4.8 \times 10^{-10} \times \frac{X}{300} \times \frac{6 \times 10^{23}}{28} \times \frac{10^{-14}}{16}$$

$$= 1.07 \times 10^{-5} X \text{ cm.}$$

In the coil, X may be 200 volts cm^{-1},

$\therefore$ $s = 2.1 \times 10^{-3}$cm.

$\therefore$ Energy of ion (max.) = 4×10^{-1}eV.

Electronic mass is $(5.15 \times 10^{4})^{-1}$ of that of a N_2^+ ion

$\therefore$ Path length of electron = 100 cms.

i.e. > dimensions of cell.

Electron energy therefore may be as high as 1 KeV. and may easily produce more highly charged ions than N_2^+.

3.2 Adsorption of discharge-activated nitrogen on glass surfaces

As the activated gas adsorbed on both glass and nickel film in the cell, adsorption on glass surfaces was studied first. A series of runs was made of adsorption of the discharge activated N_2 on glass. After each run the system was heated under the furnace to 400°C with the exit valves closed. The results are shown in Table 1.

Table 1.

Date 1964	Dosing press	Mins. disch.	Amount adsorbed ΔP	Amount desorbed ΔP by 400°C
24.9.	4.59×10^{-2}	10	0.93×10^{-2}	0.55×10^{-2}
27.9.	2.67×10^{-2}	10	1.10×10^{-2}	0.7×10^{-2}
29.9.	4.21×10^{-2}	10	1.23×10^{-2}	0.62×10^{-2}
30.9.	3.60×10^{-2}	7.5	0.72×10^{-2}	0.53×10^{-2}
30.9.	2.96×10^{-2}	10	0.79×10^{-2}	0.61×10^{-2}
1.10.	2.83×10^{-2}	10	0.76×10^{-2}	0.54×10^{-2}
2.10.	3.11×10^{-2}	10.5	0.94×10^{-2}	-
4.10.	2.42×10^{-2}	11.5	0.90×10^{-2}	0.65×10^{-2}

Volume of system isolated = 3 litres; all pressures measured at room temperature.

The total amount desorbed appears to be consistently below that adsorbed. The difference is explained by pumping through the main dekker during the rather long period (several hours) required for operation of the furnace, and therefore it appears that all gas adsorbed during the discharge time is desorbed by 400°C.

Before the results in table 2 (see below) were obtained, the pumping lead from the main dekker (D_2 in figure 6) to the cell was permanently sealed off to prevent leakage during bakeout. The effect of heating a glass surface which has taken up a dose of nitrogen, for different temperatures is also shown in table 2.

Table 2

Date	Dosing Press (torr)	Disch. time (mins)	Total adsorbed	Total desorbed	Heating time/temp.
22.10	1.7×10^{-2}	12	1.13×10^{-2}	1.08×10^{-2}	10hrs/400°C
23.10	3.2×10^{-2}	10	1.11×10^{-2}	1.29×10^{-2}	40hrs/400°C
27.10	3.4×10^{-2}	18	1.10×10^{-2}	0.06×10^{-2}	15mins/100°C
				0.32×10^{-2}	15mins/200°C

Table 2 continued:

Date 1964	Dosing Press (torr)	Disch. time (mins)	Total adsorbed	Total desorbed	Heating time/temp.
				0.52×10^{-2}	30mins/350°C
				0.7×10^{-2}	10hrs/400°C
				1.2×10^{-2}	18hrs/400°C
8.11	2.44×10^{-2}	11	0.69×10^{-2}	0.92×10^{-2}	24hrs/400°C
10.11	2.67×10^{-2}	15	1.19×10^{-2}	0.42×10^{-2}	2hrs/200°C
				0.46×10^{-2}	3hrs/250°C
				0.93×10^{-2}	15hrs/400°C
				1.07×10^{-2}	6.5hrs/400°C
				1.26×10^{-2}	14hrs/400°C
				1.44×10^{-2}	18hrs/400°C

Volume of system isolated = 3 litres; all pressures measured at room temperature.

On some occasions more gas was desorbed than was adsorbed. This must be normal outgassing of permanent gas from the glass.

In the run on 23.10.64, mercury vapour was allowed into the cell for 20 hours after dosing the glass with nitrogen and before the bakeout. There was apparently no interaction between the mercury and the adsorbed nitrogen and no desorption was observed.

FIG. 29

ADSORPTION ON GLASS OF DISCHARGE

-ACTIVATED NITROGEN

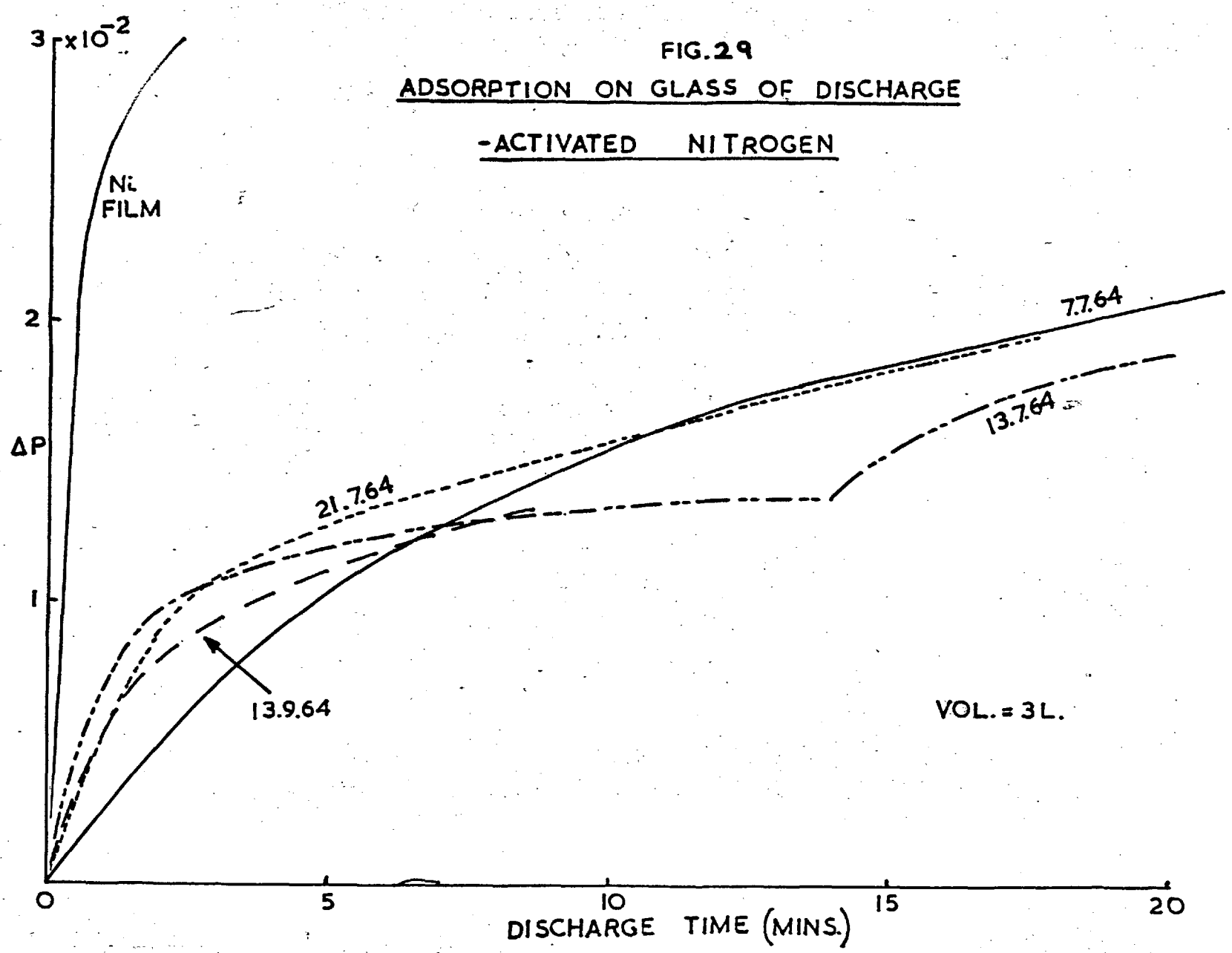

Section 3.1 demonstrated the much greater mobility of electrons than of ions in the discharge, therefore the glass will be expected to acquire a negative charge. Positive ions will be accelerated towards the glass and bury themselves, perhaps sputtering the surface, (Holland 1966). In order to prevent a similar process occurring during adsorption on filaments, the precaution was taken of earthing the filament during the discharge period. Figure 29 shows the rate of takeup of nitrogen on glass. A fall in rate after adsorption of $1x10^{-2}$torr, ($1x10^{18}$ mols), is observed corresponding to about 2 monolayers. Gas continues to be absorbed at a lower rate, perhaps because of deeper penetration into the glass, or because of adsorption on the glass on parts of the cell furthest away from the most intense part of the discharge.

Part of the adsorbed gas could be pumped away at room temperature and replaced again by a dose of activated gas. The run on 21.7.64 was interrupted after 18 minutes discharge, and the system pumped out. Evolution of gas was observed at the rate of $2x10^{15}$ mols min^{-1}. Evolution probably occurs at the same rate at the higher pressures, but it only becomes perceivable at lower pressures. After pumping for 2.5 hours, the discharge was operated with the pressure in the system

the same as before (2.2×10^{-2}torr). After this procedure 2.3×10^{17} mols were taken up during a 3 minute discharge instead of 1.2×10^{17}, and 1.4×10^{17} mols which were adsorbed during the previous two 3 minute discharges, indicating that ca. 1.1×10^{17} mols. which had desorbed during the 150 minute time lapse were replaced during the discharge period immediately following.

Dummy run

A dose of nitrogen (5×10^{-2}torr) was left in the baked out apparatus (background 2×10^{-9} torr) for one hour, then pumped out to ca. 1×10^{-6}torr.

After baking out with the mercury cut-off up for 12 hours and allowing the system to cool again, the pressure was 1×10^{-3}torr in 3 litres.

Effect of oxygen as an impurity on the take-up during a nitrogen discharge.

Several workers report that small quantities of oxygen in the nitrogen discharge increase the yield of nitrogen atoms. An experiment was conducted to investigate any variation of uptake on glass as oxygen was added to the pure nitrogen produced from sodium azide. Two mixtures were made up from air and nitrogen to give 0.1% and 4% of oxygen. Neither produced any significant effect on the take-up rate.

3.3. Adsorption of discharge-activated nitrogen on nickel films.

After adsorption behaviour on the glass had been established, and an estimate made of the amount of gas adsorbed on the nickel filament in the cell, ($\sim$10% of the amount on the glass), a film was thrown from a filament 15 cm. long and 0.5 mm. in diameter. The adsorption procedure was entirely similar to that used with glass. New doses had to be introduced more frequently to maintain the pressure at about 3×10^{-2} torr. When the discharge was first switched on, with a pressure of 4×10^{-2} torr in the cell and the dosing system and gauges isolated by dekker valves, the discharge extinguished in 5-10 seconds, as the pressure dropped to 10^{-3}torr. The rate of adsorption is shown in figure 30. This figure also shows the increased adsorption when the film was cooled to 78°K, even though 3.5×10^{18} mols had been adsorbed. A fall of adsorption rate occurred when 3×10^{18} mols had been adsorbed. This corresponds to 9×10^{15} mols cm^{-2} on a film of geometric area equal to 340 cm^2. For a roughness factor of 2-4 for the film this corresponds to ca. 3-7 monolayers. As will be seen later this agrees well with values on nickel filaments.

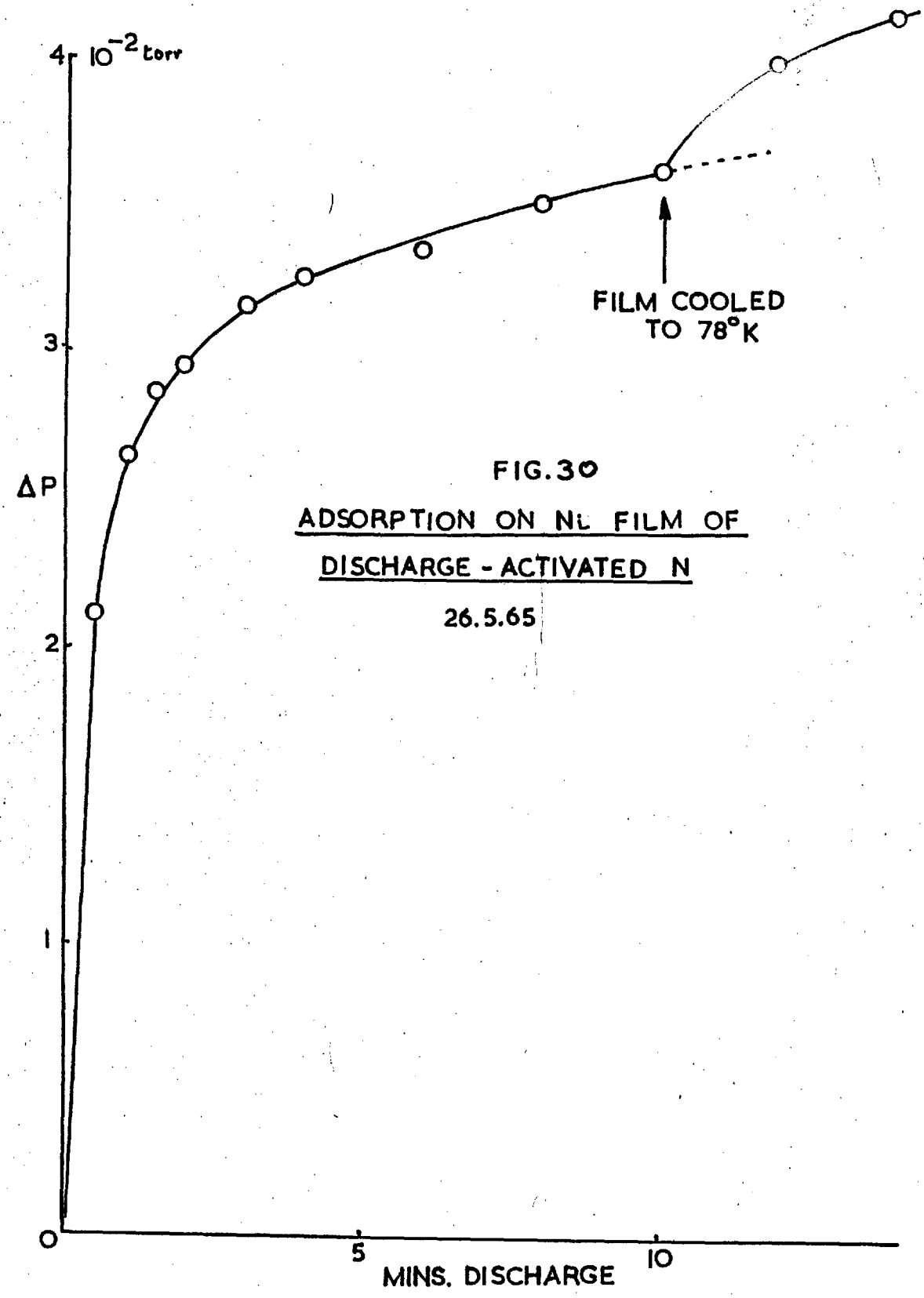

FIG. 30

ADSORPTION ON Ni FILM OF

DISCHARGE - ACTIVATED N

26.5.65

3.4. Desorption from a nickel film (26.5.65)

The technique of heating the film supported on the cell wall with an oil bath proved to have many limitations. These were principally that the rate of heating was slow, and that the highest temperature attainable was only about 300°C at which temperature the desorption would take a long time to complete.

Nevertheless these experiments did show evidence of two binding states of discharge-activated nitrogen on nickel films. Desorption from the first state occurred between 100 and 200°C. The temperature was held constant at 200°C and the rate of evolution was then found to be very low at this temperature. Heating to higher temperatures produced further evolution of gas, and when the film was held at a constant temperature of 300°C, gas was still being evolved after 4 hours.

It was estimated that 3×10^{17} molecules were desorbed from the first state. This corresponds to 8.6×10^{14} molecules per cm^2 of the geometric area of the film, and about 10% of the total uptake. The total amount desorbed was not measured.

3.5 Adsorption of discharge-activated nitrogen on nickel filaments

The study of the adsorption process was made difficult by the irreproducibility of take-up of gas.

For instance, investigations of the dependance of take-up on pressure, oscillator power, and discharge time were bedevilled by apparently random variations in discharge intensity. The latter was critically dependent on the position of the cables from the power supply to the oscillator, presumably due to a design fault in the circuit. It was therefore not easy to compare runs done on different days. Even a series of apparently identical adsorption-desorption experiments performed consecutively were typically subject to variation by a factor of 2 in the total volume of desorbed gas.

A series of typical measurements were made under the following conditions:-

Pressure 1×10^{-1} torr

Discharge power 350 Watts

Discharge time 60 secs.

Nickel filament 0.5 mm x 40 cm.

Desorption: constant voltage method.

(non-linear temperature-time profile)

A typical desorption curve is shown in figure 31 and the first and second desorption peaks are shown.

The results of a set of consecutive runs are given in the table 3.

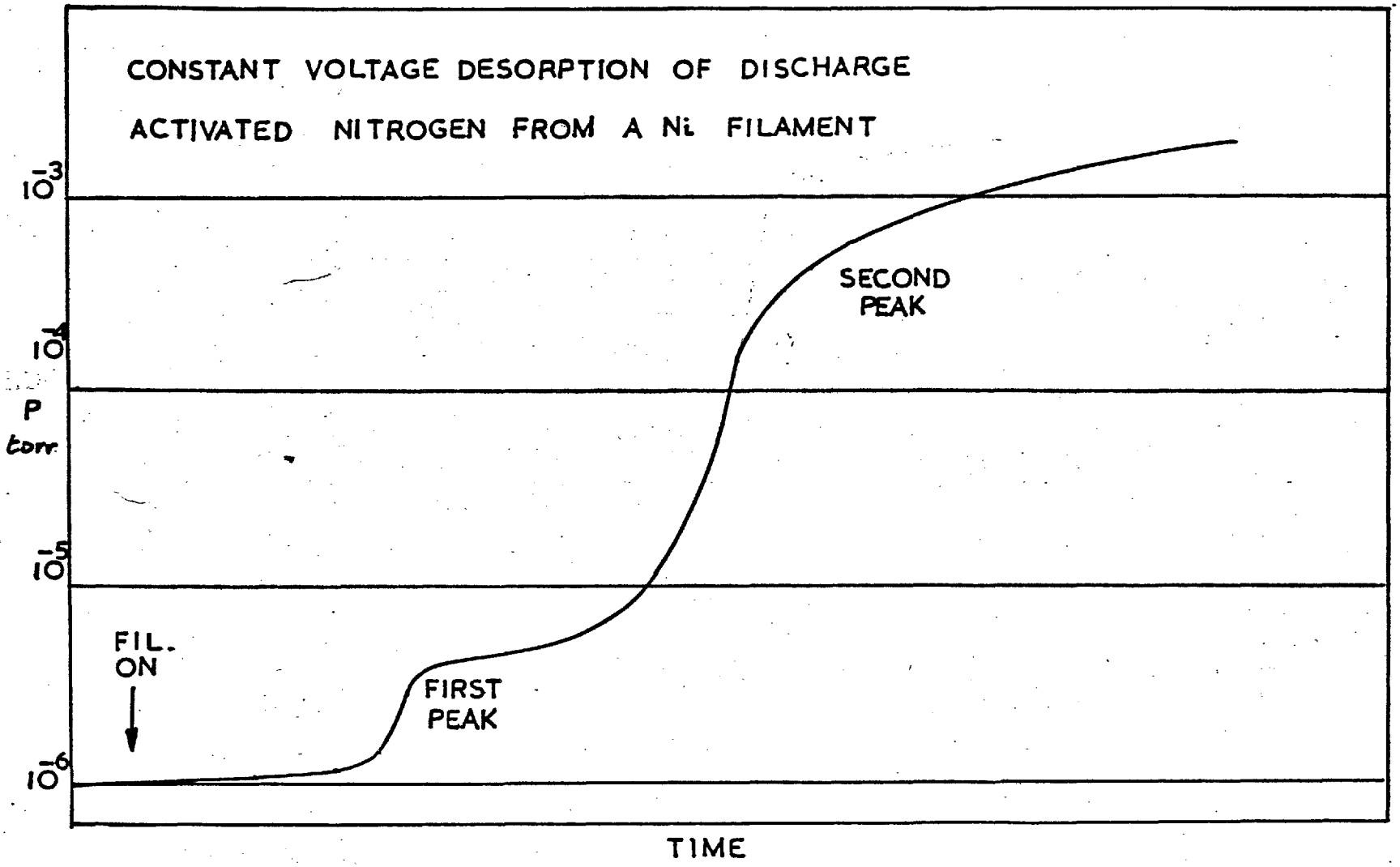
CONSTANT VOLTAGE DESORPTION OF DISCHARGE
ACTIVATED NITROGEN FROM A Ni FILAMENT
10^{-3}
10^{-4}
P
torr
10^{-5}
10^{-6}
FIL.
ON
FIRST
PEAK
SECOND
PEAK
TIME

FIG. 31

Table 3

Chart 20, July 1966.

Simple constant voltage desorptions from a 40cm. nickel wire.

Run	Discharge Press (torr)	Discharge time	ΔP_1 (first peak)	ΔP_2 (second peak)
1	1.3×10^{-1}	1 min.	3.7×10^{-6}	2.2×10^{-3}
2	1.3×10^{-1}	1 min.	-	2.4×10^{-3}
3	1.3×10^{-1}	1 min.	3.2×10^{-6}	1.6×10^{-3}
4	1.3×10^{-1}	1 min.	2.0×10^{-7}	2.2×10^{-3}
5	1.3×10^{-1}	1 min.	2.8×10^{-6}	2.1×10^{-3}
6	1.3×10^{-1}	1 min.	2.8×10^{-6}	1.0×10^{-3}
7	1.3×10^{-1}	1min.45sec.	4×10^{-6}	2.5×10^{-3}

Isolated volume during desorption = 1.13litres.

It will be noticed that in two cases (runs 2 and 4), ΔP_1 is much smaller than in the rest of the runs. This effect which long remained an enigma is now realised to be simply due to the temperature of the filament being too high during adsorption to allow the state corresponding to the first desorption peak to form.

A simple experiment showed that the operation of

the discharge caused heating of the filament due perhaps to recombination processes or eddy-current heating.

Effect of discharge on filament temperature

Pressure = 1×10^{-1} torr. Discharge power = 350 Watts

$R_{22^\circ C} = 0.0139\,\Omega$ $R_{0^\circ C} = 0.0122$ (from figure 18, p.77)

	R_T	R_T/R_0	$T^\circ C$
5 secs. discharge	.0143	1.17	25°C
20 secs. discharge	.0204	1.67	100°C
25 mins. cooling	.0137	1.12	18°C
20 secs. discharge	.0211	1.73	110°C
60 secs. discharge	.0361	3.0	235°C

As the first peak desorbs between 140 and 200°C the discharge time had to be kept below 20 - 30 secs. if the filament starts at room temperature. If outgassing has been carried out just prior to adsorption, (as was usually the case), it was necessary to allow the filament to cool.

Filament aging and its effect on size of first desorption peak.

It was noticed that in a series of runs with a new filament, the first few runs gave a relatively high value for ΔP_1, which subsequently diminished. As this

phenomenon could be explained by contamination with CO, an experiment was devised to test this.

It should be first noted that nickel wire (probably prepared by the Mond process) contains carbon. If oxygen were present as an impurity in the nitrogen, CO would be formed as the filament was heated. It has been shown (Gomer 1953) that heating nickel in oxygen removes all carbon, and subsequent reduction in hydrogen at elevated temperature removes the oxygen.

A 40 cm. nickel filament was heated in air for a few seconds until a heavy coating of oxide covered the formerly bright surface. This filament was then mounted in the apparatus and heated at about 900°C in an atmosphere of several torr of hydrogen. Reduction was rapid, but the filament, although again a metallic grey, was not polished, and it was realised, but not experimentally verified, that its surface area had been increased. It would also be reasonable to assume that the number of step and dislocation sites had increased. All carbon had however been removed.

The following table (4) presents the results of the subsequent series of runs on this filament.

Table 4

Chart 18. October 1965

Run	Discharge Press	Discharge time (total)	Desorption	
			ΔP_1	ΔP_2
2	$1x10^{-1}$	60 secs.	$5.6x10^{-5}$	$9.6x10^{-4}$
3	$1.3x10^{-1}$	60 secs.	$3.6x10^{-5}$	$1.08x10^{-3}$
4	$1x10^{-1}$	60 secs.	$1.6x10^{-5}$	$1.08x10^{-3}$
5	$1.2x10^{-1}$	60 secs.	$1.8x10^{-5}$	$9.2x10^{-4}$
6	$1x10^{-1}$	60 secs.	$5.1x10^{-6}$	$8.6x10^{-4}$
7	$1x10^{-1}$	60 secs.	$6.0x10^{-6}$	$1x10^{-3}$
	Bakeout			
8	$1x10^{-1}$	60 secs.	$6.4x10^{-6}$	$6.6x10^{-4}$
9	$1x10^{-1}$	60 secs.	$6.4x10^{-6}$	$7x10^{-4}$
10	$1x10^{-1}$	60 secs.	$6.8x10^{-6}$	$7.8x10^{-4}$
		film thrown		
11	$1.25x10^{-1}$	60 secs.	$6.8x10^{-6}$	$6.5x10^{-4}$
12	$1x10^{-1}$	60 secs.	$7.2x10^{-6}$	$1.04x10^{-4}$
	Filament reduced in H_2; bakeout			
13	$1.15x10^{-1}$	60 secs.	$6.4x10^{-6}$	$6.5x10^{-4}$
14	$1.3x10^{-1}$	60 secs.	$3.6x10^{-6}$	$6.5x10^{-4}$

Isolated volume during desorption - 1.3 litres

The following features were noted. Although the value of ΔP_2 fell during the series by a maximum of 30%, ΔP_1 decreased by a factor of 10. This is in contrast to the results presented in table 3, where the size of ΔP_2 is of the same order as in table 4, but ΔP_1 is much lower and virtually constant. This low value of ΔP_1 is of the same order as ΔP_1 towards the end of the series in table 4.

Between each run and the next, the filament was outgassed at ca. 1200°C and it was observed to become more polished as the number of runs increased.

Baking out of the apparatus, throwing a nickel film to clean the filament surface, and reduction in a hydrogen atmosphere were all tried, without any success, in an attempt to regenerate the activity of the filament in the adsorption state corresponding to the first desorption peak.

This experiment is good evidence that the first desorption peak was nitrogen and not CO as found by Mimeault and Hansen (1966) when adsorbing nitrogen activated by a hot filament on iridium.

Measurement of filament temperature during desorption

Using D.C. to heat the filament, measurement of the filament resistance is easily accomplished and

filament temperatures were calculated from figure 18 (R_T/R_{273} for nickel)

It was shown that desorption of the first peak was complete by 200°C, and the rate of evolution of the second peak increased rapidly at about 250-270°C.

A consideration of the possibility of the double desorption peak's being an experimental artefact:

A spurious double desorption peak could arise in two ways:

(a) One (or both) peaks are due to an impurity gas,

(b) an experimental artefact is causing one adsorption state to desorb in two parts, e.g. because of a temperature gradient across the adsorbent surface.

Possibility (a) is shown to be false by the mass-spectrometric evidence, and the argument against CO in Section 3.10.

Possibility (b) is considered here. The most likely cause of temperature variation along the filament is that due to cooling at the points of attachment to the tungsten pins. This is minimised (see Section 2.15.7) but must still occur to some extent. However the effect will tend to broaden any desorption peaks, and reduce resolution, rather than

give rise to separate peaks where only one should appear.

Detection of gaseous impurity.

From time to time during a series of runs a check was made on the purity of the nitrogen by dosing in gas and observing if there was any adsorption without activation. In the case of the filament experiments, this was easily tested by flashing the filament. On one occasion it was noticed that after a normal desorption run, when the filament was switched off, there appeared to be a reversible adsorption. As this had previously been shown not to take place with nitrogen and nickel, a dummy run was made as described above. On flashing the filament ca.10^{15} molecules of gas were evolved and rapidly adsorbed on the nickel film in the cell. The impurity was assumed to be oxygen which had leaked in to the supply vessel via a badly-greased tap. On repeating the above experiments with freshly prepared nitrogen the anomalous features were not observed.

3.6. Adsorption of discharge-activated nitrogen on a Palladium filament.

A 40 cm., 0.5 mm. diameter palladium filament was mounted in the cell and subjected to the same treatment

FIG. 32

DESORPTION OF DISCHARGE ACTIVATED N FROM A Pd FILAMENT

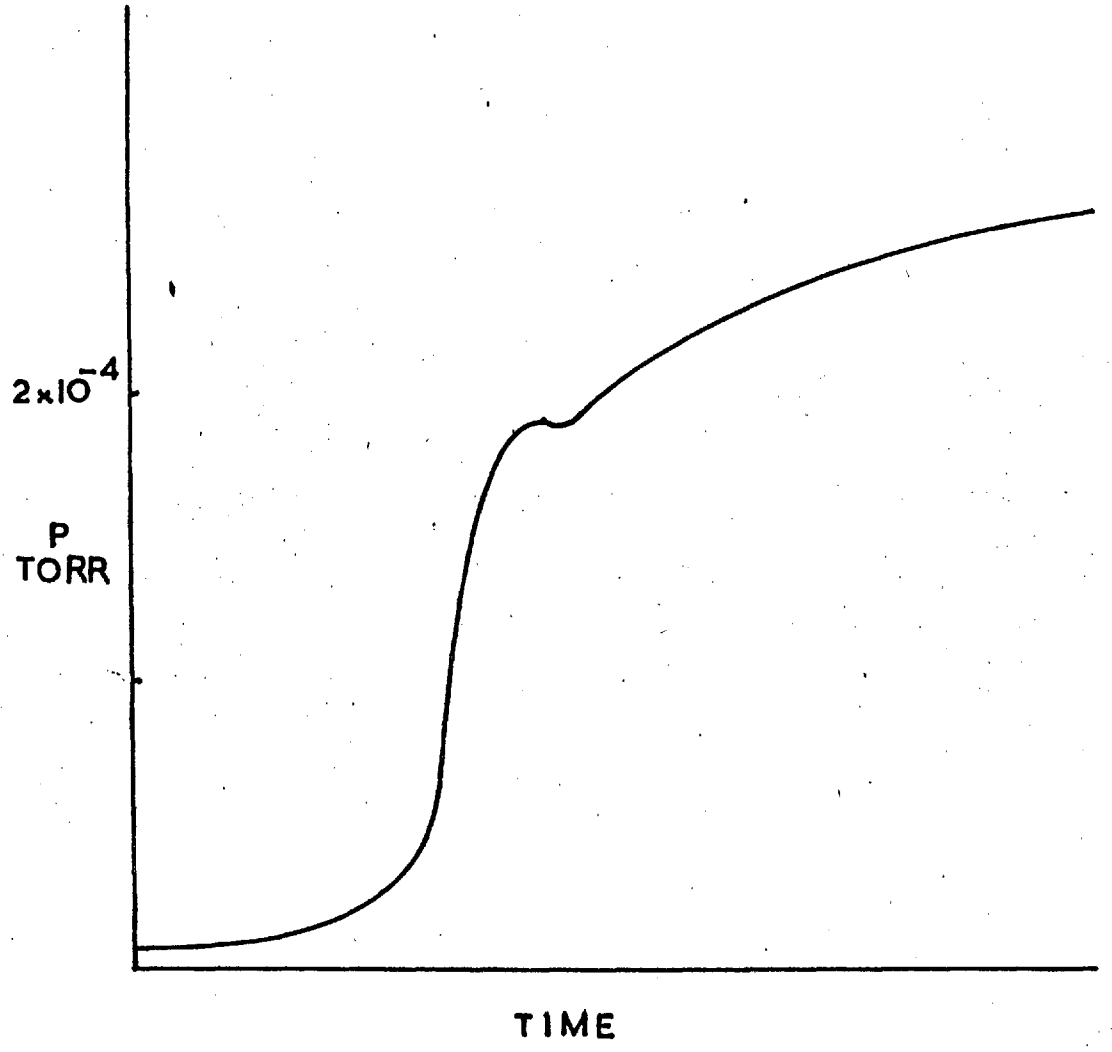

with a nitrogen discharge as described for nickel. The desorption curve is shown in figure 32. Two peaks were definitely present and were obtained many times, but further resolution did not prove possible. If the two peaks are analogous to those of the nitrogen-nickel system, the first peak in the palladium case is very much enlarged, being of the same order of magnitude as the second.

Mass-spectrometric analysis was not undertaken, but it was not believed that the double peak could have been due to impurity.

3.7. Experiments with the Mass-spectrometer

3.7.1. Mass spectra of residual gases in the system at 1 x 10^{-9} torr.

Omegatron settings: Ion current amplifier f.s.d. 1 x 10^{-13}A (its most sensitive scale)

I_{beam} = 8μA, V_{trap} = 92mV, V_{sp} = 1.45v. See figs. 33 & 34.

The peaks are assigned as follows:-

Mass	Ionic species
9.3	CO^{3+}(?)
12	C^+
14	N^+, CO^{++}, N_2^{++}
16	O^+
18	H_2O^+
22	CO_2^{++}
24	C_2^+(?)
28	CO^+, N_2^+
32	O_2^+
42	Ar^+
44	CO_2^+
54	(?)

3.7.2. Synchronous monitoring of desorption by 1G3H and omegatron tuned to mass 28.

(Desorption of discharge-activated nitrogen from a nickel filament)

The curves were of exactly the same shape up to a

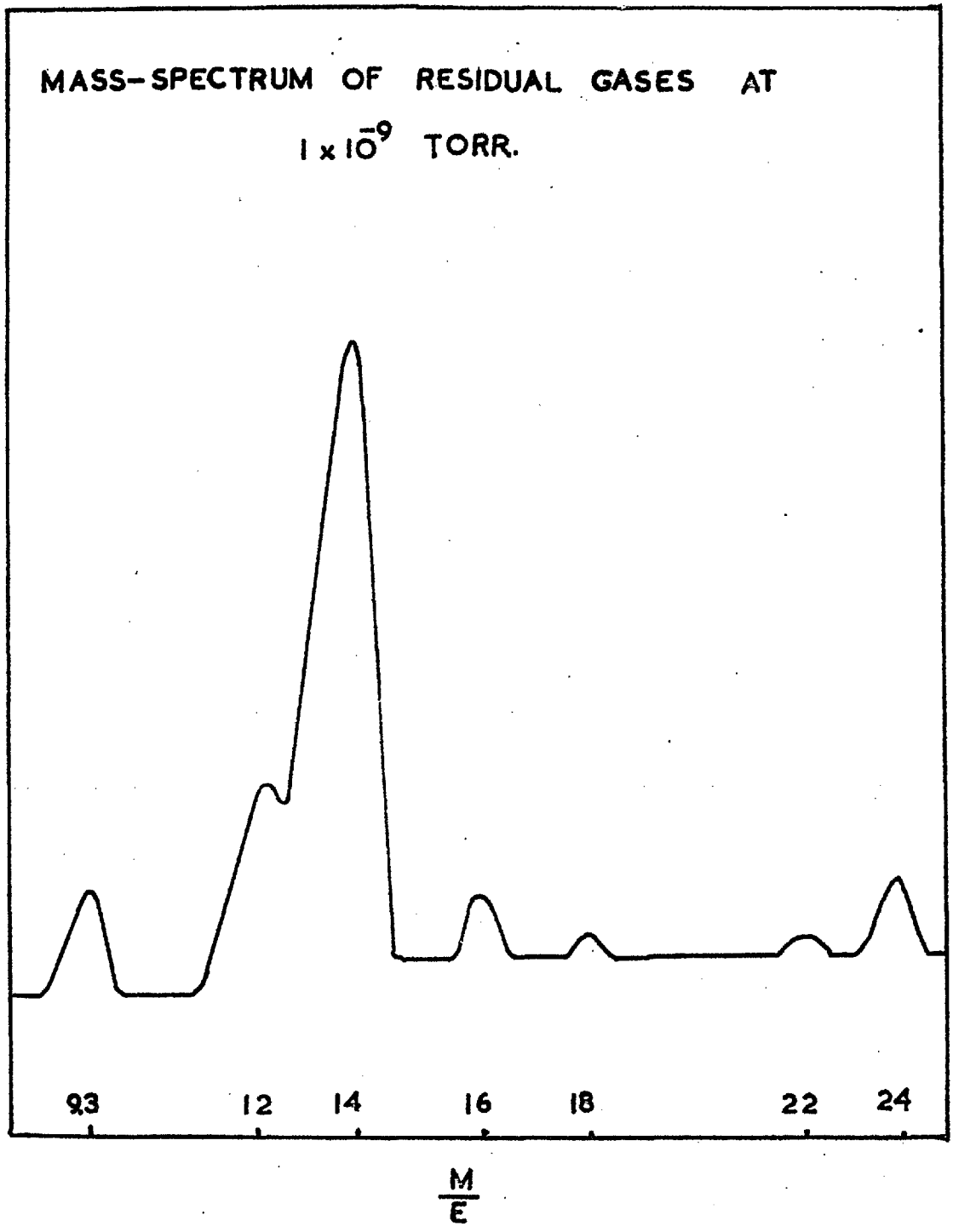
MASS-SPECTRUM OF RESIDUAL GASES AT
1 x 10⁻⁹ TORR.
93
12
14
16
18
22
24
M/E

FIG. 33

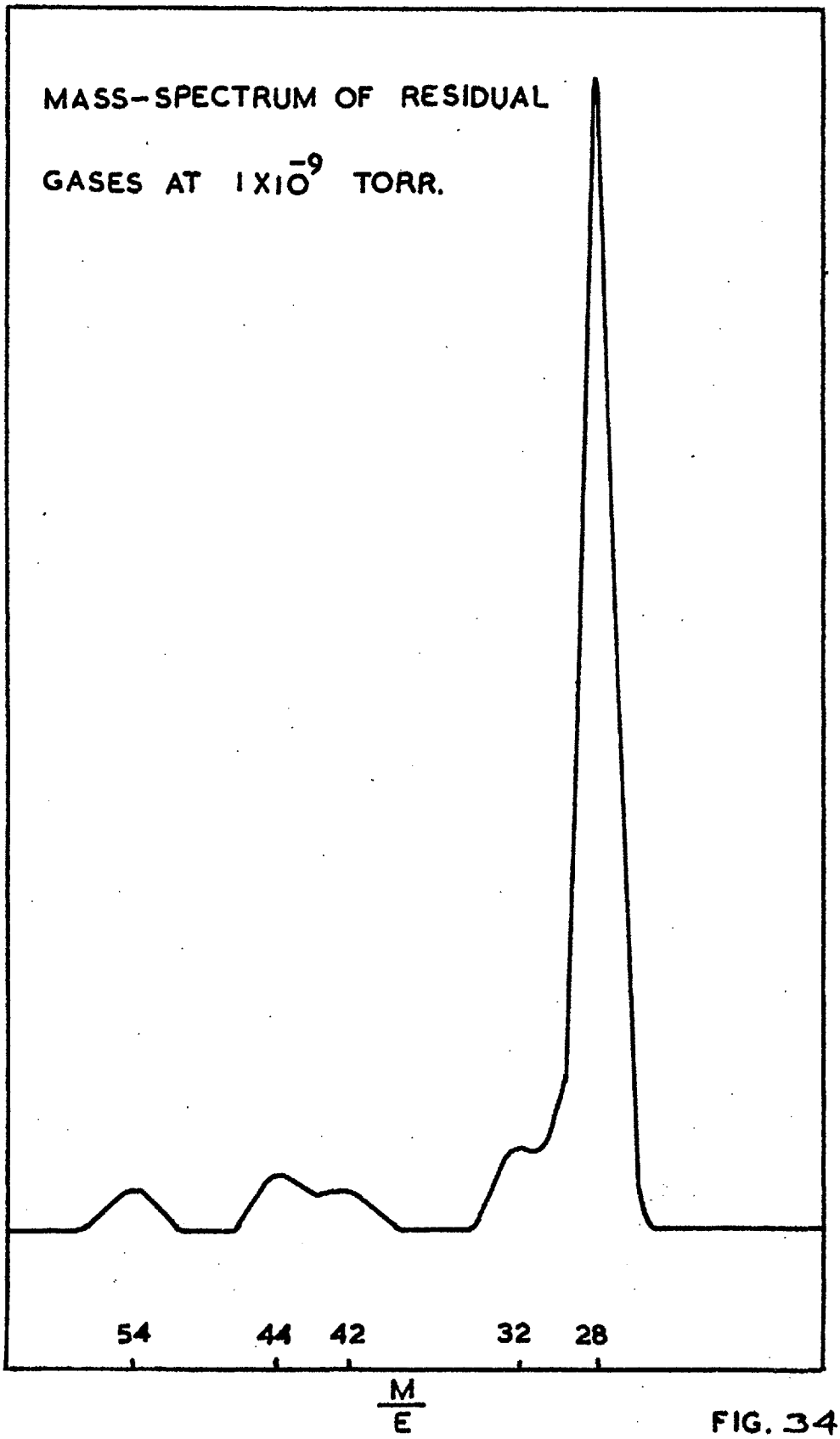
MASS-SPECTRUM OF RESIDUAL
GASES AT 1×10^{-9} TORR.
54
44
42
32
28
M/E

FIG. 34

FIG. 35

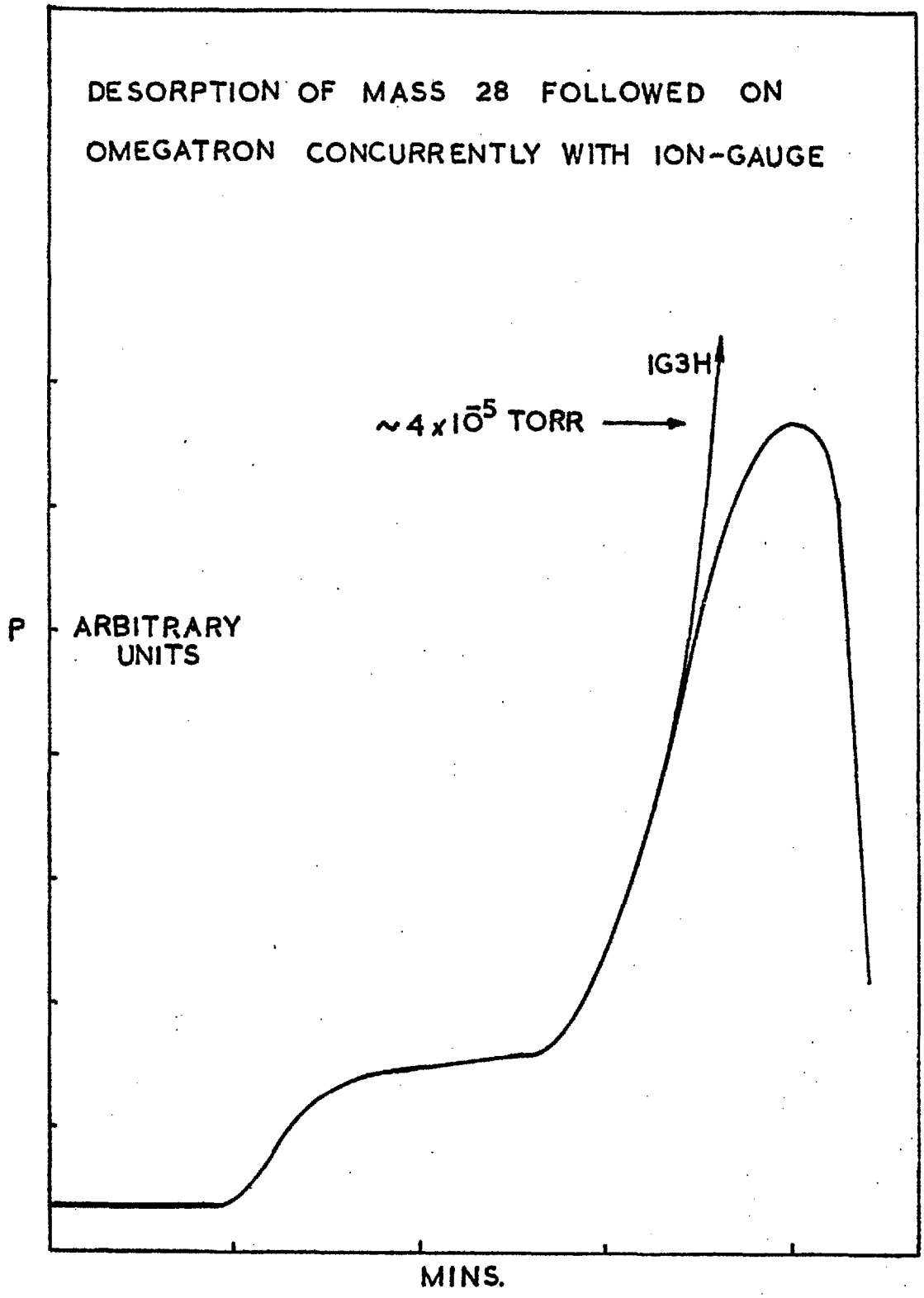
DESORPTION OF MASS 28 FOLLOWED ON
OMEGATRON CONCURRENTLY WITH ION-GAUGE
IG3H
~4x10⁻⁵ TORR
P
ARBITRARY
UNITS
MINS.

pressure of about 4 x 10^{-5}torr when the omegatron cut out because of collisions between the spiralling ions and neutral gas atoms.

The background was checked during a desorption run at a frequency near that for mass 28 but not corresponding to any particular mass number. This experiment demonstrated that the desorption curve for mass 28 was a true effect and not just due to rising background effect at these high pressures.

3.7.3. Mass spectral analysis of desorbed gases.

Desorption was stopped after the first peak and part of the second had evolved. A mass spectrogram in the mass range 10 - 20 did not indicate any C^{12} peak, which would have been produced by the only possible impurity giving rise to the mass 28 peak.

A test run with CO in the apparatus at 1 x 10^{-5}torr was made and the characteristic cracking pattern was obtained. As the C^{12} peak is approximately four times the mass 14 peak (CO^{++}), it is concluded that in the desorption runs with nitrogen, CO cannot be present in significant amounts, and in particular cannot be giving rise to the first desorption peak, as was found in the case of iridium by Mimeault and Hansen (1966).

3.7.4. Mass spectral analysis of gas in the system after operation of the H.F. discharge.

A great deal of evidence has been presented to show

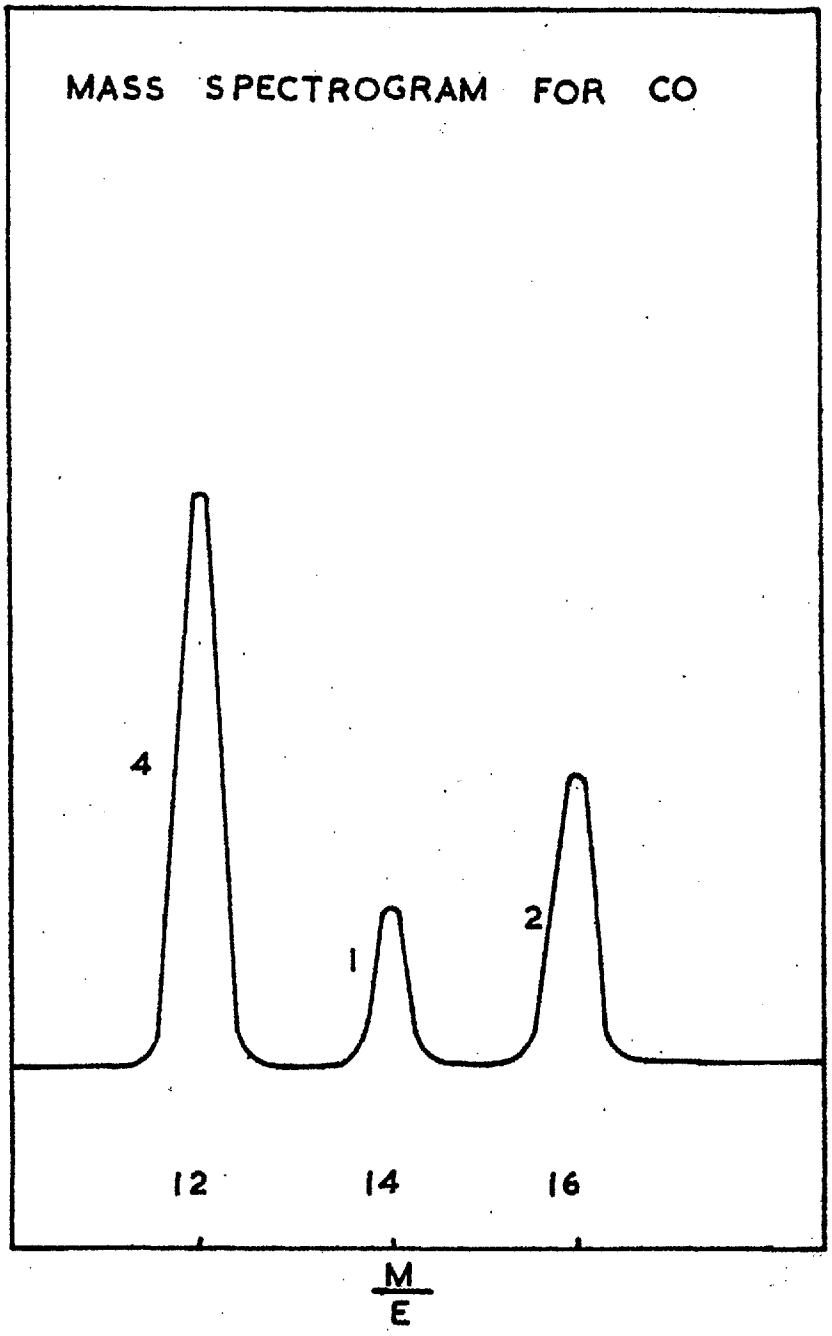

FIG. 36

that adsorbed gas molecules on solid surfaces may be desorbed if the surface is struck by energetic electrons or ions. A technique has even been developed using this phenomenon to prepare clean metal surfaces in vacuo (Farnsworth, Schlier, George and Burger, 1955).

It is very likely therefore that impurities will be desorbed from the glass walls during operation of the discharge. As previously stated, the omegatron could not be operated while the discharge was switched on, therefore the mass-spectra were obtained after the discharge had been extinguished and the system pumped down to 1×10^{-6}. No impurities were detected, but this cannot be definite proof that they were not generated during the discharge time, and rapidly readsorbed on various surfaces. As there was a thin nickel film present during all experiments with a nickel filament, and as this film has a surface area of ca. 100 times that of the filament, contamination of the filament was considered to be negligible.

3.7.5. Mass-spectral examination of gas released from tap-grease (Apiezon L)

The apparatus was evacuated to ca. 10^{-9}torr and isolated from the pumps. A greased stopcock in the nitrogen dosing system was then turned through 360 degrees several times and the pressure rose to ca.6×10^{-7} torr.

The spectrogram showed the gas to be mostly nitrogen with ca. 1% CO_2. There was a rather broad peak at mass 20 - 21 representing about 10% of the nitrogen peak. This could be ascribed to Ne^+, Ar^{2+}, or HF; but the last is unlikely as there was no peak at m = 19.

3.7.6. Mass spectral analysis of nitrogen freshly prepared from NaN_3.

Peak broadening at m = 14, 28 will mask any small peaks due to important impurities such as O_2 and CO. It was estimated that if these were present it was in concentrations < 1 part in 10^5 of nitrogen.

3.8. Adsorption of discharge-activated rare gases.

3.8.1. Experiments with argon

Attempts were made to activate argon with the discharge and adsorb it on a nickel filament to make a direct comparison with nitrogen.

The experimental technique was entirely similar to that with nitrogen, the discharge being operated for several minutes in a pressure of ca. 2×10^{-2} torr of argon. It was observed that the discharge was much less brilliant.

Desorption showed a double peak similar to that with nitrogen, ΔP for the first peak being 1×10^{-6} torr

(ca. 5×10^{13} mols) and the second 1×10^{-5}torr (ca. 5×10^{14} mols). This latter is much less that that for nitrogen, which corresponds with Winters'(1966) observation of a much lower absorption probability for argon than for nitrogen ions.

However mass-spectrometric investigation changed the picture drastically. Analysis of residual gas after 15 minutes discharge in argon, (before desorption from the filament), showed

mass	28	$\sim$ 25%	(N_2,CO)
	40	$\sim$ 65%	(Ar)
	44	$\sim$ 10%	(CO_2)

There were also peaks at 12, 13, 14, 15, 16 and 18 mass numbers.

Analysis of gas desorbed from the filament showed nitrogen was being adsorbed in very considerable amounts, and was probably giving rise to the double peak, which is therefore not attributable to argon.

Simultaneous monitoring of total pressure and mass 28, showed nitrogen to feature prominently in both the first and second peaks.

The nitrogen is probably desorbed from the walls of the cell, (which have previously been subjected to many hours of bombardment by the nitrogen discharge), and

CO_2 may be present initially in the argon, though this was not analysed.

The argon experiments were discontinued.

3.8.2. Experiments with xenon

Adsorption of discharge-activated xenon was attempted in a similar way to that with argon.

5 mins. discharge at 2×10^{-2} torr, followed by desorption, showed an increase of pressure corresponding to 3×10^{14} mols.

A desorption conducted with the omegatron tuned to the Xe^{++} peak showed that xenon was being desorbed in one peak only, however mass-spectroscopic analysis showed nitrogen to be present in large quantities. Using the data of Allan and Lang (1963) for cracking patterns and relative abundances for gases in an omegatron it was estimated that the desorbed gases contained 70 - 80% nitrogen.

3.8.3. Discussion of rare gas experiments

These observations show that under similar conditions the adsorption of xenon or argon (probably $< 1 \times 10^{14}$ molecules) is only about 1% of the corresponding adsorption of nitrogen. Calculations show (see Sect. 3.1) that the ions in the 20 Mc/s discharge have only thermal energies, therefore the results are in

qualitative agreement with the data on ion-sticking probabilities of Winters (1966); for thermal energy N_2^+ ions s = 0.15 approximately, and for A^+ ions s = 0 approximately.

No evidence was obtained of multi-state adsorption, as found for instance for Ar^+ ions on tungsten (Kornelsen, 1961) and for several rare gases on platinum and tungsten (Colligon and Leck, 1961). Kornelsen found four desorption peaks corresponding to activation energies of desorption varying from 48 to 124 K.cals. $mole^{-1}$. However he showed that for ion energies under 100eV all adsorption was confined to the state corresponding to the lowest energy. Nielsen's (1956) approximate screened nuclear scatter calculations show that a 4 KeV argon ion would only be expected to penetrate three or four lattice distance into tungsten.

If the resolution of the desorption spectra is somewhat less than that of Kornelsen only two peaks appear, as found by Colligon and Leck for several combinations of rare gas ions and metals. Their results for peak multiplicity are summarised as follows:- Atomic weights are also given

	Neon 20	Argon 40	Krypton 84
Molybdenum 96	double	single	single
Tungsten 184	double	double	single
Platinum 195	double	double	double

The explanation offered here of this variation is based on an analogy with the raising of the accommodation coefficient of a gas on a metal surface when the metal is covered with a layer of adsorbed gas molecules. In this case it is postulated that energy exchange during collision is most efficient when the two colliding bodies are of similar mass. If it is assumed that the second peak corresponding to the higher energy of desorption involves gas molecules buried more deeply under the metal surface, then those combinations of rare gas atoms and metal atoms whose atomic masses are most similar will not be expected to give rise so easily to the adsorption state corresponding to the second desorption peak.

Given the additional factor (affecting depth of penetration) of the increasing atomic diameter from neon to krypton, and the approximately equal inter-atomic spacing of the metals, a good qualitative explanation of the variations of the metal-rare gases systems is given.

3.9. Production of nitrogen atoms on a hot tungsten filament: adsorption of nitrogen atoms on a nickel filament.

The take-up of nitrogen activated by a hot tungsten filament on a nickel wire 40 cms. long and 0.5 mm. in diameter was studied in the same cell as that shown in figure 7. The lower pinch-seal supported a 25 cm., 0.2 mm. dia. tungsten wire, which was electrically heated by A.C. The temperature of the tungsten filament was measured using two optical pyrometers and checked by resistance measurements. The agreement between all methods was good after the appropriate black-body corrections were made. Temperatures in the range 2000-2600°K were estimated to be correct to ± 30°.

The take-up of nitrogen on the nickel filament was measured by flashing the filament after first pumping out the cell to background pressure. The pressure of gas thus desorbed was measured with the ionisation gauge 1G3H operating on the lower grid potential.

3.9.1. Temperature calibration for W filament

Optical pyrometry

The instruments used were an 'Optix' (Pyrowerk, G.m. b.H., Hannover), and a Foster instrument, (Foster

Instr. Co. A3/005/14.5-30.); both capable of reading temperatures up to 3000°K. Considerable difficulty was experienced in obtaining reproducible readings with the pyrometers but this was minimised as far as possible by taking 5 readings at each current setting of the tungsten filament, and taking care to approach the balance position alternately from each side on the temperature scale. The mean of these temperatures was taken and a graph plotted of temperature against current. The best line was drawn through these points which fell (over the interval 2000-2400°K) almost along a straight line (see figure 37). The emissivity of tungsten at all wavelengths is considerably less than unity, and thus pyrometers calibrated for black-body radiation give temperatures lower than the true values for tungsten. A black-body temperature correction chart was drawn up from data by Espe (1966) and Smithells (1952), and a graph of true absolute temperature against filament current was drawn, (figure 38). The effect of energy absorption by the Pyrex glass of the cell is small, and was ignored.

Resistance measurements

The optical pyrometer measurements were checked by the resistance measurements on the tungsten filament. The heating was by A.C., and the voltage measurement

FIG. 37

PYROMETER READING VS. CURRENT FOR W FILAMENT

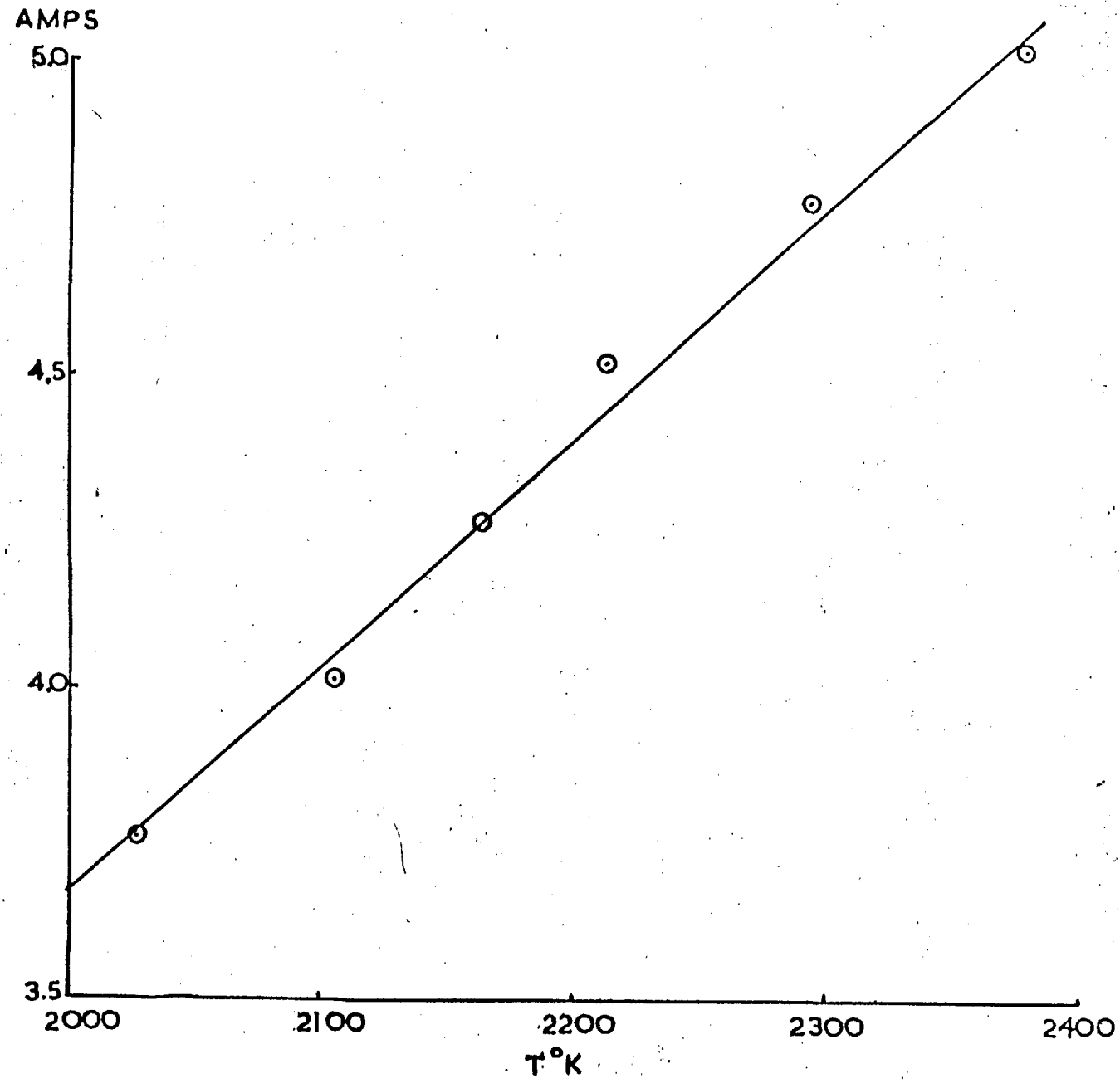

FIG. 38

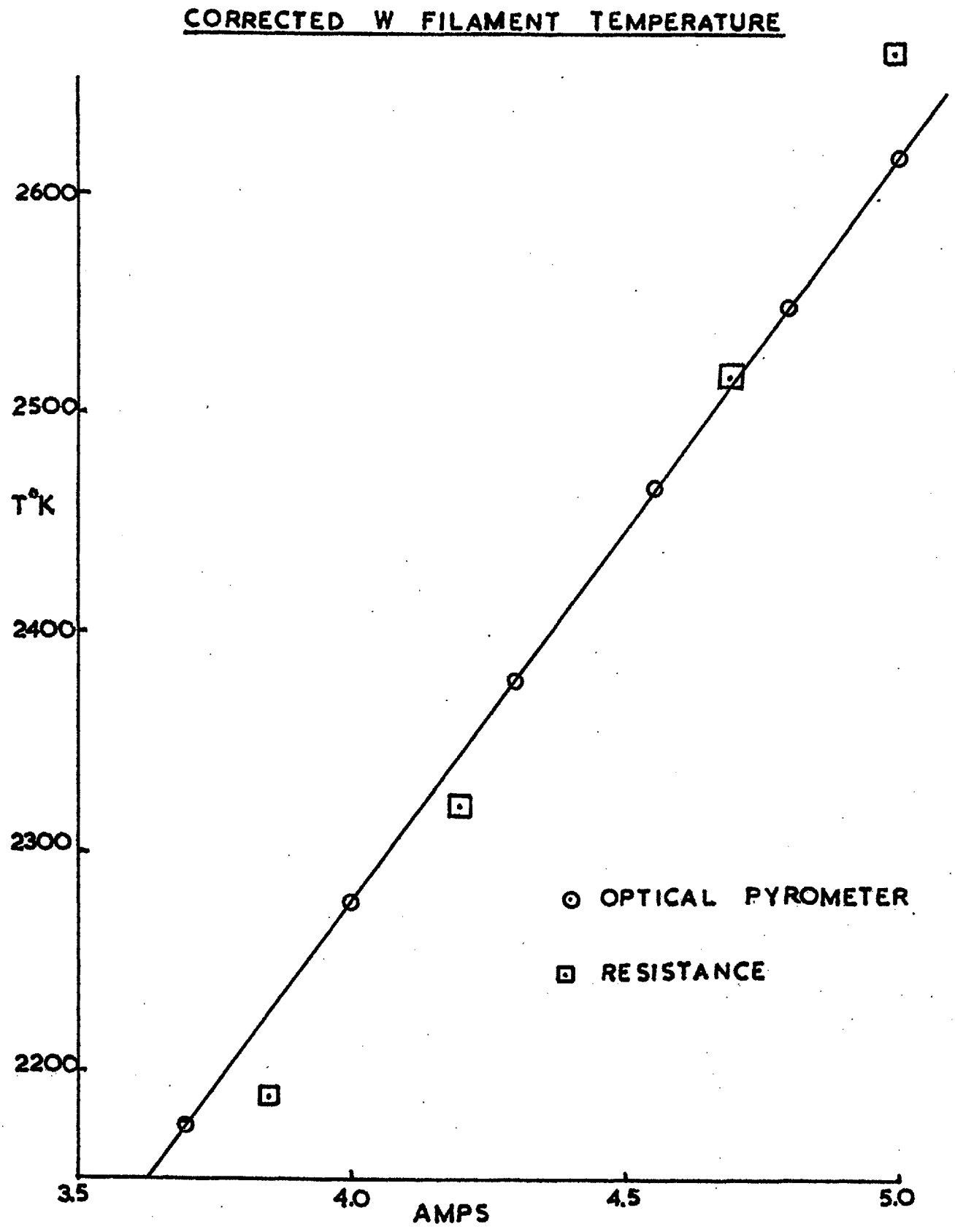
CORRECTED W FILAMENT TEMPERATURE
2600
2500
T°K
2400
2300
2200
3.5
4.0
4.5
5.0
AMPS
OPTICAL PYROMETER
RESISTANCE

was made with a Sangamo-Weston voltmeter model S103 (accuracy better than 1%; B.S.89).

The values of resistance obtained were compared with the resistance of the wire at 20°C (R_{298}) obtained accurately by D.C. measurement and these ratios were used to interpolate absolute temperatures from a graph drawn of temperature against R_T/R_{298} for tungsten. Data for this curve was obtained from Espe (1966) (See also Jones and Langmuir, 1927, and Langmuir and Taylor, 1936).

Values of temperature obtained in this way were plotted on the same curve as the optical pyrometer measurements and good agreement ($\pm$ 30°) was obtained.

3.9.2. Treatment of data

The results for 50 adsorption-desorption runs are given in Appendix I.

Figure 39 shows the variation in amount of nitrogen adsorbed with time for constant tungsten filament temperature, (2443°K in this case), and constant dosing pressure, (2.5×10^{-2}torr). As the pressure varied slightly from run to run a $P^{\frac{1}{2}}$ correction was made to normalise all runs to 2.5×10^{-2} torr. The justification for this is both theoretical (see below) and experimental, (Nornes and Donaldson, 1966). A set

FIG. 39

ADSORPTION OF N ATOMS ON Ni FILAMENT

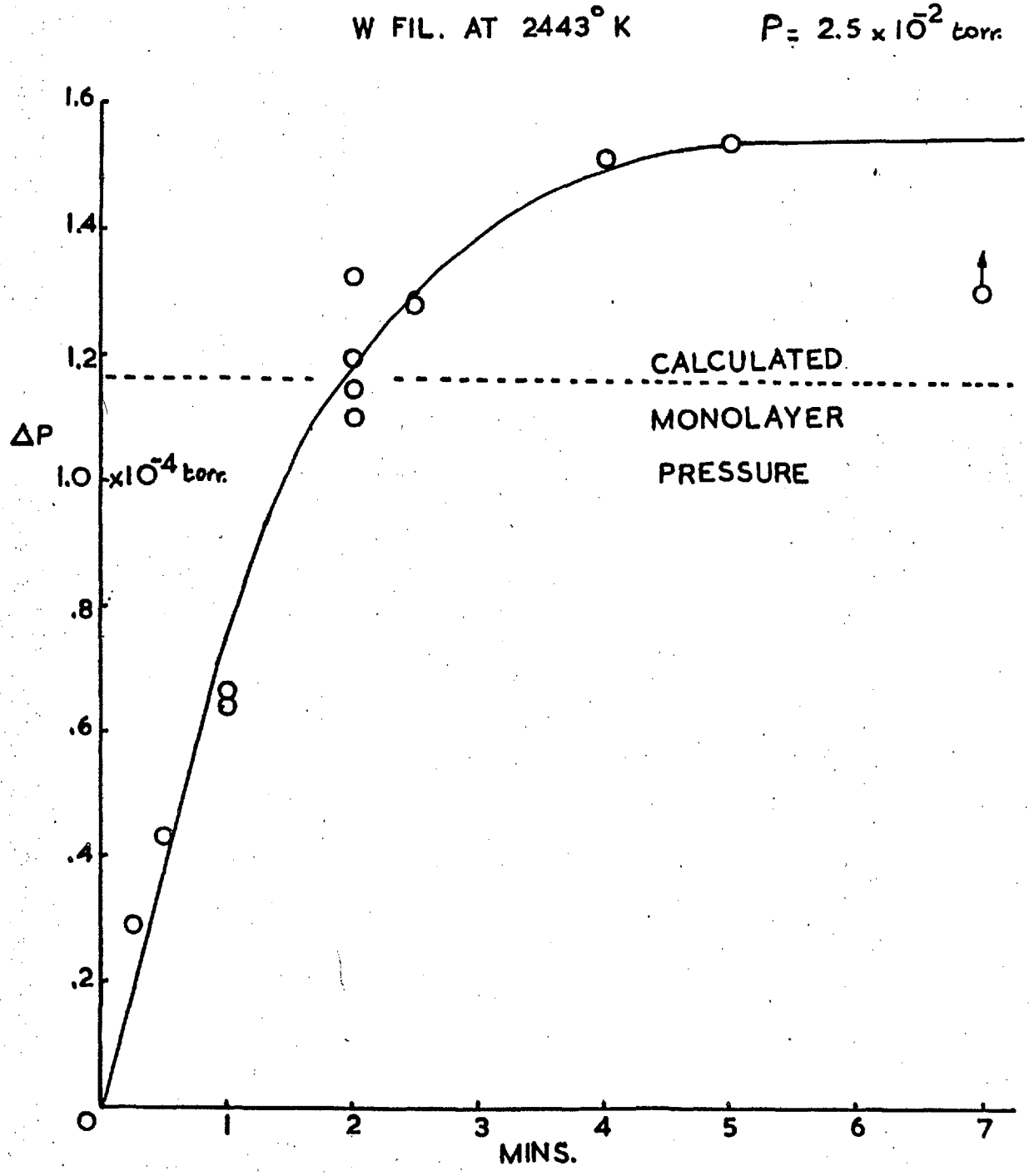

of curves of rate of adsorption for a range of temperatures from 2300-2600°K was obtained (see figure 40). The initial parts of these curves were approximately straight, and it was assumed that the rate of production of atoms on the tungsten was proportional to the rate of adsorption on the nickel. A table of initial rates of adsorption for different tungsten filament temperatures was drawn up (see table 5) and an Arrhenius plot drawn, see Figure 41.

Arrhenius plot for production of atoms

Dosing pressures corrected to 2.5×10^{-2} torr according to the $P^{\frac{1}{2}}$ law.

Table 5

Rate of atomisation (α take-up in 1 min.)		Current Amps	T_f	$1/T_f \times 10^4$
$\Delta P \times 10^5$ (torr)	$\log_{10}(\Delta P \times 10^5)$			
61.0	1.785	5.0	2617	3.795
19.7	1.294	4.75	2530	3.955
17.8	1.25	4.65	2495	4.01
11.76	1.07	4.50	2443	4.093
5.45	.736	4.30	2376	4.215
2.5	.398	4.15	2325	4.305
0.9	$\bar{1}$.954	4.1	2308	4.33
0.7	$\bar{1}$.845	4.0	2275	4.395

FIG. 40

RATE OF ADSORPTION OF N ON Ni FILAMENT

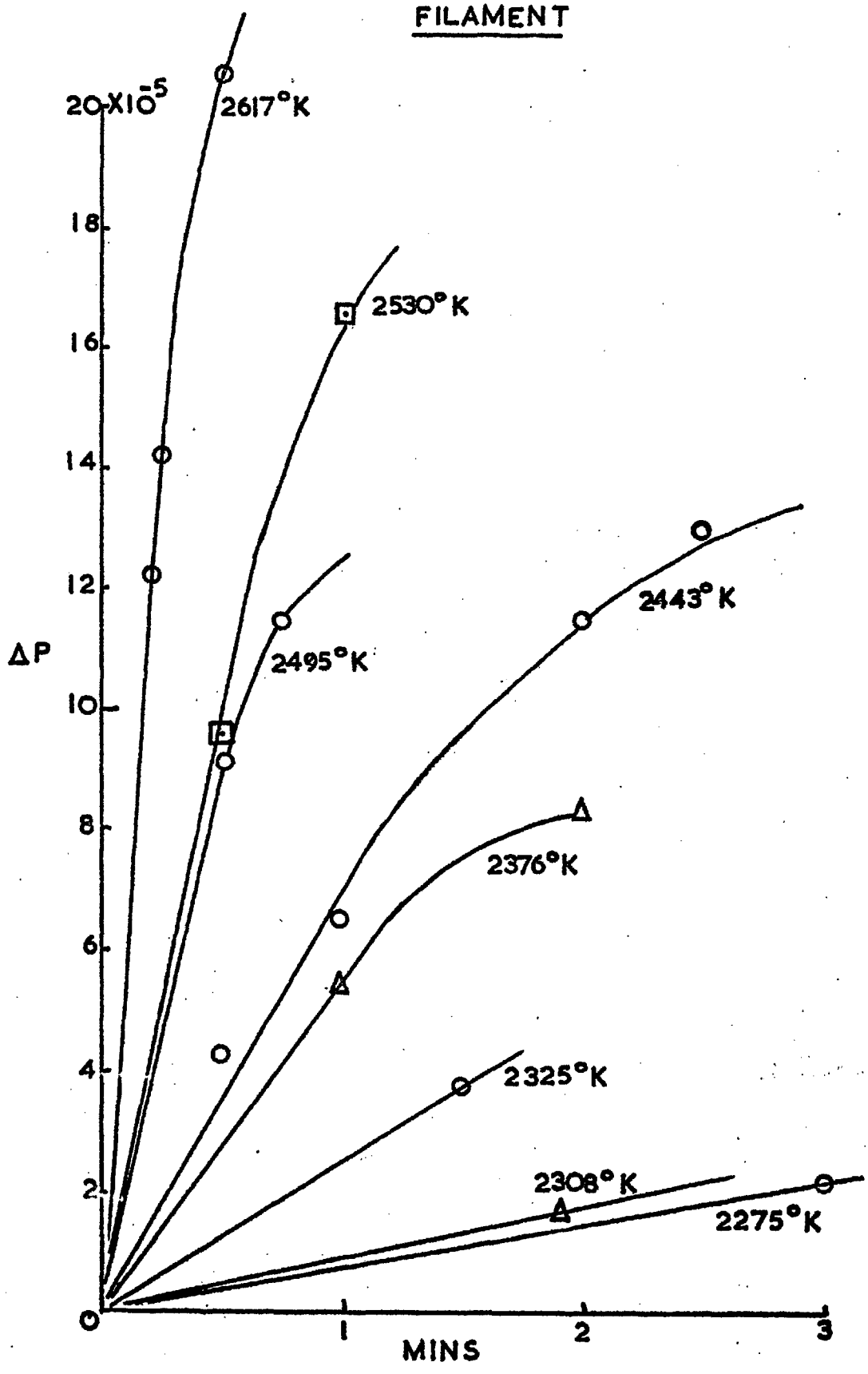

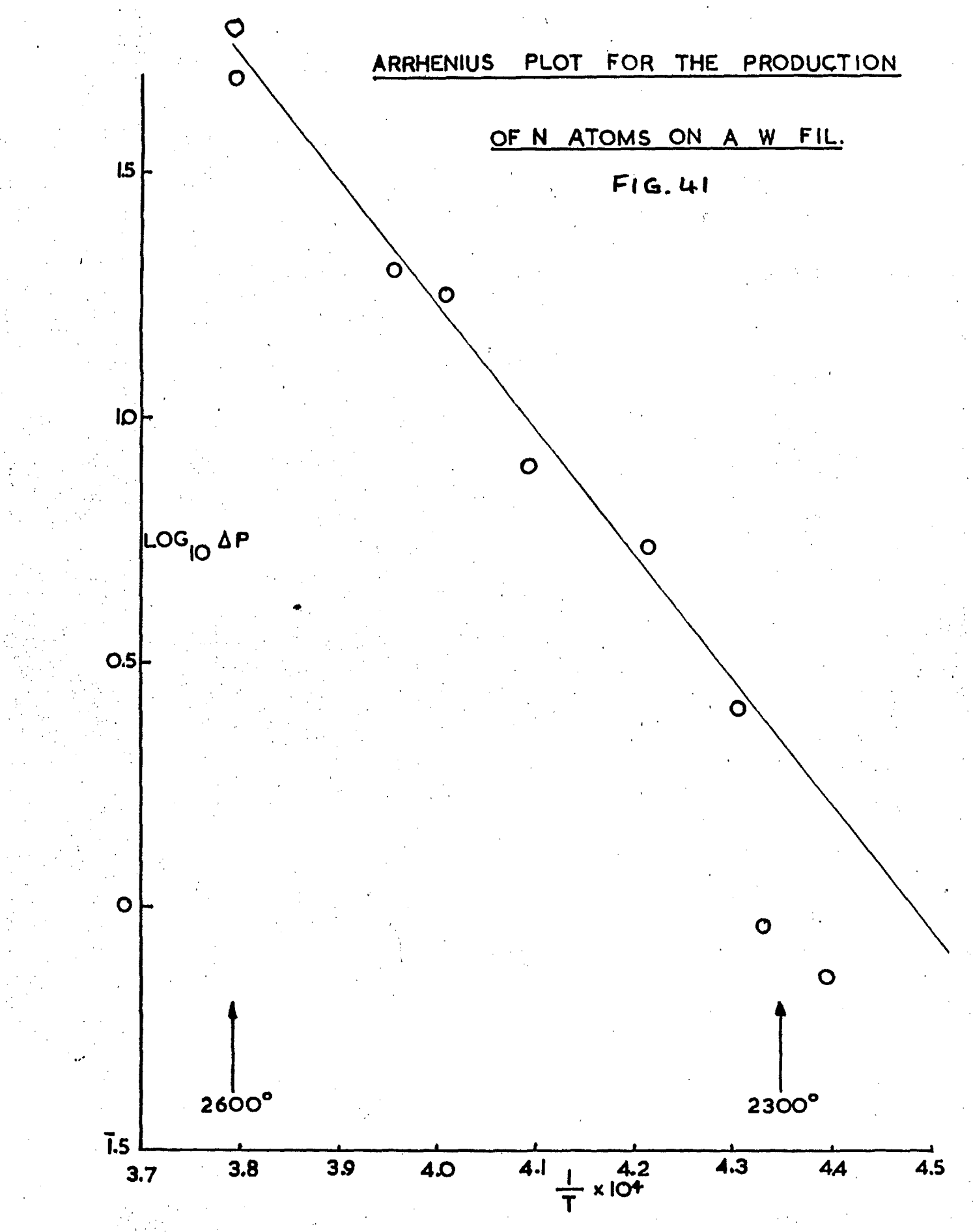
ARRHENIUS PLOT FOR THE PRODUCTION
OF N ATOMS ON A W FIL.
FIG. 41
1.5
1.0
0.5
0
$\bar{1}.5$
$\log_{10} \Delta P$
2600°
2300°
3.7
3.8
3.9
4.0
4.1
4.2
4.3
4.4
4.5
$\frac{1}{T} \times 10^4$

In estimating the rate of adsorption only data for short times are used, before any saturation has occurred. In general the highest rates are considered the most reliable.

The rates corresponding to the two lowest temperatures are not considered reliable; any attempt to include them in the calculation of the Arrhenius activation energy gives a ridiculously high value. The Arrhenius plot for the production of atoms on the tungsten filament for temperatures in the 2300-2600°K range appears to show the concave curvature towards the origin predicted by equation 11 of the theoretical treatment. The predicted values of $E_{app.}$ are 115 K cal. $mole^{-1}$ at 2600°K and 122K cal $mole^{-1}$ at 2300°K. This involves so small a change of slope that it is less than the experimental error in drawing the curve, however, the best straight line through the points gives an average value for $E_{app.}$ over the range 2300-2600 of 117 $\pm$ 3 K cals $mole^{-1}$, which is also the mean value of $E_{app.}$ derived theoretically from equation 11.

From the graph. $\frac{R_{A(2600)}}{R_{A(2300)}} = 19.7$

3.9.3. Theoretical treatment of the atomisation of nitrogen on a hot tungsten filament

Two models of the dissociation mechanism are considered,

(1)

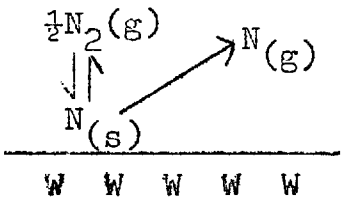

(2)

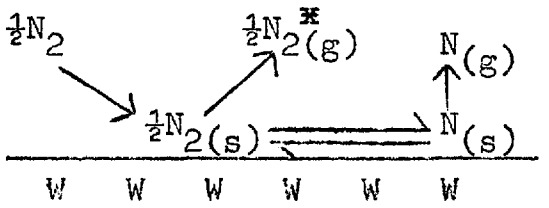

Nitrogen molecules in the gas are not in equilibrium with molecules on the surface of the hot filament. Molecules are adsorbed at 300°K and desorbed at $T_f > 2000°K$. A steady state approximation is made, (Nornes and Donaldson, 1966), in which the rate of adsorption of molecules is set equal to the rate of desorption of molecules. Model (2) therefore represents the system more properly, but it can be shown that a simple Polanyi-Wigner treatment of model (1) gives in practice essentially the same result as the more rigorous treatment given below using absolute reaction rate theorywith model (2).

(1) Rate of adsorption of molecules =

$$\frac{SP}{(2\pi mkTg)^{\frac{1}{2}}} \cdot (1 - \theta)^2 \text{ cm}^{-2}.\text{sec.}^{-1}$$

(2) Rate of adsorption of atoms =

$$\frac{S_A P_A}{(2\pi m_A kT_g)^{\frac{1}{2}}} \cdot (1 - \theta) \text{ cm}^{-2}.\text{sec}^{-1}$$

Experimental evidence indicates (2)<< (1) and the rate of adsorption of atoms is ignored.

The adsorbed layer is assumed immobile, i.e. we have site adsorption.

Rate of desorption of molecules

$$K = \frac{[N_{2\ddagger}]}{[N_s]^2} = \frac{f_{N_2}^{\ddagger}}{(fN_s)^2} \quad \exp. \frac{-\Delta H}{RT_f}$$

(3) $$\therefore R_M = \nu [N_{2\ddagger}] = \frac{kI_f}{h} \cdot \theta^2 n_s^2 \cdot \frac{fN_{2\ddagger}}{(fN_s)^2} \cdot \exp \frac{-\Delta H}{RT_f} \cdot$$

(where the weak vibration has been removed from $fN_2^{\ddagger}$).

[NOTE: Partition functions are given per cm^2 in all all cases. Some notes on the calculation of the partition functions are included at the end of this section].

Rate of desorption of atoms.

$$K_A = \frac{[N_{\ddagger}]}{[N_s]^2} = \frac{fN_{\ddagger}}{fN_s} \cdot \exp. \frac{-D(W - N)}{RT_f}$$

$$(4)\quad R_A = \nu\,[N_{\neq}] = \frac{kT_f}{h}\cdot\frac{fN_{\neq}}{fNs}\cdot\theta n_s\cdot\exp\frac{-D(W-N)}{RT_f}$$

$$(5)\quad \therefore \frac{R_M}{R_A} = \theta n_s\cdot\frac{fN_{2\neq}}{(fN_s)^2}\cdot\frac{fN_s}{fN_{\neq}}\cdot\exp.\left[\frac{-\Delta H + D(W-N)}{RT_f}\right].$$

$$\frac{fN_{2\neq}}{fN_s.fN_{\neq}} = \frac{5\times10^{21}}{8.9\times10^{18}\times 9.3\times10^{17}}$$

For $T_f = 3000^{o}K$, $\Delta H = 85$ K cal mole $^{-1}$

$D(N\equiv N) = 223$ K cal. mole^{-1}, $D(W-N) = 154$ K cal mole^{-1}.

Then $\left(\frac{R_M}{R_A}\right)_{3000} = \theta \times 0.59 \times 10^{5.0}$

$\therefore$ Moleculæs will predominate even at 3000^{o} unless θ is very small.

Calculation of coverage

We assume that the rates of adsorption and desorption of atoms are much less than the corresponding rates for molecules.

$$(6)\quad \therefore \frac{SP}{(2\pi mkT_g)^{\frac{1}{2}}}\cdot(1-\theta)^2 = \frac{kT_f}{h}\cdot\theta^2 n_s^{\,2}\cdot\frac{fN_{2\neq}}{(fN_s)^2}\exp.-\frac{\Delta H}{RT_f}$$

$$\frac{\theta}{1-\theta} = \frac{fN_s}{(fN_{2\neq})^{\frac{1}{2}}}\cdot\left(\frac{zsPh}{n_s^2kT_f}\right)^{\frac{1}{2}}\cdot\exp\frac{\Delta H}{2RT_f}\cdot$$

where $z = (2\pi mkT_g)^{\frac{1}{2}}$

$$(7)\ \therefore\ \theta = \frac{X}{1+X} \quad \text{where } X = \frac{fN_s}{(fN_2)^{\frac{1}{2}}} \cdot \frac{zsPh}{n_s kT_f}^{\frac{1}{2}} \cdot \exp. \frac{\Delta H}{2RT_f}$$

From (7); $\theta_{3000^oK} = 0.035$

$$\therefore \frac{R_M}{R_A} = 2 \times 10^3$$

$\therefore$ Our a priori assumptions are justified.

The full rate equation for atoms is (from [4])

$$(8)\ R_A = \frac{kT_f}{h} \cdot n_s \cdot \frac{fN_{\ddagger}}{fN_s} \cdot \frac{fN_s}{(f_{\ddagger}N_2)^{\frac{1}{2}}} \cdot \left(\frac{zsPh}{n_s^2 kT_f}\right)^{\frac{1}{2}} \exp. \left[\frac{\frac{\Delta H}{2} - D(W-N)}{RT_f}\right]$$

$$1 + \frac{fN_s}{(fN_{2\ddagger})^{\frac{1}{2}}} \cdot \left(\frac{zsPh}{n_s^2 kT_f}\right)^{\frac{1}{2}} \exp. \frac{\Delta H}{2RT_f} \cdot$$

In the limit of low coverage, when $\theta \ll 1$ or $X \ll 1$,

$$R_A = \frac{kT_f}{h} \cdot n_s \cdot \frac{fN_{\ddagger}}{fN_s} \cdot \frac{fN_s}{(f_{\ddagger}N_2)^{\frac{1}{2}}} \cdot \left(\frac{zsPh}{n_s^2 kT_f}\right)^{\frac{1}{2}} \exp. \left[\frac{-D(W-N) + \frac{\Delta H}{2}}{RT_f}\right]$$

If we put $C_{N_{2(g)}} = \frac{P}{kTg}$, we obtain equation (9)

$$(9)\ R_A = s^{\frac{1}{2}} \left(\frac{kT_f}{h}\right)^{\frac{1}{2}} \cdot \left(\frac{kT_g}{h}\right)^{\frac{1}{2}} \cdot C_{N_{2(g)}}^{\frac{1}{2}} \left(\frac{h^2}{2\pi mkT_g}\right)^{1/4} \cdot \frac{f_{\ddagger}N}{(f_{\ddagger}N_2)^{\frac{1}{2}}} \cdot$$

$$\exp. \left[\frac{-D(W-N) + \frac{\Delta H}{2}}{RT_f}\right]$$

Equation (9) is identical to equation (8) of Nornes and Donaldson (1966)

<u>An independent calculation of $\frac{R_M}{R_A}$ from considerations of equilibrium</u>

For a filament in equilibrium with a gas

$$R_{M(ads.)} = Z_M S_M P_{N_2} = R_M$$

and $$R_{A(ads.)} = Z_A S_A P_N = R_A$$

$$\frac{R_M}{R_A} = \frac{Z_M S_M P_{N_2}}{Z_A S_A P_N}$$

Data for the reaction

$\frac{1}{2}N_2 \rightleftharpoons N$ is given by Stull and Sinke (1956)

$$K_p = \frac{P_{N_g}}{(P_{N_{2g}})^{\frac{1}{2}}} \quad \text{(pressures in atm.)}$$

Converting the pressures to torr:

$$P_{N_g} = \sqrt{760} \cdot K_p \times p^{\frac{1}{2}}_{N_{2g}}.$$

$K_{p(3000)} = 1.38 \times 10^{-5}$

$K_{p(2000)} = 10^{-9}$ and for $P_{N_{2g}} = 10^{-2}$ torr.

$$\therefore \left(\frac{R_M}{R_A}\right)_{3000} = 264. \text{ cf. } 2\times10^3 \text{ by kinetic method}$$

$$\left(\frac{R_M}{R_A}\right)_{2000} = 3.62 \times 10^6 \text{ cf. } 2.97 \times 10^6 \text{ by kinetic method.}$$

Variation of activation energy for production of atoms under different conditions of temperature and pressure.

From equation (8), by taking logs and differentiating w.r.t. $\frac{1}{T_f}$, we have, to a first approximation,

$$(10)\quad \frac{d \ln R_A}{d\frac{1}{T_f}} = -\left[\frac{D(W-N)-\frac{\Delta H}{2}}{R}\right] \cdot \frac{f_{\ddagger} N \cdot \frac{fN_s}{fN_s}}{(f_{\ddagger} N_2)^{\frac{1}{2}} \left(\frac{zsPh}{n_s^2 kT_f}\right)^{\frac{1}{2}} \cdot \frac{\Delta H}{2R} \cdot \exp \cdot \frac{\Delta H}{2RT_f}}{1 + \frac{fN_s}{(f_{\ddagger} N_2)^{\frac{1}{2}}} \cdot \left(\frac{zsPh}{n_s^2 kTf}\right)^{\frac{1}{2}} \exp \cdot \frac{\Delta H}{2RT_f}}$$

whence the apparent activation energy for production of nitrogen atoms

$$(11)\quad E_{(app)} = D(W-N) - \frac{\Delta H}{2} + \theta \cdot \frac{\Delta H}{2} .$$

This equation demonstrates the effect of varying coverage on the apparent activation energy. The treatment of Nornes and Donaldson (1966) does not consider site adsorption, and so is incapable of demonstrating this. Calculated values of $E_{(app)}$ are shown below, (Table 6).

The two limiting cases are

when $1 \gg X$, i.e. $\theta \ll 1$ (low P, high T)

(12) $E_{(app)} = D(W\text{-}N) - \frac{\Delta H}{2} = \frac{1}{2}D(N\text{-}N)$

These conditions would appear to apply in the work of Nornes and Donaldson and Mimeault and Hansen.

When $1 \ll X$, i.e. $\theta \backsim 1$ (high P, low T)

(13) $E_{(app)} = D(W\text{-}N)$. (approx. 155 K cal mole^{-1})

Table 6 (for P = 2.5×10^{-2} torr)

$T^{o}K$	θ	$E_{(app)}$
2000	0.60	136 K cal.
2300	0.26	121
2600	0.10	115
3000	0.035	112

Total nitrogen take-up during the tungsten filament experiments.

Only a small fraction of the decrease in pressure during passage of current through the tungsten filament was due to adsorption on the nickel filament, the rest being due to adsorption on the walls of the cell. This part of the work was not done systematically as it was not intended to use these results when the experiments were planned.

Table 7

Run	T_f °K	Time (secs)	Decrease in press. $\times 10^3$ torr	mols.sec^{-1} ads.on cell	mols.sec^{-1} on 1 cm^2 of cell	mols.sec^{-1} on 1 cm^2 of Ni fil.
26	2530	60	0.9	1.14×10^{15}		
19	2450	150	1.5	7.6×10^{14}		
20	2450	120	1.2	7.6×10^{14}	2.2×10^{12}	5×10^{12}
10	2450	180	2.7	1.14×10^{15}		
12	2450	300	4.3	1.09×10^{15}		

Volume of system isolated during atomisation experiments = 2.26 litres

Volume of system isolated during desorption experiments = 1.16 litres

As the fall of pressure during atomisation was small compared with P, there is a large error in the McLeod gauge reading (estimated at 20-30%).

The experimental rate of production of atoms on tungsten at 2,450°K is thus about 1×10^{15} cm^{-2}. sec^{-1}. This is higher than that predicted by the theoretical rate equation by a factor of about 70. We do not yet have a satisfactory explanation for this, but it may be due to an additional mode of adsorption operating in parallel to that described. Gettering by evaporating tungsten atoms does not give a high enough rate, if it is

assumed one tungsten atom will remove one nitrogen atom. Another possibility is solution of nitrogen in the tungsten wire, as found by Nornes and Donaldson (1966). It should be noted that the experimental technique used in the present work for obtaining the activation energy for production of atoms is independent of the two side-effects just described, whereas the technique of Nornes and Donaldson does not have this advantage.

Discussion of atomisation on tungsten

Nornes and Donaldsons' observation that neither saturation nor recombination occurs on the glass surface can only be true for low coverages, because Mimeault and Hansen find that nitrogen atoms can diffuse through a glass system and be adsorbed on a clean filament when there is no unimpeded path between the adsorbing filament and the atom-generating filament. The present work also suggests that both saturation and recombination occur. In many of the runs a thin nickel film was present. As the curves in figure 40 show, a few minutes operation of the filament at $\sim$2400^{o}K in a pressure of 10^{-2} torr results in at least partial saturation. (This saturation condition appeared less at higher filament temperatures). Thus after this time the walls must have reached this

stage for all runs. These effects must be investigated further, but for the present we assume that, for a constant current and pressure, the amount adsorbed on the nickel filament was proportional to the length of time for which the current passed. The experimental results bore this out for $\theta < 0.5$ equally when the glass walls were clean or when covered with a nickel film. We further assume that the same fraction of atoms is intercepted by the nickel filament irrespective of the rate of atomisation as determined by the temperature of the tungsten filament. This is borne out experimentally:

(1) by the ratio of the rates of atomisation at two temperatures, 2300 and 2600°K, as determined by the experimental method which involves the above assumptions, agreeing well with the ratio predicted theoretically from absolute reaction rate theory.

(2) By the reproducibility of rates of adsorption at different temperatures even when successive run temperatures are selected in a random way.

Two observations of the dissociation of molecular nitrogen have recently been published in the literature (Nornes and Donaldson, 1966; Mimeault and Hansen, 1966). These papers are critically examined

and a treatment of the atomisation process using absolute reaction rate theory is presented which is at variance with the work of Mimeault and Hansen, but which includes the equation of Nornes and Donaldson for the rate of production of atoms as a special case, valid only in part of the pressure-temperature range.

In reference to the paper of Farber and Darnell (1953), (mentioned in Section 1.4.1.), who investigated the interaction of molecular nitrogen on a tungsten filament at temperatures up to 3000°K, but failed to discover any dissociation, it is important to assess their experimental method. Their means of detection of dissociation was by power dissipation at the tungsten wire. While this technique is adequate in the case of hydrogen where an appreciable percentage of the molecules striking the filament are dissociated, it is not so with nitrogen. As has been shown below, the corresponding fraction for nitrogen is ca. 0.01%. This would not be expected to produce a deviation in the power dissipation curve, and indeed one was not observed. It seems strange however that a fall in pressure was not observed.

Mimeault and Hansen (1966) present a treatment of atomisation of nitrogen on tungsten which, it is

believed, is both theoretically and experimentally unsound. Their technique (using iridium as adsorbent) is similar to that used in the present work. After dosing with a mixture of $^{28}N_2$ and $^{30}N_2$ they find (predictably) that the desorption peak from iridium shows the nitrogen isotopes have been completely scrambled. They maintain that this is evidence that nitrogen is present on iridium as a mobile layer of atoms just below the desorption temperature, when it is clear that scrambling must have occurred on the tungsten surface before the nitrogen atoms reached the iridium.

They obtain an effective activation energy of atomic nitrogen adsorption on iridium as $\frac{1}{4}D(N\equiv N)$ both experimentally and theoretically from a model assuming a steady state of nitrogen atoms in the gas phase due to recombination at the glass walls.

The method should be independent of the metal used, if, as seems reasonable from our results and those of Mimeault and Hansen, almost all incident atoms are adsorbed (at coverages < 0.5). In the present work with a nickel wire the activation energy is greater than $\frac{1}{2}D(N\equiv N)$, as predicted by an absolute rate treatment.

Mimeault and Hansen do not give full experimental details of their method of measurement of the temperature of the tungsten wire, but as this can only be a few cms.

long (as it is the filament of an ion gauge) the temperature variation along its length must be hundreds of degrees per cm. Whether optical pyrometer readings or resistance measurements were used the temperatures obtained cannot be meaningful.

Mimeault and Hansen's theoretical model is probably wrong in the step

(1) $N_{gas} \underset{}{\overset{K'}{\rightleftharpoons}} N_{Gl.}$ (adsorption on glass)

where there is probably no equilibrium

and in

(2) $2N_{Gl.} \xrightarrow{K''} N_{2(gas)}$ (Catalytic recombination)

which probably does not occur without heating.

The steady state is probably reached by

(3) $N_{(gas)} + N_{Gl.} \longrightarrow N_{2(gas)}$ which is the non-equilibrium interaction of a gas phase atom on an adsorbed atom on the glass.

Rate of recombination on glass $\left(\frac{-d\,N_g}{dt}\right)_G = Z.N_g\,N_G$

If N_G is almost constant (for which there is evidence for bombardment of nickel with nitrogen at $T_{fil} < 2400^oK$), the steady state equations of Mimeault and Hansen then becomes

$$P_{N_2}^{\frac{1}{2}} \cdot A.e^{\frac{-\Delta H_1}{RT}} = \text{constant} \times N_g.$$

As the rate of adsorption of nitrogen on iridium is assumed $\alpha\ N_g$, the effecting activation energy for adsorption is the activation energy for production of nitrogen atoms on tungsten (viz. $\frac{1}{2}$ D(N≡N)).

Note on partition functions used in the calculations

All partition functions used refer to 1 cm^2 of surface and are evaluated for $T = 2000^oK$.

Translational partition functions

$$f_{trans} = \left(\frac{2\pi mkT}{h^2}\right)^{\frac{1}{2}} \cdot \ell \quad \text{(1 degree of freedom)}$$

$$fN_{trans} = 9.65 \times 10^{8} \times \ell$$

$$fN_{2\ trans} = 1.36 \times 10^{9} \times \ell$$

Rotational partition functions

$$f_{rot} = \left(\frac{8\pi IkT}{2h^2}\right)^{\frac{1}{2}}$$ per site (1 degree of freedom)

$$fN_{2\ rot} = 13.2 \text{ per site}$$

Vibrational partition functions

$$f_{vib} = \frac{1}{(1 - e^{\frac{-h\nu}{kT}})}$$ (1 degree of freedom)

$\nu = 10^{12}\,sec^{-1}$ $\quad f_{vib} = 43.5$ per site

$\nu = 10^{13}\,sec^{-1}$ $\quad f_{vib} = 4.7$ per site

$\nu = 10^{14}\,sec^{-1}$ $\quad f_{vib} = 1.1$ per site

fN_s is assumed to contain 3 vibrations with frequencies $\nu = 10^{13}, 10^{12}, 10^{12}$.

$\therefore$ $fN_s = 8.9 \times 10^{3}$ per site

$fN_s = \underline{8.9 \times 10^{18}\ cm^{-2}}$

$f\ddagger N$ contains 2 degrees of translational freedom

$\therefore$ $f\ddagger N = \underline{9.3 \times 10^{17}\ cm^{-2}}$

$f\ddagger N_2$ contains 2 translational

1 rotational

and 2 vibrational ($\nu = 10^{13}, 10^{12}$) degrees of freedom

$$f\ddagger N_2 = 5 \times 10^{21}\ cm^{-2}.$$

or it may contain 2 translational
2 rotational
and 1 vibrational ($\nu = 10^{13}$)
degrees of freedom

Then $f_{\neq N_2} = 1.51 \times 10^{21}$ cm^{-2}.

3.10 The argument against carbon monoxide being responsible for either peak of the desorption spectrum.

It is important to examine the possibility of contamination by carbon monoxide for the following reasons:-

(1) The adsorption heat of CO on nickel (40 K cals $mole^{-1}$) is about right to explain the first desorption peak.

(2) Mimeault and Hansen (1966) found that the first peak, (low temperature; not specified), of their desorption spectrum of nitrogen (activated by a hot tungsten filament) on iridium was attributable to CO.

(3) Energetic electrons, nitrogen atoms or ions may desorb CO from the glass walls.

(4) The same energetic species may desorb O_2 and H_2O from the glass walls which will then adsorb onto the nickel filament. When the filament is heated, and if it contains some carbon impurity, CO may then be desorbed.

(5) Carbon very probably occurs in nickel manufactured by the Mond process. No analysis figure is given for carbon as the analysis technique uses an arc struck between carbon electrodes.

(6) Evidence has been presented for the diminution in

size of the first peak during a series of runs with a new filament. This could be ascribed to the effect of depletion of carbon in the filament, or of oxygen on the glass walls.

Argument against carbon monoxide contamination

In discharge experiments	In W filament experiments
(1) N_2 from NaN_3 analysed with mass spectrometer. Free from CO, O_2.	N_2 from NaN_3 analysed with mass spectrometer. Free from CO .O_2.
(2) Dummy run with N_2 but no discharge: no desorption peak.	Dummy run with N_2 but no W filament current: no desorption peak.
(3) Dummy run with discharge power on but no N_2; no desorption peak.	Dummy run, W. filament at 2600°K but no N_2 ($P < 10^{-7}$torr); no desorption peak.
(4) Desorbed gas analysed C^+_{12} with mass spec., and not detected.	-
(5) An oxidised nickel filament, reduced with H_2 gives larger ΔP_1.	-

(6) Adsorbed rare gases were desorbed in a single peak. –

The desorption spectrum in these experiments was very similar to that in the discharge experiments. Therefore the implication of points (4), (5) and (6) applies by analogy.

3.11 Measurement of the activation energy of desorption of activated nitrogen adsorbed on a nickel filament

The method of operation of the filament controller has been described in sections 2.15.2 and 3 (p.68). The nickel filament was dosed with activated nitrogen in the usual way, and the glass walls of the cell heated to 80°C to remove the low energy states on the glass. The current and voltage recorders were synchronised and started and the filament was switched into the Kelvin bridge of the controller and a comparison resistance selected on the control panel.

As gas was evolved from the filament (the pressure being recorded on a third recorder) the control resistor was abruptly raised, the Kelvin bridge was unbalanced, and the out of balance current, suitably amplified, heated the nickel filament rapidly to the new selected resistance and temperature. At the same time there is an abrupt change in rate of desorption of gas at the filament.

$$(\text{rate})_{T_1} = k.f(c).\ \exp\ \frac{-\Delta E}{RT_1}$$

and $$(\text{rate})_{T_2} = k.f(c).\ \exp\ \frac{-\Delta E}{RT_2}$$

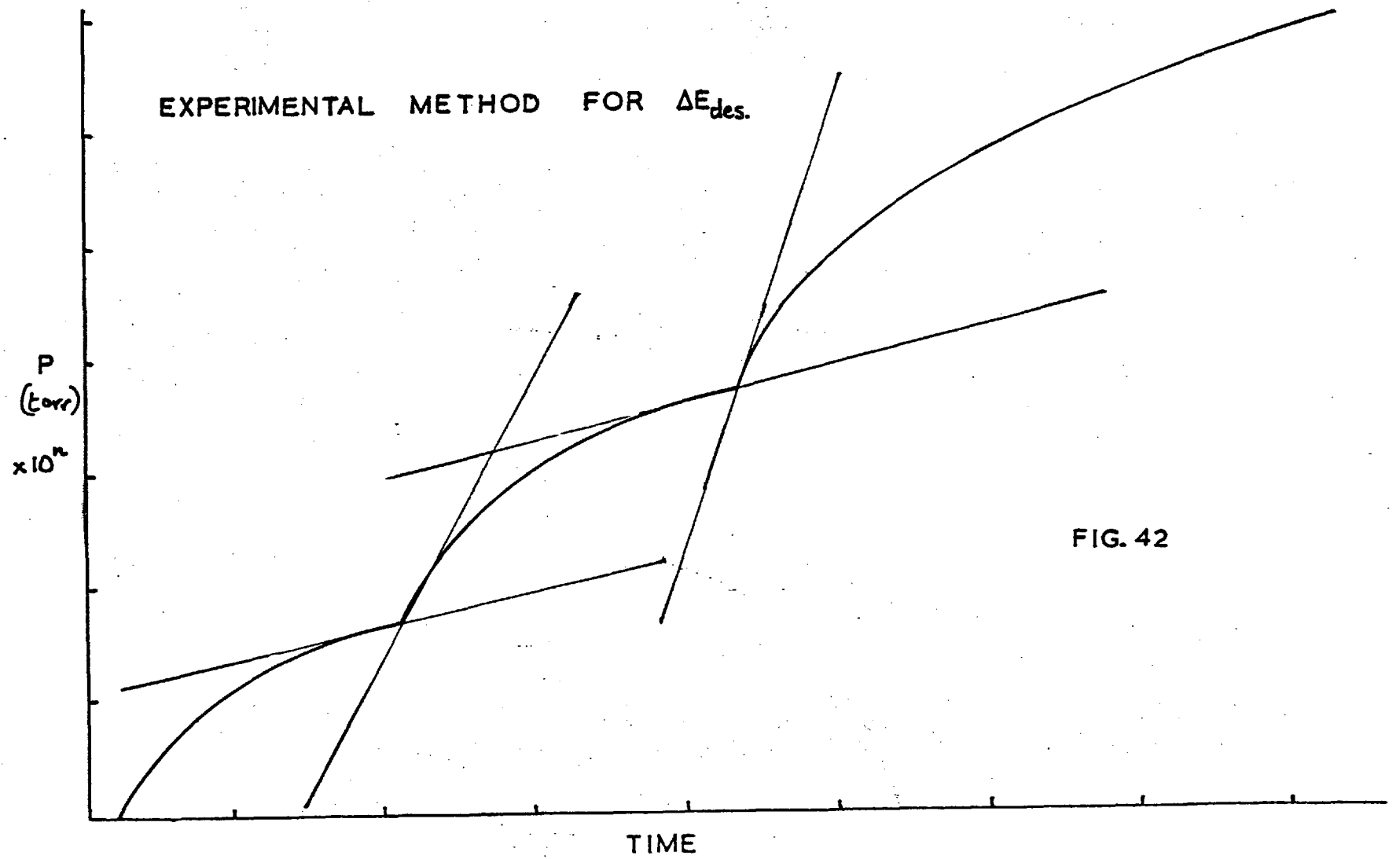

FIG. 42

whence $\Delta E = 2.303\ R \log_{10} \frac{r_2}{r_1} \cdot \frac{T_1 T_2}{T_2 - T_1}$

Thus although the concentration of reacting species (and the reaction order) are unknown, if we assume that f(c) does not appreciably change during the time required to determine experimentally the desorption rates, we may obtain a value for the activation energy of desorption. To determine these rates, tangents are drawn to the pressure time curve, as shown in figure 42.

By raising the filament temperature in a series of jumps in this manner a set of values of the activation energy at different coverages was obtained.

Measurement of filament temperature was described in section 2.15.5, (p.76). The results for the activation energy of desorption from nickel of discharge activated nitrogen are shown in figure 43 and of nitrogen activated by a hot tungsten filament in figure 44.

The scatter of the points is large both because of errors in measurement of the rate and of the temperature. The filament controller was not specifically designed to heat a filament of the characteristics of the nickel filaments used, and during the time taken to reach a higher temperature

(ca. 15 seconds) it may well be that f(c) is significantly altered.

FIG.43

ΔE_{des} FROM Ni OF DISCHARGE

ACTIVATED NITROGEN

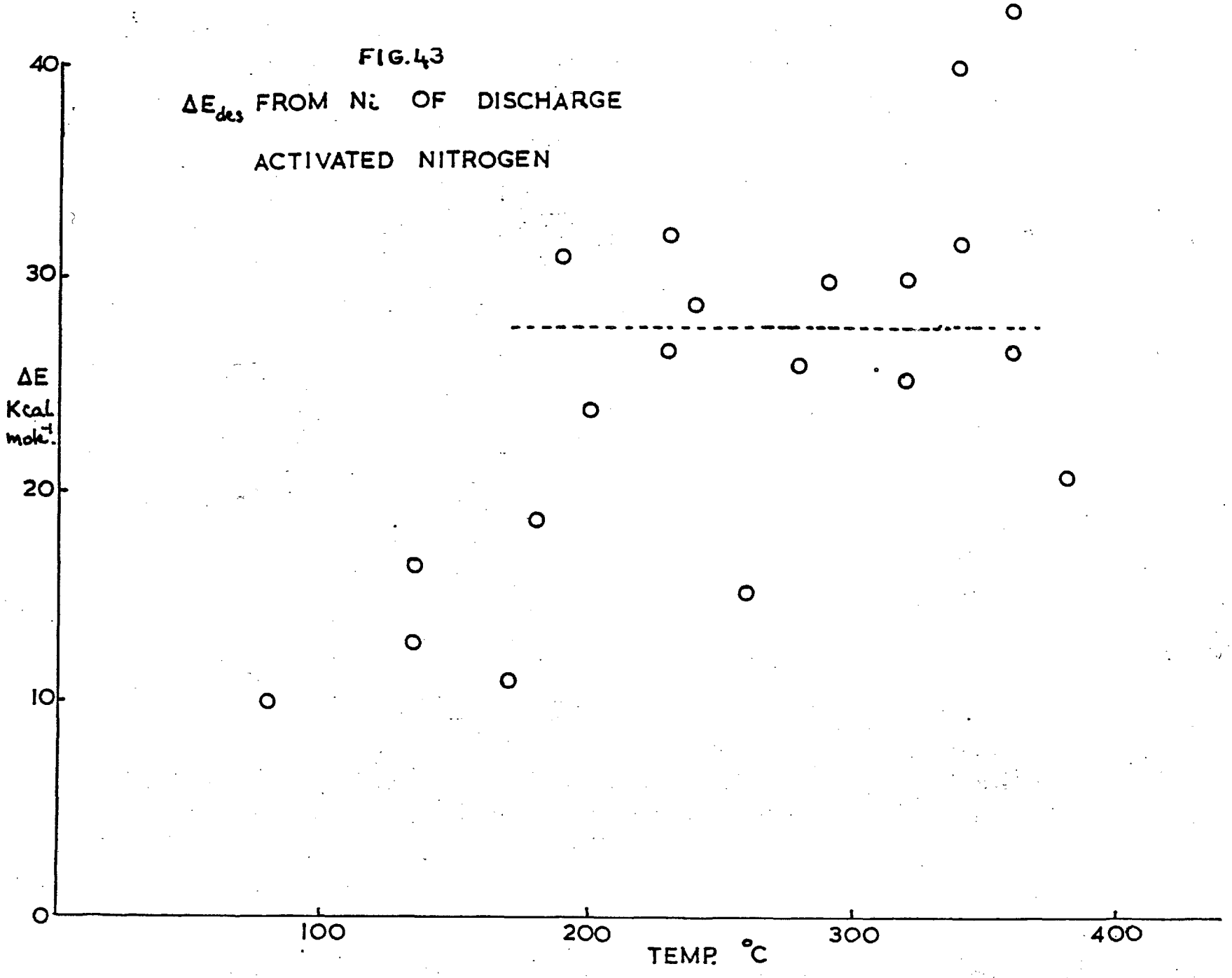

FIG. 44

$\Delta E_{des.}$ FROM Ni FILAMENT OF NITROGEN ACTIVATED ON A W FILAMENT.

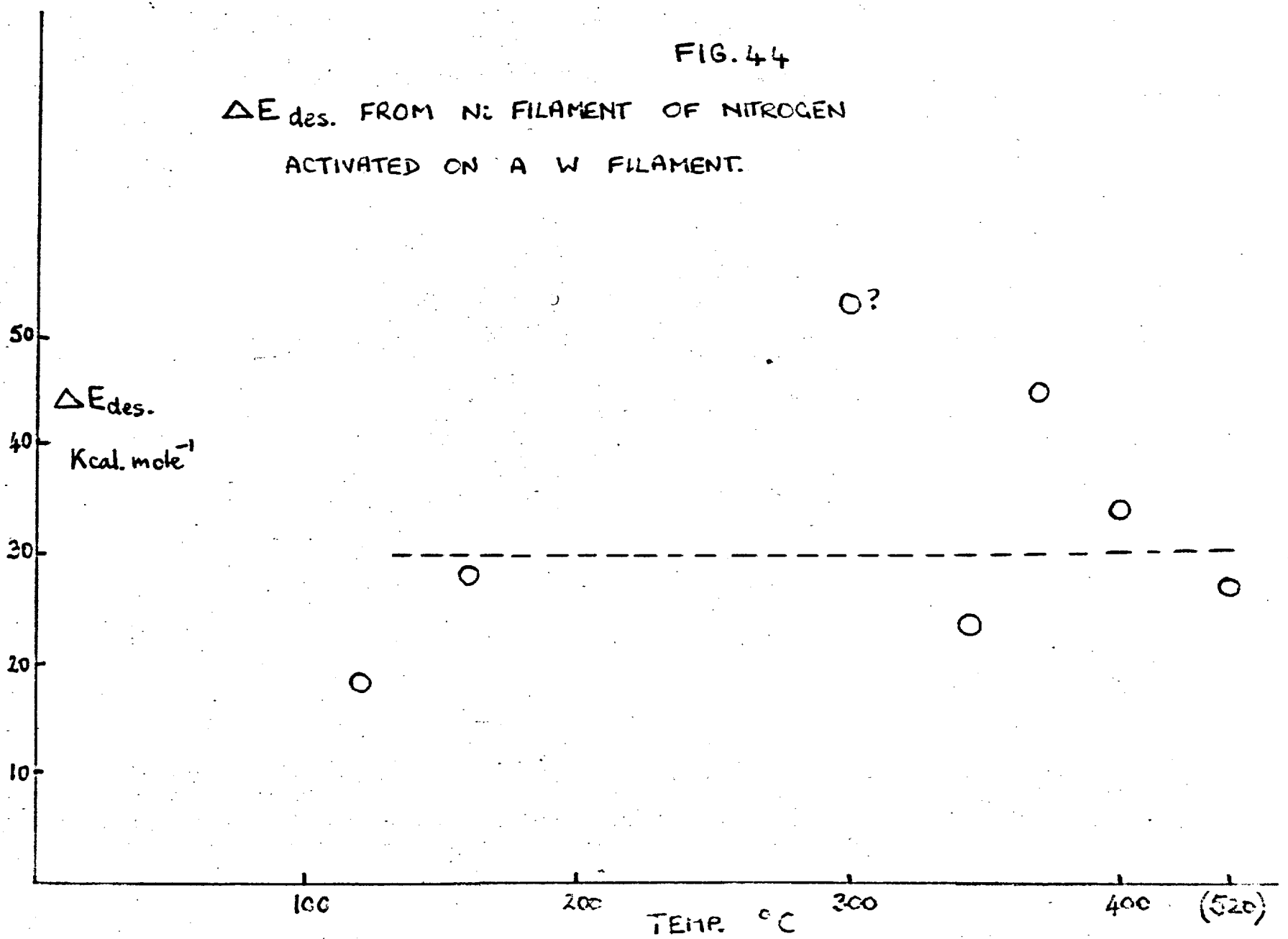

3.12 Conclusions on the nickel-nitrogen system.

Nitrogen atoms produced on a hot tungsten filament have been found to chemisorb onto films and filaments of nickel.

Desorption spectra following adsorption on nickel of discharge-activated nitrogen and nitrogen atomised on tungsten are so markedly similar in desorption temperature, activation energy of desorption, and to a lesser extent, in population density of states, that it is inferred that the same surface complexes are produced in both cases, and that these consist of atomic nitrogen.

Section 1 described the facility with which predissociation can occur in the nitrogen system, and it is postulated that neutralisation of a N_2^+ ion from the discharge activated nitrogen results in the release of sufficient energy to dissociate the molecule, which is then chemisorbed as atoms.

This is supported by the fact that low energy N_2^+ ions, impinging on a metal surface, give a surprisingly low yield of Auger electrons. This is explained if all of the energy released in a neutralisation transition is not absorbed by an electron, but a fraction is transferred to excitation of the adsorbed molecule enabling it to dissociate. Low

energy Auger electrons have a higher probability of scattering from electrons in adsorbed molecules and thereby producing electronic excitation.

The nitrogen atoms taken up by the nickel may exist in a genuine chemisorbed state on the surface, as a subsurface compound, or as a uniform solid solution throughout the metal. The last possibility can probably be dismissed as in this work, and that of Sieverts and Krumbhaar (1910) solution could not be detected even at temperatures up to 1500°K, indicating that the equilibrium for the reaction

$$\frac{x}{2}\ N_2 + yNi \rightleftharpoons Niy\ Nx \text{ (solid solution)}$$

must be well over to the left hand side.

The reaction between nitrogen molecules and nickel is probably endothermic, or slightly exothermic. This work is unable to distinguish between these possibilities.

The activation energy for desorption was found to be 28 ± 10 K cals $mole^{-1}$.

Examination of the properties of nickel nitride, Ni_3N, reveals several interesting parallels

(1) The heat of formation from the elements at 20°C = 0.2 ± .1 K cal $mole^{-1}$. (Hahn and Konrad, 1951), i.e. virtually zero. Nickel nitride is one of many examples in nitrogen chemistry of a thermodynamically unstable compound existing at normal temperatures. This special feature of nitrogen chemistry is a consequence of the unique bond strength and stability of the N≡N molecule.

(2) Mathis (1951) estimates the temperature of onset of decomposition to be 290°C, and Trillat et al. (1957) describe an increase in magnetic susceptibility occuring at 250°C. In the present work the second desorption peak (comprising 90-99% of the total gas) started to evolve at 250°C and the rate rapidly increased in the range 250-300°C.

(3) Trillat (1957) and Terao (1959) describe the expansion of the nickel f.c.c. lattice at 150-175°C in the presence of ammonia. At 175°C the hexagonal form of Ni_3N is obtained. In the present work the first desorption peak occurred at 150-180°C.

(4) From Mathis' results it is possible to calculate the activation energy for decomposition of Ni_3N obtained in his system. This has been done, see figure 45 and $E_{act.} = 25.5$ K cals $mole^{-1}$.

The activation energy of desorption in this work was found to be 28 ± 10.

From this comparison it is maintained that a close analogy exists between bulk Ni_3N and the nickel nitrogen surface states observed here.

The larger second peak is identified with nitrogen atoms which have penetrated below the first layer of nickel atoms and are occupying interstitial positions in the nickel lattice. Where the coverage rises to several monolayers (as in the case with the discharge activated gas, and with the tungsten filament experiments at the higher temperatures), it is postulated that penetration occurs to several monolayers depth.

The long 'tail' observed during desorption even at high temperatures (> 700°C) may be due to nitrogen atoms diffusing into the bulk, or to the effusion of atoms which were deeply buried by a channelling mechanism, (Zscheile, 1966).

It is postulated that the take-up of nitrogen atoms onto nickel at 20°C is not properly ordered.

FIG. 45

$\Delta E_{diss.}$ OF Ni_3N CALCULATED FROM MATHIS' DATA

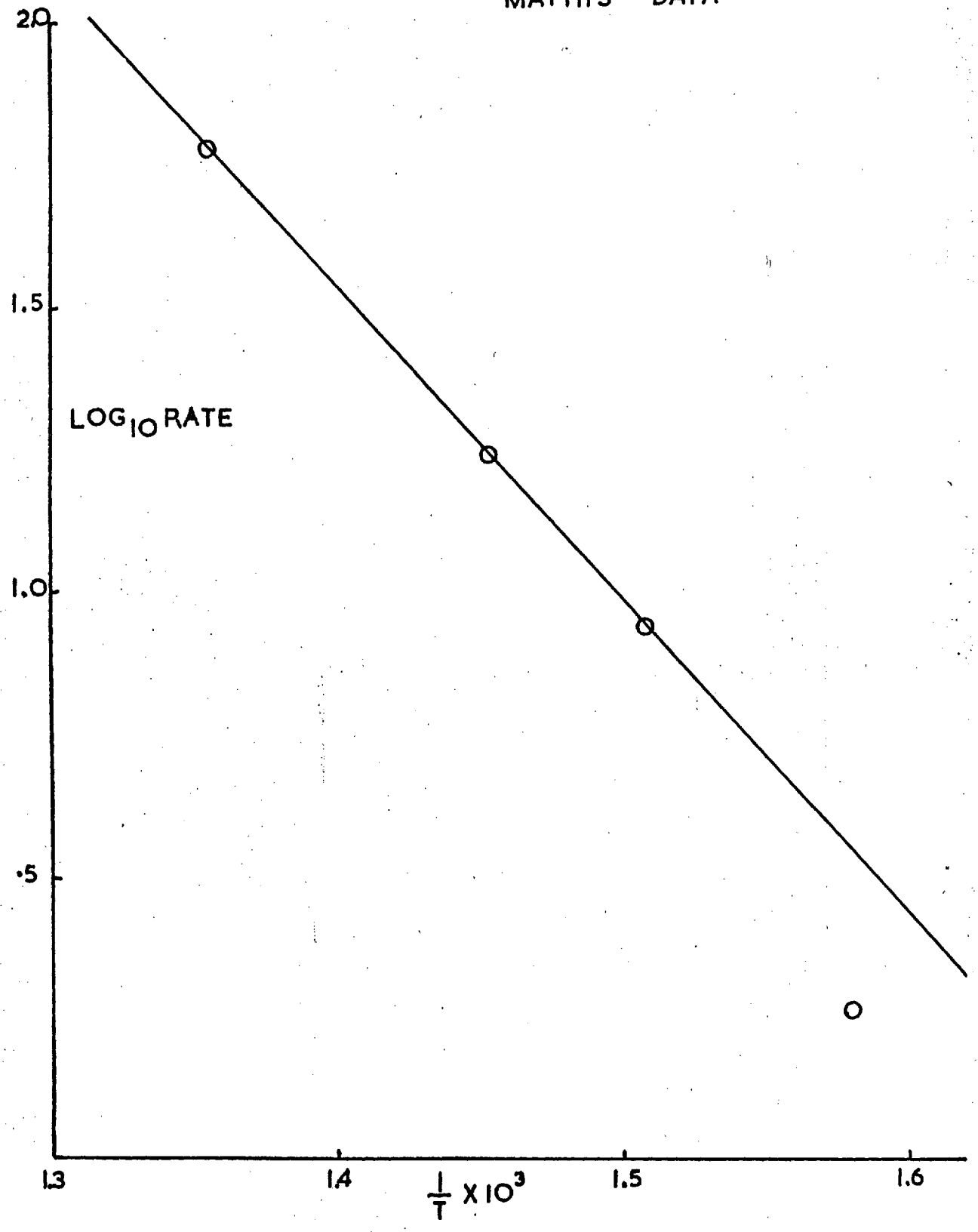

Method of Activation	Substrate	Adsorption in 60 secs. (molecules)	No. of mols. in 1st peak	$\frac{\Delta P_1}{\Delta P_2}$	Area of substrate cm^2	Rough-ness factor	Coverage (mono-layers)
Discharge	Glass	$1x10^{18}$	-	-	500	2	1.5
Discharge	Ni film	$3x10^{18}$	$3x10^{17}$	10%	340	2 - 4	7 - 3
Discharge	Ni filament	$8.4x10^{16}$	$1.26x10^{14}$	0.6%	6.25	1.4	9
Discharge	roughened Ni filament	$4.3x10^{16}$	$2.4x10^{15}$	5.5%	6.25	?	
W filament	Ni filament	$5x10^{15}$	$8x10^{13}$	1.6%	6.25	1.4	0.8

At 150°C the nickel atoms possess enough energy to relax the normal interatomic distances of the nickel f.c.c. lattice. This enables most nitrogen atoms to take up metastable equilibrium positions corresponding in the limit to the octahedral coordination of Ni_3N, while a small proportion of N atoms near the surface or perhaps held in corners or multi coordinate sites in the surface are able to escape.

Figure 46 shows the dependence of ΔP_1 on ΔP_2 in the case of the W filament experiments. In terms of the postulated model we may say that when the coverage < 0.5 of a calculated monolayer there are plenty of free sites for nitrogen atoms in which to assume their metastable positions at 150-180°C. If the coverage is higher there is more chance of two nitrogen atoms combining to form a molecule and being desorbed during the lattice rearrangement.

The metastable N atoms remain in interstitial positions in the lattice until at 350°C their thermal energy enables a significant number to surmount the activation energy barrier and desorb irreversibly.

No exact comparison can be made for the interrelation of ΔP_1 and ΔP_2 in the case of the discharge experiments as no experiments were done with low enough coverages. Evidence is provided that ΔP_1 is

FIG. 46

DEPENDENCE OF FIRST DESORPTION PEAK ON SECOND

(NITROGEN : W FIL. : Ni FIL.)

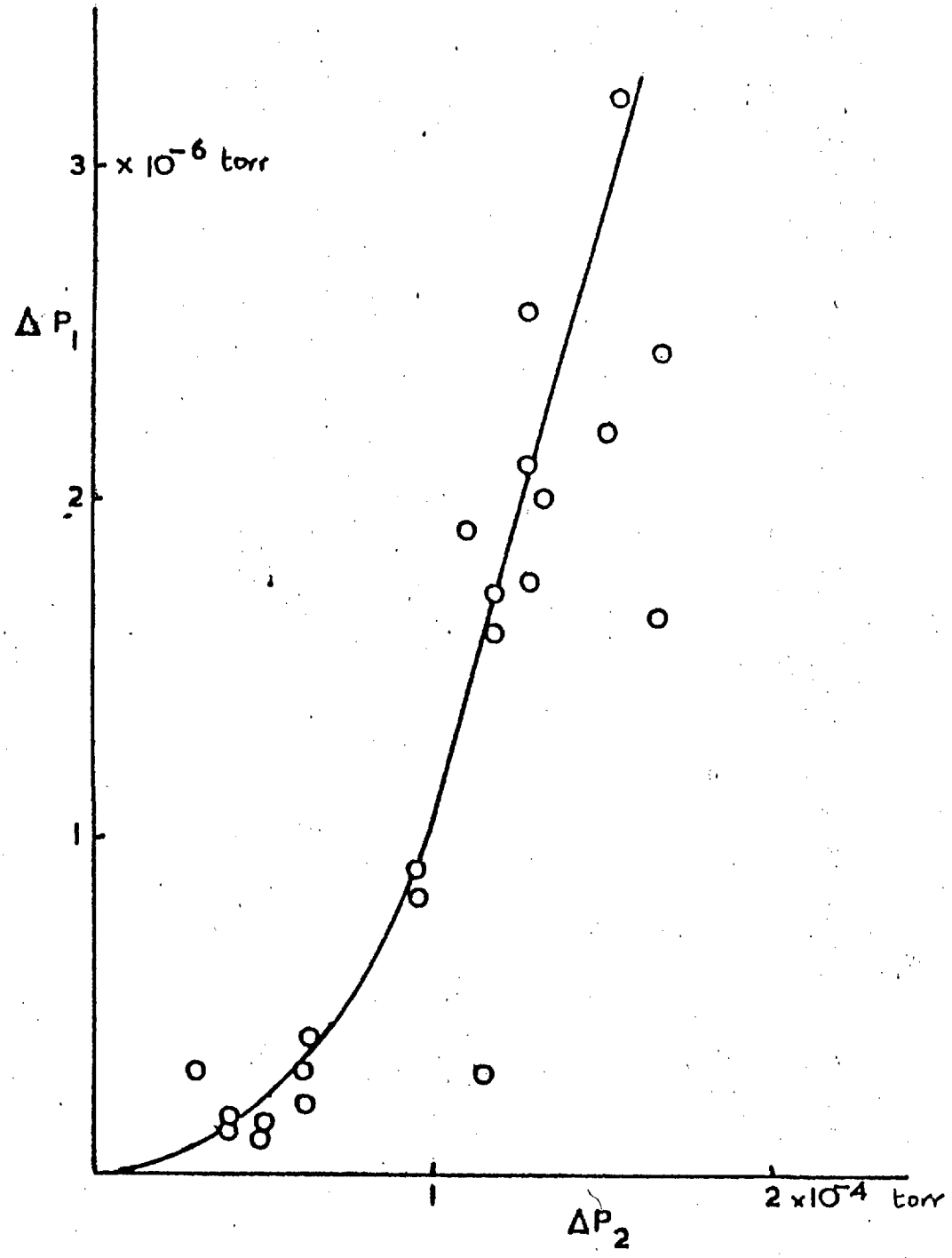

associated with the surface layer and perhaps with multi coordinate sites by the experiment with a roughened filament in which ΔP_1 was greatly increased.

The activation energy for desorption of the surface states, and also of decomposition of bulk Ni_3N appears too low for a state only starting to desorb appreciably at 250°C. As qualititative explanation of this an analogy is made with the treatment of Delchar and Tompkins for the incorporation of oxygen into the nickel lattice. Here also, the experimental rate is much lower than examination of the activation energy and system temperature would suggest. The explanation offered is that oxygen atoms only move when four nickel atoms in the plane through which the oxygen atom is passing move outwards simultaneously along the diagonals of a rectangle. The probability of this occurring is low, and therefore so is the rate of diffusion.

APPENDIX I

Rates of atomization of nitrogen on a tungsten filament

Area of W fil. = $1.25cm^2$. Area of Ni fil. = $6.25cm^2$

Isolated volume during desorption = $1,150cm^3$.

Run No.	Dosing Press (torr)	Time (secs)	Current (A)	Tf. (^oK)	Desorption from Ni 1st peak(ΔP_1) (torr)	Total (torr)
1	$2.5x10^{-2}$	60	4.4		-	$4.5x10^{-5}$
2	$2.5x10^{-2}$	60	4.5	2443	$1.5x10^{-7}$	$6.0x10^{-5}$
N.C.X 3	$2.5x10^{-2}$	60	4.5	2443	$1x10^{-7}$	$1.8x10^{-4}$
4	$2.5x10^{-2}$	60	4.5	2443	$1x10^{-7}$	$4.2x10^{-5}$
5	$2.5x10^{-2}$	60	4.5	2443	$1x10^{-7}$	$4.35x10^{-5}$
6	$2.4x10^{-2}$	60	4.5	2443	$3.8x10^{-7}$	$6.4x10^{-5}$
7	$2.3x10^{-2}$	60	4.5	2443	$1.9x10^{-7}$	$6.15x10^{-5}$
8	$2.4x10^{-2}$	60	4.5	2443	$1.3x10^{-7}$	$4.1x10^{-5}$
9	$2.4x10^{-2}$	120	4.5	2443	$3.0x10^{-7}$	$1.19x10^{-4}$
10	$2.3x10^{-2}$	180	4.5	2443	$2.8x10^{-7}$	$1.47x10^{-4}$
N.C.X = filament supports not cooled						
11	$2.3x10^{-2}$	60	4.5	2443	$3.2x10^{-7}$	$6.2x10^{-5}$
12	$2.3x10^{-2}$	240	4.5	2443	$2.2x10^{-6}$	$1.51x10^{-4}$
13	$2.4x10^{-2}$	420	4.5	2443	$1.75x10^{-6}$	$1.28x10^{-4}$
14	$(2x10^{-7})$	90	4.5	2443	$< 1x10^{-7}$	

Run No.	Dosing Press (torr)	Time (secs)	Current (A)	Tf. (^{o}K)	Desorption from Ni 1st peak(ΔP_1) (torr)	Total (torr)
15	2.4×10^{-2}	-	-	293	$< 1\times10^{-7}$	6×10^{-7}
16	2.4×10^{-2}	30	4.5	2443	1.5×10^{-7}	4.35×10^{-5}
17	2.3×10^{-2}	15	4.5	2443	3.2×10^{-7}	2.94×10^{-5}
18	2.3×10^{-2}	300	4.5	2443	3.2×10^{-6}	1.54×10^{-4}
19	2.13×10^{-2}	150	4.5	2443	2.1×10^{-6}	1.28×10^{-4}
20	2.24×10^{-2}	120	4.5	2443	1.9×10^{-6}	1.1×10^{-4}
21	2.15×10^{-2}	60	4.0	2275	-	4.5×10^{-7}
22	2.13×10^{-2}	60	4.0	2275	-	2.56×10^{-7}
23	2.13×10^{-2}	180	4.0	2275	-	1.1×10^{-6}
24	2.07×10^{-2}	180	4.3	2376	-	1.67×10^{-5}
25	2.07×10^{-2}	90	4.3	2376	-	1.28×10^{-5}
26	2.55×10^{-2}	60	4.75	2530	1.6×10^{-6}	1.66×10^{-4}
27	2.55×10^{-2}	30	4.75	2530	8.2×10^{-7}	9.6×10^{-5}
28	2.75×10^{-2}	90	4.15	2325	7×10^{-8}	3.97×10^{-5}
29	2.75×10^{-2}	90	3.90	2241	-	9.0×10^{-7}
30	2.75×10^{-2}	60	4.30	2376	1.3×10^{-7}	5.45×10^{-5}
31	2.70×10^{-2}	30	4.65	2496	9×10^{-7}	9.6×10^{-5}
32	2.70×10^{-2}	45	4.65	2496	1.6×10^{-6}	1.19×10^{-5}
33	2.70×10^{-2}	120	4.30	2376	-	8.3×10^{-5}
34	2.70×10^{-2}	180	4.15	2325	-	3.97×10^{-5}
35	2.75×10^{-2}	-	-	-	-	-
36	2.75×10^{-2}	120	4.5	2443	1×10^{-7}	5.12×10^{-5}

Run No.	Dosing Press (torr)	Time (secs)	Current (A)	Tf. (^{o}K)	Desorption from Ni 1st Peak(ΔP_1) (torr)	Total (torr)
37	2.75×10^{-2}	120	4.5	2443	2.56×10^{-6}	1.28×10^{-4}
38	2.56×10^{-2}	120	4.5	2443	1.73×10^{-6}	1.19×10^{-4}
39	2.37×10^{-2}	120	4.5	2443	1.99×10^{-6}	1.33×10^{-4}
40	2.37×10^{-2}	180	4.0	2275	-	2.18×10^{-5}
41	2.37×10^{-2}	270	4.0	2275	-	2.56×10^{-6}
42	2.37×10^{-2}	120	4.1	2308	-	1.28×10^{-5}
43	2.37×10^{-2}	120	4.1	2308	-	1.67×10^{-5}
44	2.37×10^{-2}	120	4.1	2308	-	-
45	2.37×10^{-2}	30	5.0	2617	2.18×10^{-6}	2.0×10^{-4}
46	2.20×10^{-2}	150	4.1	2308	-	-
47	3.38×10^{-2}	120	4.5	2443	2.43×10^{-6}	1.67×10^{-4}
48	3.35×10^{-2}	15	5.0	2617	-	1.64×10^{-4}
49	3.2×10^{-2}	12	5.0	2617	-	1.38×10^{-4}
50	3.2×10^{-2}	90	5.0	2617	-	2.75×10^{-4}

APPENDIX II

Construction of a valve-voltmeter

A simple valve-voltmeter was constructed for use with the filament controller. The circuit is shown overleaf. The instrument was calibrated and shown to be linear over all three voltage ranges. However, in use with the filament controller, its response deviated markedly from linearity due to some incompatibility in the two circuits. The stability of the controller was also affected. Thereafter voltages were directly recorded as described in Section 2.15.4.

SIMPLE VALVE-VOLTMETER

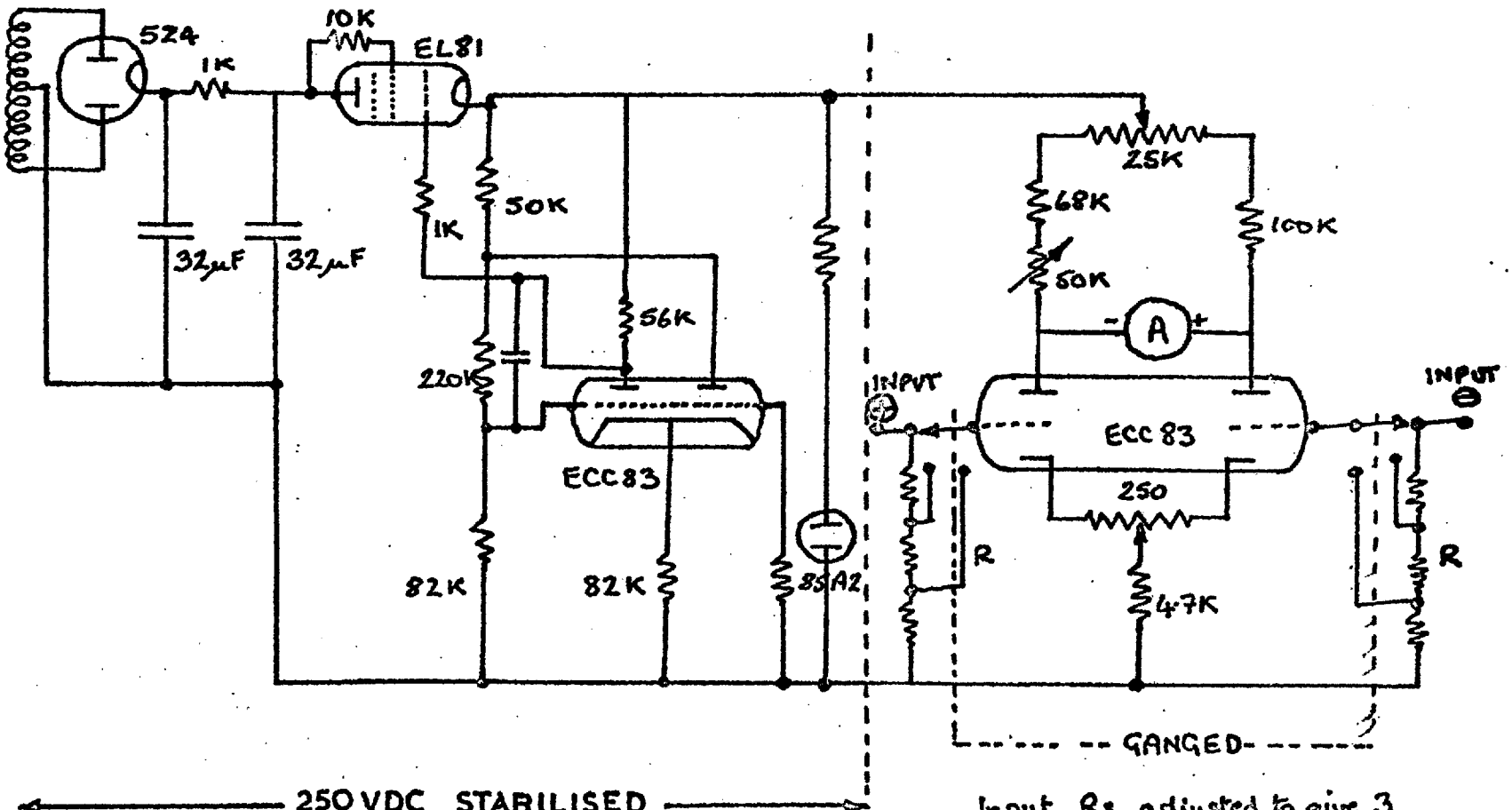

Input Rs adjusted to give 3 ranges of 0.25, 1·0, 2·5 V f.s.d. total R = 4·75 MΩ approx.

FIG. 47

References

Ackley J.W., Lothrop, C.F., and Wheeler, W.R.,
9th Nat. Vac. Symp., 492, (1962)

Allan, R.G.W., and Lang, B,
Vacuum 13, 359, (1963).

Anderson, P.A.,
Phys. Rev. 47, 958, (1935)

Bayard, R.T., and Alpert, D.,
Rev. Sci. Instr. 23, 571, (1950)

Becker, J.A., and Hartmann, C.D.,
J. Phys. Chem. 57, 153, (1953)

Beeck, O., Smith, A.E., and Wheeler, A.,
Proc. Roy. Soc. A177, 62, (1941)

Berkowitz, J., Chupka, W.A., and Kistiakowsky, G.B.,
J. Chem. Phys. 25, 457, (1956)

Blodgett, K.B., and Vanderslice, T.A.,
J. Appl. Phys. 31, 1017, (1961)

Bowden, P., and Brandon, D.G.,
Phil. Mag., 8, 935, (1963)

Broida, H.P., and Lutes, O.S.,
J. Chem. Phys. 24, 484, (1956)

Brown, F., and Davies, J.A.,
Can. J. Phys. 41, 844, (1963)

Campbell, I.M., and Thrush, B.A.,
Proc. Roy. Soc. A296, 201, (1966)

Carmichael, J.H., and Knoll, J.S.,

Trans. Nat. Vac. Symp. 5, 18, (1958)

Carter, G.,

Vacuum 9, 190, (1959)

Carter, G., and Leck, J.M.,

Proc. Roy. Soc., A261, 303, (1961)

Carter, G., Colligon, J.S., and Leck, J.M.,

Proc. Phys. Soc. 79, 299, (1962)

Carter et al. (1962) see Smeaton, Carter and Leck (1962).

Colligon, J.S., and Leck, J.M.,

8th Vac. Symp. 275, (1961)

Dekker, R.W.,

J. Appl. Phys., 25, 1441, (1954)

Delchar, T.A., and Tompkins, F.C.,

Gen. Elec. Rep. (1966)

Dushman, S.,

"The Production and Measurement of high vacua,"

Gen. Elec. Rev. (1922)

Dushman, S.,

Vacuum Techniques, 333, (1949)

Dushman, S., and Lafferty, J.M.,

Scientific Foundations of Vacuum Technique,

2nd ed. p.87, (1961)

Ehrlich, G., and Hudda, F.G.,

J. Chem. Phys. 35, 1421, (1961)

Ehrlich, G.,

Adv. in Catalysis 14, 391, (1963)

Eischens, R.P., and Jacknow, J.,

in " Proc. 3rd Int. Congress on Catalysis"

N-Holland, Amsterdam, p.641. (1965)

Espe, W.,

" Materials of High Vacuum Technology" Vol.1.

Metals and Metalloids, (Pergamon) (1966)

Farber, M., and Darnell, A.J.,

J. Chem. Phys., 21, 172, (1953)

Farnsworth, H.E., Schlier, R.E., George, T.H., and

Burger, R.M.,

J. Appl. Phys., 26, 252, (1955)

Farnsworth, H.E., and Tuul, J.,

J. Phys. Chem. Solids, 9, 48, (1958)

Foner, S.N., and Hudson, R.L.,

J. Chem. Phys. 37, 1662, (1962)

Gaede, W.,

Ann. Phys., Lpz., 46, 357, (1915)

Germer, L.H., Scheibner, E.J., and Hartmann, C.D.,

Phil. Mag. [8], 5, 222 (1960)

Gilmore, F.R.,

J. Quant. Spec. Rad. Transfer 5, 369, (1965)

Gmelin

Handbuch der Anorg. Chem., System 59, Nickel,

Part D2, p.253, (1959)

Gomer, R.,

J. Chem. Phys. 21, 293, (1953)

Gomer, R., and Zimmerman, D.,

Rev. Sci. Instr. 36, 1046, (1965)

Groth, W., and Warneck, P.,

Z. Physik. Chem. 10, 523 (1957)

Gundry, P.M.,

in " Actes du 2me Congres International de Catalyse", Vol.1, Paris, p.1083, (1961)

Gundry, P.M., Haber, J, and Tompkins, F.C.,

J. Catalysis 1, 363, (1962)

Hagstrum, H.D.,

Phys. Rev. 104, 317, (1956)

Hahn, H., and Konrad, A.,

Z. Anorg. Allgem. Chem. 264, 181, (1951)

Hayward, D.O., and Trapnell, B.M.W.,

" Chemisorption" Butterworths, London (1964)

Hayward, D.O., King, D.A., and Tompkins, F.C.,

(In press) (1966)

Hemstreet, R.A., and Hamilton, J.R.,

J.Chem. Phys. 34, 948, (1961)

Herzberg, G.,

in " Molecular Spectra and Molecular Structure: Part I: Diatomic moleclues" Van Nostrand., New York, (1950)

Hickmott, T.W. and Ehrlich, G.,

J. Phys. Chem. Solids, 5, 47, (1958)

Hildebrandt, A.F., Barth, C.A., and Booth, F.B.,

Planetary Space Sci., 3, 194, (1961)

Holland, L.,

" The Properties of Glass Surfaces" (Chapman and Hall), p. 277 (1966)

Ishii, H., and Nakayama, K.,

Trans. 8th. Nat. Vac. Symp., 519, (1961)

Jackson, D.S., and chiff, H.I.,

J. Chem. Phys. 21, 2233, (1953)

Jackson, D.S., and Schiff, H.I.,

J. Chem. Phys. 23, 2333, (1955)

James, L.H., and Carter, G.,

Trans. Nat. Vac. Symp. 9, 502, (1962)

Jansen, C.G.J., and Venema, A.,

Vacuum, 9, 219 (1959)

Jennings, K.R., and Linnett, J.W.,

Quart. Revs., 12, 116, (1958)

Jones, H.A., and Langmuir, I.,

Gen. Elec. Rev. 30, 310, (1927)

Juza, R., and Hahn, H.,

Z. Anorg. Allgem. Chem. 241, 172, (1939)

King, D.A.,

Disc. Far. Soc. 109, (1966)

Klemperer, O.,

J. Sci. Inst. 21, 88, (1944)

Knewstub, P.F., and Tickner, A.W.,

J. Chem. Phys. 37, 2941, (1962)

Kokes, R.J., and Emmett, P.H.,

J. Am. Chem. Soc. 82, 1037, (1960)

Kornelsen, E.V.,

8th Nat. Vac. Symposium p.281, (1961)

Langmuir, I., and Taylor, J.B.,

Phys. Rev., 50, 68, (1936)

Leck, J.H.,

Pressure Measurement in Vacuum Systems

(Chapman and Hall) (1964)

Lewis, B.,

J. Amer. Chem. Soc., 51, 564, (1929)

Lewis, P.,

Astrophys. J., 12, 8, (1900)

Lichten, W.,

Phys. Rev. 120, 848, (1960)

McLeod, H.,

Phil. Mag. 48, 110, (1874)

Madden, H.H., and Farnsworth, H.E.,

J. Chem. Phys., 34, 1186, (1961)

Mannella, G.G.,

Chem. Revs., 1, (1962)

Massey, H.W.S., and Burhop, E.H.S.,
"Electronic and Ionic Impact Phenomena,"
(O.U. Press) p.263 (1952)

Mathis, M.,
Bull. Soc. Chim. Fr., 443, (1951)

Mignolet, J.C.P.,
Disc. Far. Soc. 8, 105, 326, (1950)

Mimeault, V.J., and Hansen, R.S.,
J. Phys. Chem. 70, 3001, (1966)

Mitra, S.K.,
"Active Nitrogen - A New Theory" Calcutta (1945)

Nielsen, K.O.,
in "Electromagnetically enriched isotopes and
mass spectrometry",(N.Y. Acad. Press) p.68 (1956)

Nornes, S.B., and Donaldson, E.E.,
J. Chem. Phys. 44, 2968, (1966)

Nottingham, W.B.,
J. Appl. Phys. 8, 762, (1937)

Pietsch, E.,
Ergeb. Exakt. Naturw. 5, 213, (1926)

Plücker, J.,
Pogg. Ann., 105, 84, (1858)

Porter, A.W.,
Trans. Far. Soc. 29, 702, (1933)

Propst, F.M., and Lüscher, E.,
Phys. Rev., 132, 1037, (1963)

Rayleigh, Lord,

Proc. Roy. Soc. A176, 1, (1940)

Redhead, P.A.,

Rev. Sci. Instr. 31, 343, (1960)

Redhead, P.A.,

Trans. 7th Nat. Vac. Symp. (N.Y.), 108, (1961)

Redhead, P.A.,

Vacuum. 12, 267, (1962)

Ricca, F., and Saini, G.,

Ann. Chim. (Rome) 54(6), 572, (1964)

Rosenberg, P.,

Rev. Sci. Instr. 9, 258, (1938)

Rosenberg, P.,

Rev. Sci. Instr. 10, 131, (1939)

Schiff, H.I.,

Ann. N.Y. Acad. Sci. 67, 518, (1956)

Schuit, G.C.A., and De Boer, N.H.,

J. Chim. Phys., 51, 482, (1954)

Schulz, G.J.,

J. Appl. Phys. 28, 1149, (1957)

Schulz, G.J., and Phelps, A.V.,

Rev. Sci. Instr. 28, 1051, (1957)

Smeaton, P.G., Carter, G., and Leck, J.H.,

Trans. Nat. Vac. Symp. 9, 491, (1962)

Sieverts, A., and Krumbhaar, W.,

Ber. Deut. Chem Ges. 43, 893, (1910)

Smithells, C.J.,

" Tungsten, a Treatise on its Metallurgy, Properties and Applications" London, 3rd Ed. (1952)

Stout, V.L., and Vanderslice, T.A.,

8th Vac. Symp., 400, (1961)

Stull, D.R., and Sinke, G.C.,

Thermodynamic Properties of the Elements Advances in Chemistry Series, 18. American Chemical Society, (1956)

Suhrmann, R., and Schultz, K.,

Z. Naturforsch. 10B, 517, (1955)

Tanaka (1956) see Schiff (1956)

Terao, N., and Berghezan, A.,

J. Phys. Soc. Japan 14, 139, (1959)

Thompson, J.B.,

Proc. Roy. Soc. A262, 503, (1961)

Trapnell, B.M.W.,

Proc. Roy. Soc. A218, 566, (1953)

Trillat, J.J., Tertian, L., Terao, N., Lecomte, C.,

Bull. Soc. Chim. Fr. 804, (1957)

Van Hardeveld, R., and Van Montfoort, A.,

Surf. Sci., 4, 396, (1966)

Wagener, S.,

J. Phys. Chem. 61, 267, (1957)

Wehner, G.K.,

8th Vac. Symp. p.239 (1962)

Winters, H.F., Horne, D.E., and Donaldson, E.E.,

J. Chem. Phys. 41, 2766, (1964)

Winters, H.F.,

J. Chem. Phys. 44, 1472, (1966)

Yarwood, J., and Close, K.J.,

Proc. 2nd European Symp. on Vac. p.3. (1963)

Zscheile, H.,

Phys. Status Solidi, 14, K15, (1966)